On the SU(2) theory of the t-J model.

by

Dmitri A. Ivanov
M.Sc., Moscow Institute of Physics and Technology, 1995

Submitted to the Department of Physics
in partial fulfillment of the requirements for the degree of

Doctor of Philosophy

at the

MASSACHUSETTS INSTITUTE OF TECHNOLOGY

September 1999

© Massachusetts Institute of Technology 1999. All rights reserved.

Author .....
Department of Physics
June 30, 1999

Certified by .....
Patrick A. Lee
William and Emma Rogers Professor of Physics
Thesis Supervisor

Accepted by .....
Thomas J. Greytak
Professor, Associate Department Head for Education

MASSACHUSETTS INSTITUTE OF TECHNOLOGY
WITHDRAWN
SEP 21 1999
MIT LIBRARIES
LIBRARIES
Science

On the SU(2) theory of the t-J model.

by
Dmitri A. Ivanov
M.Sc., Moscow Institute of Physics and Technology, 1995

Submitted to the Department of Physics
on June 30, 1999, in partial fulfillment of the
requirements for the degree of
Doctor of Philosophy

Abstract

The t-J model proposed to simulate the electronic structure of high-temperature cuprate superconductors, is itself a very complex system, many of its properties still being a subject of controversy. The physics of the t-J model in the regime pertaining to the underdoped cuprates can be understood in the framework of an SU(2) theory employing the slave-boson decomposition together with a particle-hole symmetry for spinons. The SU(2) theory is of a mean-field type without a small parameter, and without including all fluctuations, its results must be interpreted with caution.

In the first part of my thesis, I propose to account for the no-double-occupancy constraint by a Gutzwiller-type projection of the SU(2) mean-field function. The projection is also constructed in an SU(2) gauge invariant way. The resulting wave function coincides with the d-wave Gutzwiller-projected wave function known to give a very good variational energy. The SU(2) symmetry of the construction allows us to link this wave function to the staggered-flux phase of the SU(2) theory, which explains the correlations of the staggered vorticity of holes. A loop-soup construction based on the staggered-flux description provides an understanding of the hole pairing. The discussion is supported by variational Monte Carlo simulations.

The second part of the thesis is devoted to applying the SU(2) theory to two-leg t-J ladders. In the low-temperature staggered-flux phase, we can exclude the spin degrees of freedom which have an energy gap. For gapless charge excitations the effective theory is the Luther-Emery liquid. Our analysis is applicable at low doping and in the "physical" range of parameters $t/J \sim 3$ where there is only one massless mode in the charge sector and no massless modes in the spin sector. Within our model we make predictions about correlation exponents and the superconductivity order parameter.

In the last part of the thesis, we study the nuclear spin-lattice relaxation rate $1/T_1$ in the two-leg antiferromagnetic spin-1/2 Heisenberg ladder. More specifically, we consider the contribution to $1/T_1$ from the processes with momentum transfer (π, π). In the limit of weak coupling between the two chains, this contribution is of activation type with gap 2Δ at low temperatures (Δ is the spin gap), but crosses over to a slowly-decaying temperature dependence at the crossover temperature $T \approx \Delta$. We also discuss applicability of our results to weakly doped t-J two-leg ladders.

Thesis Supervisor: Patrick A. Lee
Title: William and Emma Rogers Professor of Physics

Acknowledgments

I would like to express my sincere gratitude to those who have made this work possible.

First of all, I would like to thank my advisor Patrick Lee for his kindly guidance throughout my studies in MIT. I have benefited from his deep physical insight and from his gentle tutorship. He encouraged independent thinking, but was always open for discussions and questions. I felt some very special warm and inspiring atmosphere around Patrick, and working with him was a pleasure.

I would also like to thank Xiao-Gang Wen and Takashi Imai, who kindly agreed to serve in my thesis committee. Xiao-Gang's thoughts greatly contributed to my work on the second chapter of the thesis. The experiments of Takashi Imai and his collaborators motivated the last chapter of the thesis. I would like to thank Takashi Imai for sharing with us their experimental data before publication.

I want to express my deepest thanks to my friend and former office mate Don Kim. I must confess that I shared with Don not only our office cubicle, but also his encyclopedical knowledge of physics, his beautiful physics library, and his love for classical music. Topics of our discussions ranged from the history of physics to Thoreau, from saltwater fishing to Russian literature. His friendship was of invaluable help in my work, and much more.

During the last year of my work on the thesis, I enjoyed frequent and extensive discussions with Sasha Abanov, usually accompanied by tea and cookies. In addition to being of a substantial help in my studies, tea sessions with Sasha revived my enthusiasm for the mathematical elegance of physics.

In the progress of my work, I benefited from many interactions. I enjoyed many discussions with Naoto Nagaosa during his visits to MIT, especially on one-dimensional physics. I am grateful to Chris Mudry for helpful remarks, particularly regarding the third chapter of the thesis. Many thanks to Andrey Shytov, my college friend and former office mate, for our helpful conversations and for his Russian-style physics. During the last stage of my work, I often shared my thoughts and ideas with my new office mates Guobin Sha and Walter Rantner. I benefited a lot from their response.

With pleasure I mention the support of my Russian advisor and collaborator Misha Feigel'man. I would like to thank him for his kind care throughout my American education and for making my frequent trips to Moscow pleasant and productive.

During my undergraduate years, I was fortunate to work with Andrei Losev and then with my undergraduate advisor Leonya Levitov, with whom I still discuss more than just physics.

Finally, my thanks go to Yu. P. Rybkin, A. R. Zilberman, B. M. Davidovich, Volodya Fock, and Yura Chekanov who taught me the beauty of physics and mathematics during my school time, as well as to my classmates without whom my education would be impossible and whose support I always felt during these years.

Contents

1 Introduction **8**
1.1 Hubbard and t-J models and cuprate superconductors 8
1.2 SU(2) theory of the t-J model 12
1.3 Outline of the thesis. 13

2 An SU(2) approach to variational wave functions of the t-J model in two dimensions. **17**
2.1 Introduction 17
2.2 Construction of the wave function. 19
2.2.1 SU(2)-invariant construction. 19
2.2.2 Variational wave function in the staggered-flux gauge. 22
2.2.3 Variational wave function in the pairing gauge. 27
2.2.4 Symmetry of the wave function. 28
2.2.5 Optimizing the wave function and the "chemical potential" μ. 28
2.3 Loop-soup interpretation of the wave function. 30
2.4 Correlation functions computed by the VMC method. 35
2.4.1 Spin correlations. 35
2.4.2 Density correlations. 36
2.4.3 Single-particle equal-time Green's function. 38
2.4.4 Vorticity correlations. 41
2.5 Discussion and conclusion. 43

3 An SU(2) theory of t-J two-leg ladders **48**
3.1 Introduction 48
3.2 $SU(2)$ mean-field theory of the ladder 50
3.3 Luther-Emery liquid and correlation exponents 60
3.4 Modified d-wave relation on superconducting order parameter 63
3.5 Conclusion 66

4 Staggered-spin contribution to nuclear spin-lattice relaxation in two-leg antiferromagnetic spin-1/2 ladders. **69**
4.1 Appendix A. Case of weakly doped ladders 76
4.2 Appendix B. On the validity of neglecting magnon interaction in computing $1/T_1$ 77

List of Figures

1-1 A schematic view of the copper-oxide layer. 10
1-2 Phases of superconducting cuprates. 11

2-1 Ordering convention for the wave function. 23
2-2 A possible realization of the staggered-flux phase in the abelian gauge. Links with arrows correspond to $a_{ij} = \varphi/2$ in the direction of the arrow. Links without arrows have $a_{ij} = 0$. The two sublattices A and B are labeled. 24
2-3 An example of partitioning the lattice into non-intersecting cycles. All cycles have either length one or even length. 31
2-4 The four possible configurations of a hole in the "loop-soup". 32
2-5 An illustration of the "alignment" sign rule. The loop (A) is aligned ("alignment" sign +1). The loop (B) requires the direction of two segments to be reversed for alignment (sign +1). The loop (C) requires the direction of one or three segments reversed (sign -1). 32
2-6 Diagrams for spin-spin (A) and hole-density (B) correlation functions. The shaded box denotes the summation over loop coverings; lines without arrows assume summation over directions. 33
2-7 Diagrams for the Green's functions $\langle c_\uparrow(i)c_\uparrow^\dagger(j)\rangle$ (A) and $\langle c_\downarrow(i)c_\downarrow^\dagger(j)\rangle$ (B). 34
2-8 Diagram for the pairing correlation $\langle c_\uparrow(i_1)c_\downarrow(i_2)c_\downarrow^\dagger(j_1)c_\uparrow^\dagger(j_2)\rangle$ (A). As the distance between the pairs of sites (i_1, i_2) and (j_1, j_2) goes to infinity, the correlation function factorizes (B). 34
2-9 Staggered spin correlation $(-1)^{R_x+R_y}\langle\sigma_z(0)\sigma_z(R)\rangle$ as a function of R^2 for the undoped system. Lattice size 20×20, number of samples 10^4. 36
2-10 Staggered spin correlation $(-1)^{R_x+R_y}\langle\sigma_z(0)\sigma_z(R)\rangle$ as a function of R^2 at various values of doping x. The gap value is $\tilde{\Delta} = 0.55$ (optimal gap at zero doping). Lattice size 20×20, number of samples 10^4. 37
2-11 Hole density and staggered vorticity correlations for two holes in the 18×18 lattice at $\tilde{\Delta} = 0.55$ as a function of R^2. Number of samples: $2 \cdot 10^4$. Both correlation functions are normalized to the density of holes n_h. 38
2-12 The same as previous figure, but at $\tilde{\Delta} = 2.0$. The hole correlations at the even sites of the same sublattice (with even R_x and R_y) identically vanish. 39
2-13 The same as previous figure, but at $\tilde{\Delta} = 0.1$. 39

2-14 Nearest-neighbor and $(1,1)$-neighbor hole correlations for two holes in the $N \times N$ lattice as a function of N (in log-log scale). The gap value is fixed $\tilde{\Delta} = 2.0$. Each point is the result of averaging over $2 \cdot 10^4$ samples. 40
2-15 The same as fig. 2-11, but for 16 holes in the 18×18 lattice. $\tilde{\Delta} = 0.55$. Log-log scale for vorticity and log-linear scale for density. Number of samples: $2 \cdot 10^3$. 40
2-16 The same as the previous figure, but for 32 holes in the 18×18 lattice. $\tilde{\Delta} = 0.55$. Log-log scale for vorticity and log-linear scale for density. Number of samples: $1 \cdot 10^3$. 41
2-17 Momentum distribution of holes for 10% doping of 10×10 lattice and $\tilde{\Delta} = 0.57$. 42
2-18 (A) Current-current correlations for 10 holes in the 10×10 lattice at $\tilde{\Delta} = 0.55$ and $\mu = -0.16$ (normalized to hole density). The number on a link is the correlation of the current on this link and of the current on the circled link. The arrows point in the direction of the positive correlations of the current. The error bars are one or two units in the last digit. (B) The same, but in the form of vorticity correlations. The number on a plaquet is the vorticity correlation of this plaquet and the crossed plaquet. 44

3-1 Two-leg t-J ladder. 51
3-2 The two closed contours used in constructing mean-field order parameters. 53
3-3 Space of mean-field phases. The two corners correspond to the π-flux and uRVB phases, boundaries — to the uniform-flux and staggered-flux phases. 54
3-4 Mean-field phase diagram at isotropic coupling and $t/J = 3$. 55
3-5 sF phase order parameters in the translationally invariant gauge. . . . 56
3-6 sF order parameters in the abelian gauge. 56
3-7 Typical fermionic-bosonic spectrum. Both bands are doubly degenerate. 57
3-8 Gauge fields describing the fluctuations of the order parameter. We choose the gauge with $A_\perp = 0$. 58
3-9 Lowest-order diagram responsible for the dynamics of the gauge field. Solid lines denote spinon propagators. This diagram gives mass to the out-of phase mode and 1+1-dimensional QED dynamics for the in-phase mode. 59
3-10 Fluctuating singlets in the spin ladder. 60
3-11 Misplaced singlet bonds between two holes in the t-J ladder. The energy cost is proportional to the distance between the holes. 60

4-1 Three-magnon processes contributing to $(1/T_1)_{q=\pi}$. 73
4-2 The three limiting asymptotics of the temperature dependence of $(1/T_1)_{q=\pi}$. Dashed line is the qualitative interpolation of the actual temperature dependence. 75

Chapter 1

Introduction

The men of principled simplicity
Will have no traffic with our subtle doubt.
The world is flat, they tell us, and they shout:
The myth of depth is an absurdity!

For if there were additional dimensions
Beside the good old pair we'll always cherish,
How could a man live safely without tensions?
How could he live and not expect to perish?

In order peacefully to coexist
Let us strike one dimension off our list.

If they are right, those men of principle,
And life in depth is so inimical,
The third dimension is dispensable.

From *The poems of Knecht's student years*,
The Glass Bead Game, Hermann Hesse
(translated by Richard and Clara Winston)

1.1 Hubbard and t-J models and cuprate superconductors

The first high-temperature superconductor, $(LaBa)_2CuO_4$, with the critical temperature $T_c = 33K$ has been discovered in 1986 [1]. Since then, many more superconducting cuprates have been found, such as $(LaSr)_2CuO_4$ ($T_c = 34K$) and YBCO ($T_c = 92K$). The critical temperatures reach as high as $164K$ [2], but the explanation of the phenomenon of high-temperature superconductivity still remains a challenge for theoretical physics.

The characteristic feature of cuprate superconductors is the copper-oxide planes where copper atoms form a square lattice with oxygen atoms in the centers of the

links (fig. 1-1). An analysis of atomic levels suggests that the electronic properties are determined by the nearly half-filled $Cu_{(3d)}$-$O_{(2p)}$ hybridized orbitals. At half filling, the layer becomes a Mott insulator, with antiferromagnetically ordered electron spins (electrons may be visualized as localized on copper atoms). When doped with mobile holes, the antiferromagnetic long-range order quickly disappears, and a superconducting phase emerges. The critical temperature is maximal at the "optimal doping" (typically, about 15%), and decreases with further doping (fig. 1-2). The underdoped region is very different in many respects from the overdoped one, the latter resembling the conventional Fermi liquid in the normal state. The work presented in the thesis is related to the underdoped case which exhibits anomalous behavior in both superconducting and normal states.

The layered crystal structure is responsible for the inhomogeneous superconductivity: the superconducting electrons are mostly confined within copper-oxide planes, and the Josephson coupling between planes provides the three-dimensional phase coherence. The superconducting order parameter has experimentally been shown to have a d-wave structure [3]. But the most unusual feature of the superconducting state is the relation between the superconducting gap Δ and the critical temperature T_c. In the underdoped region, the gap Δ only weakly depends on the hole concentration, while T_c is roughly proportional to the doping, thus the BCS relation between Δ and T_c does not hold.

Moreover, above T_c, in the underdoped region, the gap Δ manifests itself as a spin gap observable in NMR [4] and photoemission experiments [5], specific heat [6] and c-axis conductivity [7]. This gap affects only spin degrees of freedom, and is not observable, for example, in the in-plane optical conductivity. Another interesting feature of the underdoped cuprates is the evolution of the Fermi-surface from small segments ("hole pockets") near wave vector $(\pi/2, \pi/2)$ at low doping [8] to a full Fermi surface with area $(1-x)$ in optimally doped cuprates [9].

Such a collection of anomalous features requires a non-Fermi-liquid description with possible spin-charge separation. The mechanism of superconducting pairing is not the phonons, but the spin fluctuations of electrons in Cu-O planes. It has been suggested (the first three "Dogmas" of Anderson [13]) that most of the anomalous properties are contained in a simple strongly-correlated two-dimensional model: the one-band Hubbard model or its strong-coupling limit $t-J$ model.

The Hubbard model describes fermions on a lattice with an on-site repulsion:

$$H = -t \sum_{ij} c_i^\dagger c_j + U \sum_i (c_i^\dagger c_i)^2, \tag{1.1}$$

where the hopping term, in the simplest case, connects only nearest-neighbor sites (next-nearest-neighbor hopping is also sometimes included, but its physical relevance is unclear). In the limit of $U \gg t$, the low-energy effective Hamiltonian is that of the $t-J$ model:

$$H = -t\mathcal{P}\left(\sum_{ij} c_i^\dagger c_j\right)\mathcal{P} + J\sum_{ij}\left(\vec{S}_i\vec{S}_j - \frac{n_i n_j}{4}\right), \tag{1.2}$$

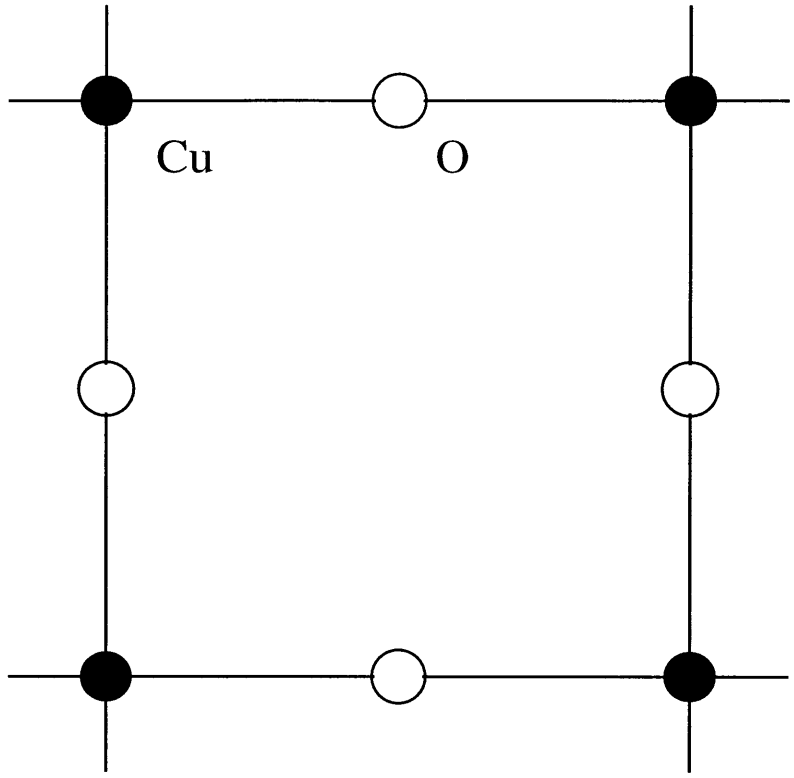

Figure 1-1: A schematic view of the copper-oxide layer.

where $\mathcal{P}$ is the projector onto the states without doubly occupied sites, $J = 2t^2/U$ is the exchange constant appearing in the second-order perturbation theory in U. (A more consistent derivation uses a canonical transformation to exclude higher-energy states [11].)

With the seemingly simple Hamiltonians, the physics of the Hubbard and t-J models is complicated and inaccessible to regular perturbation-expansion-type treatment. The properties of the t-J and Hubbard models are believed to be qualitatively similar (in the low-energy regime), but it is still not clear if these models alone are able to reproduce the anomalous behavior of superconducting cuprates, or further complications (such as next-nearest-neighbor hopping) may be required. The discussion of the present thesis is limited to the $t - J$ model with nearest-neighbor hopping only.

In understanding the origin of high-temperature superconductivity, we may benefit from studying "ladder" compounds [12]. With a microscopic structure similar to planar materials, "ladder" compounds have copper atoms organized in ladders with number of legs depending on the stoichiometric composition and on fabrication details. The inter-ladder interactions are frustrated and at the first approximation may be neglected. The (quasi)-one-dimensionality of ladders allow us to apply a much more powerful machinery of methods including bosonization and mapping onto exactly solvable systems. Besides attempts of extrapolating the theory from ladders onto two-dimensional layers [13], ladder cuprates also provide an additional insight into the microscopics of cuprates and a testing ground for approximations and models.

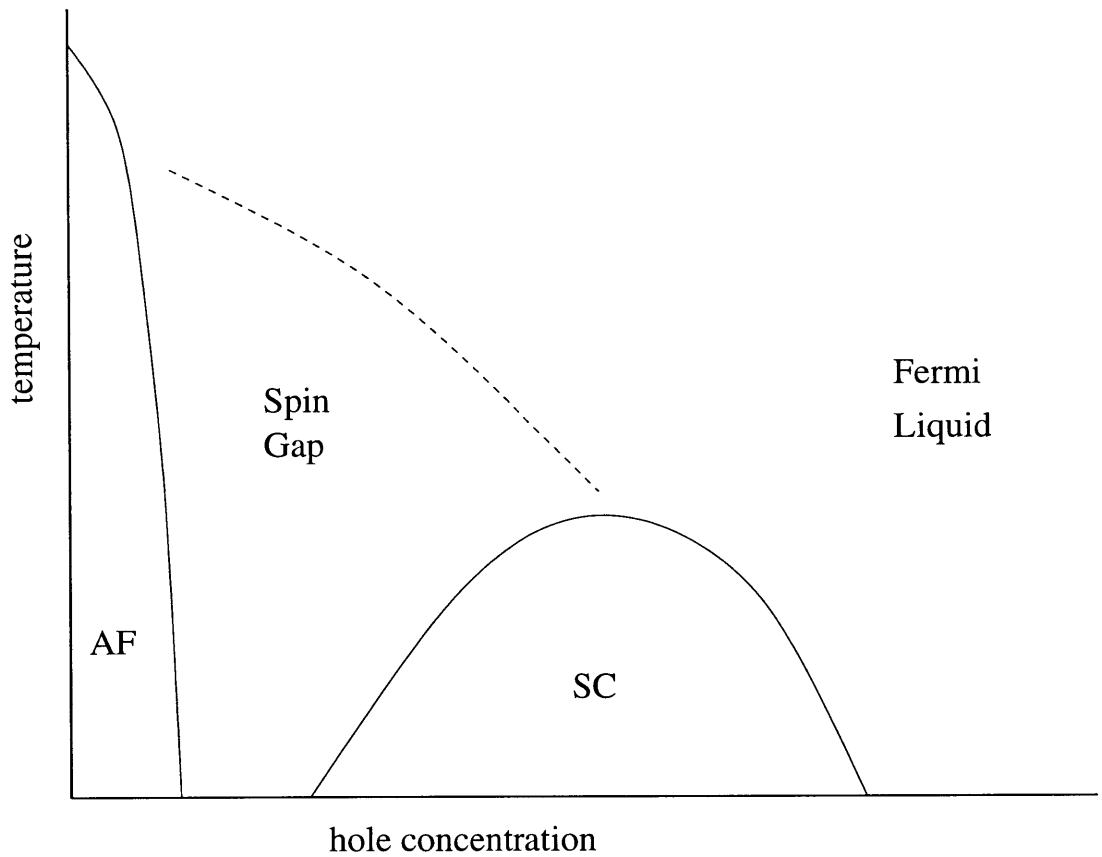

Figure 1-2: Phases of superconducting cuprates.

1.2 SU(2) theory of the t-J model

One of the most straightforward treatments of the t-J model is the mean-field approach [14, 15, 16, 17]. The no-double occupancy constraint may be dealt with by representing the electron as a product of auxiliary fermion and boson particles (a spinon and an holon): $c_\sigma = f_\sigma b^\dagger$. Then the constraint becomes a linear one requiring that the total number of particles (spinons and holons) on each site is equal to one. On one hand, such a slave-boson approach implies a certain degree of separation of spin and charge degrees of freedom, which is helpful for explaining the spin-gap phenomenon in the underdoped region. On the other hand, this will eventually lead to the physical picture of a hole-doped resonating-valence-bond (RVB) state proposed by Anderson [18].

The mean-field phase diagram based on the slave-boson representation captures the physics of cuprates remarkably well. In particular, in the underdoped region, the spinon-pairing temperature T^* is higher than that of the Bose-condensation T_c, leaving a region of the spin gap in the normal phase. However, not very much can be done beyond the mean-field theory. In fact, including gauge-field fluctuations around the mean-field state has been shown to lead to instabilities [19, 20].

A more advanced $SU(2)$ version of the slave-boson decomposition which already includes some of the fluctuations over the $U(1)$ mean-field state has been proposed by Wen and Lee [21, 22]. The $SU(2)$ approach extends the particle-hole symmetry present at half-filling [23] to the doped case. This is done by doubling the number of bosons. In addition to the fermionic $SU(2)$ doublets

$$\Psi^\dagger_{i\uparrow} = \begin{pmatrix} f^\dagger_{i\uparrow} \\ f_{i\downarrow} \end{pmatrix} \tag{1.3}$$

and

$$\Psi^\dagger_{i\downarrow} = \begin{pmatrix} f^\dagger_{i\downarrow} \\ -f_{i\uparrow} \end{pmatrix}, \tag{1.4}$$

we introduce a bosonic doublet

$$b^\dagger_i = \begin{pmatrix} b^\dagger_{i1} \\ b^\dagger_{i2} \end{pmatrix} \tag{1.5}$$

(i is the index for the lattice site). A physical hole may now be represented as either a no-spinon site with a $b^\dagger_1$ holon or as a two-spinon site with a $b^\dagger_2$ holon. The physical subspace of the spinon-holon space on each site consists of the only three $SU(2)$-invariant states: $f^\dagger_\uparrow|0\rangle$, $f^\dagger_\downarrow|0\rangle$, and $\frac{1}{\sqrt{2}}(b^\dagger_1 + b^\dagger_2 f^\dagger_\uparrow f^\dagger_\downarrow)|0\rangle$, corresponding to a spin-up site, a spin-down site, and a hole, respectively.

The electron operators are represented as

$$\begin{aligned} c^\dagger_\uparrow &= \frac{1}{\sqrt{2}}\Psi^\dagger_\uparrow b = \frac{1}{\sqrt{2}}(f^\dagger_\uparrow b_1 + f_\downarrow b_2), \\ c^\dagger_\downarrow &= \frac{1}{\sqrt{2}}\Psi^\dagger_\downarrow b = \frac{1}{\sqrt{2}}(f^\dagger_\downarrow b_1 - f_\uparrow b_2), \end{aligned} \tag{1.6}$$

and the spin operators (when projected onto the physical subspace) contain only

spinon variables:

$$\vec{S} = \frac{1}{2} c_\alpha^\dagger \vec{\sigma}_{\alpha\beta} c_\beta = \frac{1}{2} f_\alpha^\dagger \vec{\sigma}_{\alpha\beta} f_\beta. \tag{1.7}$$

This representation is redundant: it is invariant with respect to an $SU(2)$ gauge symmetry:

$$\begin{aligned} \Psi_{i\alpha} &\mapsto W_i \Psi_{i\alpha}, \\ b_i &\mapsto W_i b_i, \end{aligned} \tag{1.8}$$

where W_i are arbitrary site-dependent $SU(2)$ matrices.

Any physical observable must be an $SU(2)$ gauge-invariant quantity; correlation functions of non-gauge-invariant quantities are equal to zero after averaging over gauge transformations (1.8). The mean-field phase diagram and the electronic spectral function in the $SU(2)$ approach were derived in [21, 22].

In the present thesis I am making an attempt to explain the physical meaning of the $SU(2)$ ansatz. In the next two chapters I develop the $SU(2)$ approach for the two-dimensional lattice (in the variational formalism) and for the two-leg ladder. Being very different in physics and in the methods, those two problems have a common feature — pairing of holons into an $SU(2)$ singlet. This suggests that the $SU(2)$ approach may be beneficial for describing hole pairing in the $t - J$ model.

1.3 Outline of the thesis.

The main part of the thesis consists of three chapters devoted to different aspects of the physics of the t-J model.

The first part (Chapter 2) studies the $SU(2)$ theory of the t-J model in two dimensions in the variational formulation in terms of Gutzwiller-projected wave functions. We find that the d-wave Gutzwiller-projected wave function [24, 25] may be alternatively viewed as a $SU(2)$-projected staggered-flux wave function. The signature of the staggered flux is the staggered pattern of the correlations of local electrical current, which suggests that pairs are formed of holes circulating in opposite directions. In the staggered-flux description, the paired holes have opposite $SU(2)$ indices. This variational wave function describes a superconducting phase transition at zero temperature as binding-unbinding of hole pairs. The $SU(2)$ variational approach may also be useful for describing quantum phase transitions into phases with broken time-reversal or translational symmetry (e.g. Neel antiferromagnetic phase).

The second part (Chapter 3) is devoted to application of the $SU(2)$ approach to two-leg t-J ladders. The physics of the $t - J$ model in two-leg ladders is now very well understood. The even-leg antiferromagnetic spin-1/2 ladders are known to have a spin gap similar to the Haldane gap in integer-spin chains. This gap persists at low hole doping. Both in the limits of weak and strong coupling between the two legs of the ladder, analytic studies show that the low-energy charge excitations are massless and carry charge two (we call such hole pairs bipolarons). We derive a similar picture from the $SU(2)$ slave-boson formalism in the case when the inter-chain and

intra-chain couplings are of the same order of magnitude. The gapped spin degrees of freedom may be integrated out, and holes of opposite $SU(2)$ charge are confined into pairs by fluctuations of the gauge field. Our approach also predicts the d-wave structure of pairing correlations.

Finally, the third part (Chapter 4) reports the theoretical study of the spin-lattice relaxation in two-leg antiferromagnetic spin-1/2 ladders. Inspired by the NMR experiments by Imai et al [26], we have developed a simple theory of the temperature dependence of the staggered-spin contribution to $1/T_1$ in the weak-interchain-coupling limit. Our theory is based on scaling-type arguments and predicts a crossover from an activational behavior of $(1/T_1)_\pi$ at low T to a weakly decreasing temperature dependence at high T. A crossover, with a maximum of $(1/T_1)_\pi$, is shown to occur at a temperature close to the spin gap. This type of temperature behavior is predicted for both undoped and weakly doped ladders.

The material of Chapter 3 and most of the material of Chapter 4 have been previously published in [27, 28].

Bibliography

[1] J. G. Bendorz and K. A. Müller, Z. Phys. B 64 (1986) 189.

[2] L. Gao, Y. Y. Xue, F. Chen, Q. Xiong, R. L. Meng, D. Ramirez, C. W. Chu, J. H. Eggert, and H. K. Mao, Phys. Rev. B 50 (1994), 4260.

[3] D. J. van Harlingen, Rev. Mod. Phys. 67 (1995), 515;
C. C. Tsuei, J. R. Kirtley, C. C. Chi, L. S. Yu-Jahnes, A. Gupta, T. Shaw, J. Z. Sun, and M. B. Ketchen, Phys. Rev. Lett. 73 (1994), 593.

[4] M. Takigawa et al., Phys. Rev. B 43 (1991), 247.

[5] A. G. Loeser et al., Science 273 (1996), 325;
H. Ding et al., Nature 382 (1996), 51.

[6] J. W. Loram, K. A. Mirza, J. R. Cooper, and W. Y. Liang, Phys. Rev. Lett. 71 (1993), 1740.

[7] C. C. Homes et al., Phys. Rev. Lett. 71 (1993), 1645.

[8] B. O. Wells, Z.-X. Shen, A. Matsuura, D. M. King, M. A. Kastner, M. Greven, and R. J. Birgeneau, Phys. Rev. Lett. 74 (1995), 964.

[9] Z. X. Shen and D. S. Dessau, Phys. Rep. 253(1995), 1.

[10] P. W. Anderson, The theory of Superconductivity in the High-T_c Cuprates, Princeton Univ. Press (1997).

[11] W. Kohn, Phys. Rev. A 133 (1964), 171.

[12] Z. Hiroi, M. Azuma, M. Takano, and Y. Bando, J. Solid State Chem. 95 (1991), 230.

[13] T. M. Rice, S. Haas, M. Sigrist, and F.-C. Zhang, Phys. Rev. B 56 (1997), 14655.

[14] G. Baskaran, Z. Zou and P. W. Anderson, Solid State Commun. 63 (1987), 973.

[15] I. Affleck and J. B. Marston, Phys. Rev. B 37 (1988), 3774.

[16] G. Kotliar and J. Liu, Phys. Rev. B 38 (1988), 5142.

[17] Y. Suzumura, Y. Hasegawa, and H. Fukuyama, J. Phys. Soc. Jpn. 57 (1988), 2768.

[18] P. W. Anderson, Science 235 (1987), 1196.

[19] M. U. Ubbens and P. A. Lee, Phys. Rev. B 49 (1994), 6853.

[20] R. Hlubina, W. Putikka, T. M. Rice, and D. Khveshchenko, Phys. Rev. B 46 (1992) 11224.

[21] X.-G. Wen and P. A. Lee, Phys. Rev. Lett. 76 (1996), 503.

[22] P. A. Lee, N. Nagaosa, T.-K. Ng, and X.-G. Wen, Phys. Rev. B 57 (1998), 6003.

[23] I. Affleck, Z. Zou, T. Hsu, and P. W. Anderson, Phys. Rev. B 38 (1988), 745.

[24] C. Gros, Ann. Phys. 189 (1989), 53.

[25] H. Yokoyama and M. Ogata, J. Phys. Soc. Jpn. 65 (1996), 3615.

[26] T. Imai, K. R. Thurber, K. M. Shen, A. W. Hunt, and F. C. Chou, Phys. Rev. Lett. 81 (1998), 220.

[27] D. A. Ivanov and P. A. Lee, Phys. Rev. B 57 (1998), 2118.

[28] D. A. Ivanov and P. A. Lee, Phys. Rev. B (1999).

Chapter 2

An SU(2) approach to variational wave functions of the t-J model in two dimensions.

2.1 Introduction

The $SU(2)$ theory of the t-J model proposed by Wen and Lee has proven effective in describing superconducting cuprates. Its mean-field phase diagram explains the spin-gap phenomenon in the normal state of underdoped cuprates, while the physical electron spectral function shows an evolution from Fermi-surface segments at small doping to a large Fermi surface as the doping increases [1, 2, 3].

At the same time, there are questions essential for the $SU(2)$ theory that remain open. Firstly, the questions of interpreting the $SU(2)$ formalism: the physical meaning of the $SU(2)$ order parameter ("flux") and the mechanism of the superconducting transition. Secondly, we need to understand the effect of fluctuations about the mean-field state and the interplay between charge and spin degrees of freedom. In the present paper we address these questions with the variational formulation of the $SU(2)$ approach which allows us to go beyond the mean-field theory. The no-double-occupancy constraint can be imposed exactly in the Gutzwiller-projected wave functions [4]. While the Gutzwiller approximation is equivalent to treating the slave bosons at the mean-field level [5], the Gutzwiller projection corresponds to averaging over gauge fluctuations responsible for the constraint. This reasoning can be straightforwardly extended to the $SU(2)$ formalism.

The $SU(2)$ version of the Gutzwiller projection involves not only fermions (spinons), but also bosons (holons). A hole may be represented by either a no-spinon site with a type-one holon or from a two-spinon site with a type-two holon. This construction simply recasts the $SU(2)$ slave-boson decomposition into the language of Gutzwiller projection. We apply the $SU(2)$ projection to a mean-field state corresponding to the staggered-flux (sF) or to the $d_{x^2-y^2}$-wave (pairing) mean-field phase which are SU(2) gauge-equivalent and represent the mean-field solution at low temperatures. The holons are taken Bose-condensed, which implies that the resulting

wave function is superconducting. Since the projection is formulated in an $SU(2)$-covariant form, the wave function after the projection is the same for the sF and pairing phases (we shall further call it the $SU(2)$ wave function to stress its dual origin). Moreover, we prove that it coincides with the d-wave pairing wave function projected by means of the conventional ($U(1)$) Gutzwiller projection.

If we use variational wave functions only as a computational tool, the $SU(2)$ approach provides no new result, because the resulting wave function is the same as in the conventional $U(1)$ theory. However, we learn two lessons from the alternative sF description of the wave function.

The first lesson is to look at the staggered-flux signatures in the wave function. We compute the equal-time current-current correlation function by the variational Monte Carlo method and find that it has a well-pronounced pattern of staggered vorticity. A natural explanation arising from the sF picture is the formation of pairs of holes of opposite staggered vorticity.

The second lesson is that the staggered-flux formulation provides a useful "loop-soup" picture of the variational wave function. Correlation functions are given by statistical averages over all loop coverings of the lattice such that every site belongs to exactly one loop. The statistical weights of configurations are not necessarily positive, but contain minus-one factors arising from fermionic loops. We conjecture that for our choice of the mean-field phase (which features four nodal points instead of a Fermi surface at the mean-field level) the weight of large loops decays as a power of the size of the loop (the exponent depends continuously on the parameters of the wave function). The attraction of spinons and holons is represented as loops connecting them. This leads to the power-law behavior of many correlation functions. In particular, the staggered-spin correlations decay as power law at any concentration of holes. The density-density correlation function for two holes also decays as power law. For the realistic values of parameters, the results of the variational Monte Carlo computations give the exponent less than two, which results in the unbound state in the thermodynamic limit. The power-law dependence on the distance is also found in the current-current correlations.

The rest of the paper provides the details of the above outline arranged in a somewhat different order. In the second section, we define the wave function, rigorously prove some of its properties, and present explicit expressions in the sF and pairing gauges. The last part of the second section is devoted to optimizing the variational energy by adjusting the variational parameter and by introducing the antiferromagnetic order or the "chemical potential". In the third section we develop the loop-soup theory of the wave function. The fourth section contains data on correlation functions obtained by the VMC method and their interpretation from the point of view of the $SU(2)$ theory. Finally, in the last section we speculate on the possible interpretations of our results for the theory of the t-J model and of high-temperature superconductivity.

2.2 Construction of the wave function.

2.2.1 SU(2)-invariant construction.

In this section we construct a variational ground-state wave function by means of a Gutzwiller-type projection of a mean-field spinon-holon state. Our projection differs from the conventional Gutzwiller projection [4] in that we represent a hole by either an empty or a doubly occupied with spinons site, in agreement with the $SU(2)$ "particle-hole" symmetry (we shall nevertheless call our wave function "Gutzwiller-projected" (GP) reserving the name "conventional Gutzwiller projection" for the projection of a purely fermionic state prohibiting doubly-occupied sites). We shall prove later that our wave function in fact coincides with the $d_{x^2-y^2}$ wave function studied by Gros [6] and by Yokoyama and Ogata [7]. However, we present our SU(2)-invariant construction in the belief that it provides an additional insight in the physics of the wave function by reconciling its superconducting and staggered-flux properties. Our derivation of the $SU(2)$ invariance follows the argument of Zhang et al [8] and extends it to the doped case.

In a few words, to construct the GP wave function we start from the bands of the mean-field theory, with the half-filled fermionic bands, and put bosons at the bottom of the bosonic bands. Finally, we perform the projection onto the only three allowed states at each site: $f_\uparrow^\dagger|0\rangle$, $f_\downarrow^\dagger|0\rangle$, and $\frac{1}{\sqrt{2}}(b_1^\dagger + b_2^\dagger f_\uparrow^\dagger f_\downarrow^\dagger)|0\rangle$ ($f_\uparrow^\dagger$ and $f_\downarrow^\dagger$ are the spinons with spins up and down, $b_1^\dagger$ and $b_2^\dagger$ is the $SU(2)$ doublet of holons, $|0\rangle$ is the "empty" site; we follow the notation of [1]). Below we elaborate this construction for a particular case of the staggered-flux (or, equivalently, d-wave-pairing) phase.

We start from the mean-field Hamiltonian for the spinons and the holons:

$$H = J\sum_{ij} \begin{pmatrix} f_{i\uparrow}^\dagger & f_{i\downarrow} \end{pmatrix} U_{ij} \begin{pmatrix} f_{j\uparrow} \\ f_{j\downarrow}^\dagger \end{pmatrix} + \text{h.c.} + \\ +t\sum_{ij} \begin{pmatrix} b_{i1}^\dagger & b_{i2}^\dagger \end{pmatrix} U_{ij} \begin{pmatrix} b_{j1} \\ b_{j2} \end{pmatrix} + \text{h.c.}, \tag{2.1}$$

where U_{ij} are unitary 2x2 matrices [1]. At the moment we neglect the Lagrange multiplier terms for no-double-occupancy constraint assuming their mean-field value is zero and postpone their discussion until later. We also disregard the overall energy scale of the Hamiltonian and may, without loss of generality, take U_{ij} normalized: $\det U_{ij} = -1$.

The physical electrons $c_\uparrow^\dagger$ and $c_\downarrow^\dagger$ are expressed as

$$c_\uparrow^\dagger = \frac{1}{\sqrt{2}}(f_\uparrow^\dagger b_1 + f_\downarrow b_2), \\ c_\downarrow^\dagger = \frac{1}{\sqrt{2}}(f_\downarrow^\dagger b_1 - f_\uparrow b_2). \tag{2.2}$$

This slave-boson representation is redundant and enjoys the $SU(2)$ gauge symmetry:

$$U_{ij} \mapsto W_i U_{ij} W_j^\dagger, \tag{2.3}$$

$$\begin{pmatrix} f_{i\uparrow}^\dagger \\ f_{i\downarrow} \end{pmatrix} \mapsto W_i \begin{pmatrix} f_{i\uparrow}^\dagger \\ f_{i\downarrow} \end{pmatrix}, \qquad \begin{pmatrix} f_{i\downarrow}^\dagger \\ -f_{i\uparrow} \end{pmatrix} \mapsto W_i \begin{pmatrix} f_{i\downarrow}^\dagger \\ -f_{i\uparrow} \end{pmatrix}, \tag{2.4}$$

$$\begin{pmatrix} b_{i1}^\dagger \\ b_{i2}^\dagger \end{pmatrix} \mapsto W_i \begin{pmatrix} b_{i1}^\dagger \\ b_{i2}^\dagger \end{pmatrix}, \tag{2.5}$$

where W_i are arbitrary site-dependent $SU(2)$ matrices.

In particular, the staggered-flux configuration

$$U_{ij} = ie^{ia_{ij}\sigma_z}, \tag{2.6}$$

where the gauge field a_{ij} has alternating flux $\pm\varphi$ around plaquets, is gauge-equivalent to the d-wave-pairing configuration

$$U_{ij} = -\chi\sigma_z \pm \Delta\sigma_x \tag{2.7}$$

with plus for horizontal links and minus for vertical links. The staggered flux φ is related to the gap $\tilde{\Delta}$ as

$$\frac{\tilde{\Delta}}{2} \equiv \frac{\Delta}{\chi} = \tan\frac{\varphi}{4}. \tag{2.8}$$

Let Ξ be the ground state of the fermionic Hamiltonian. In the sF gauge, Ξ is the half-filled fermionic state:

$$\Xi^{\mathrm{sF}} = \prod_k \left(f_{k\uparrow}^-\right)^\dagger \prod_k \left(f_{k\downarrow}^-\right)^\dagger |0\rangle, \tag{2.9}$$

where the product is performed over all negative-energy states. In the pairing gauge, Ξ is of the BCS form:

$$\Xi^{\mathrm{pair}} = \prod_k \left(u_k + v_k f_{k\uparrow}^\dagger f_{-k\downarrow}^\dagger\right) |0\rangle. \tag{2.10}$$

The bosonic part of the Hamiltonian has two degenerate minima (representing the two species of bosons) — except in the case of π-flux (or, equivalently, $\tilde{\Delta} = 2$), but the variational value of the flux is always less then π (see also subsection 2.2.5). Denote $B_1^\dagger$ and $B_2^\dagger$ the operators creating holons at the bottom of the bosonic bands.

The unprojected (spinon-holon) wave function is the product of Ξ and the Bose condensate of holons. There is an apparent ambiguity in populating the two minima of the bosonic bands, so in general we write the spinon-holon wave function as

$$\Psi_{\mathrm{s-h}} = \sum_{m=0}^{N_h} c_m \left(B_1^\dagger\right)^m \left(B_2^\dagger\right)^{N_h - m} \Xi, \tag{2.11}$$

with some undetermined coefficients c_m. N_h is the number of holes.

Finally, we apply the projection operator

$$P_G = \prod_i \left(|\uparrow\rangle_i\langle\uparrow|_i + |\downarrow\rangle_i\langle\downarrow|_i + |\star\rangle_i\langle\star|_i \right), \tag{2.12}$$

where the product is taken over all sites of the lattice and at each site

$$\begin{aligned} |\uparrow\rangle &= f_\uparrow^\dagger|0\rangle, \\ |\downarrow\rangle &= f_\downarrow^\dagger|0\rangle, \\ |\star\rangle &= \frac{1}{\sqrt{2}}(b_1^\dagger + b_2^\dagger f_\uparrow^\dagger f_\downarrow^\dagger)|0\rangle. \end{aligned} \tag{2.13}$$

Thus, for any choice of gauge we end up with a Gutzwiller-projected wave function

$$\Psi_{GP} = P_G\Psi_{\text{s-h}} = \sum_{m=0}^{N_h} c_m P_G \left(B_1^\dagger\right)^m \left(B_2^\dagger\right)^{N_h-m} \Xi. \tag{2.14}$$

With different choices of coefficients c_m, Ψ_{GP} spans some subspace of a dimension not greater than $N_h + 1$.

We shall now prove the two properties of this subspace:

A) It is one-dimensional, i.e. Ψ_{GP} is defined unambiguously, and

B) It is $SU(2)$-gauge-invariant, i.e. Ψ_{GP} is the same for gauge-equivalent configurations of U_{ij}.

We start with proving part B.

First, recall that the $SU(2)$ gauge symmetry may be extended from operators (eqs. (2.4),(2.5)) to the Hilbert space of unprojected (spinon-holon) wave functions. Let $H_i^{(f)}$ and $H_i^{(b)}$ denote the fermionic and the bosonic Hilbert spaces at the site i (the total Hilbert space H_i at the site i is the product of $H_i^{(f)}$ and $H_i^{(b)}$, and the total spinon-holon Hilbert space is the product of all H_i). To extend the $SU(2)$ rotations of spinons (2.4) onto $H_i^{(f)}$, we need to rotate the vacuum so that it will be annihilated by the images of $f_\uparrow$ and $f_\downarrow$. Obviously, this consistently and uniquely defines the $SU(2)$ rotation of the space $H_i^{(f)}$ (this space is four-dimensional, and transforms as the $(s = 1/2) \otimes (s = 0) \otimes (s = 0)$ representation of $SU(2)$: the states with a nonzero spin $f_\uparrow^\dagger|0\rangle$ and $f_\uparrow^\dagger|0\rangle$ are $SU(2)$ singlets, and the zero-spin states $|0\rangle$ and $f_\uparrow^\dagger f_\uparrow^\dagger|0\rangle$ form an $SU(2)$ doublet).

The $SU(2)$ action on $H_i^{(b)}$ is obvious: it rotates $b_1^\dagger$ to $b_2^\dagger$ and vice versa, leaving the vacuum invariant. By acting with different $SU(2)$ rotations on different sites, we realize the $SU(2)$ gauge action on the whole space H of unprojected wave functions.

Further, the eigenfunctions of the Hamiltonian (2.1) map into the eigenfunctions of the transformed Hamiltonian, with the total number of holons preserved. Therefore, the subspace of unprojected wave functions $\Psi_{\text{s-h}}$ as defined in (2.11) maps under any $SU(2)$ gauge transformation into the subspace $\Psi_{\text{s-h}}$ corresponding to the transformed Hamiltonian.

Finally, we remark that the projection operator P_G defined by (2.12) is $SU(2)$

gauge-invariant, namely $P_G G = P_G$ for any $SU(2)$ gauge transformation G. This guarantees that $SU(2)$-equivalent unprojected wave functions $\Psi_{\mathrm{s-h}}$ result in the same projected wave function Ψ_{GP}, which proves our statement B.

To prove property A, it suffices to check it in the sF gauge. The number of fermions in Ξ^{sF} is equal to the number of lattice sites, and therefore the number of empty sites is equal to the number of doubly-occupied sites. As a result, after the projection (2.14) only the term with $m = N_h/2$ will survive, all the other terms projected out. As we proved above, the subspace Ψ_{GP} is the same in all gauges. It is one-dimensional in the sF phase and therefore in any gauge-equivalent phase. This proves property A.

When applied to the case of zero doping, the above argument of the $SU(2)$ gauge invariance establishes the exact equivalence between the $d_{x^2-y^2}$ Gutzwiller-projected wave function of Gros [6], Yokoyama and Ogata [7] on one side and the staggered-flux GP wave function of Dmitriev et al. [9] and the present work on the other side (this equivalence is also implicitly suggested in [10]). The gap Δ/t in the notation of [6, 7] is equal to $\tilde{\Delta}$ in our notation and converts into the flux through plaquet φ according to (2.8). This relation explains the symmetry $\Delta/2t \mapsto 2t/\Delta$ noticed in [7]: in the flux-phase description this transformation is equivalent to $\varphi \mapsto \varphi + 2\pi$.

The values of the energy as a function of Δ/t at half filling numerically computed in [6, 7] agree with those in [9]. In particular, both [9] and [7] find that the energy is minimized not at $\varphi = \pi$, but at a much smaller flux $\varphi/\pi = 0.32..0.35$.

At a finite doping, we establish equivalence of our wave function to $d_{x^2-y^2}$ wave function of Yokoyama and Ogata [7] and of Gros [6]. Working in the pairing gauge (2.7), the minima of the bosonic bands are $B_1^\dagger = \sum_i b_1^\dagger$ and $B_2^\dagger = \sum_i (-1)^i b_2^\dagger$. Now we use a freedom to choose the coefficients c_m in (2.14) as long as the result of the projection is non-zero. In particular, we may choose $c_{N_h} = 1$, all the other c_m to be zero. In that case only B_1 bosons are allowed, and the projection becomes the conventional Gutzwiller projection.

We must also remark that the $SU(2)$ wave function does not exist at finite doping and zero flux: the doped spinon-holon wave function projects to zero by the $SU(2)$ projection (2.12). To prove this, observe that at zero flux, U_{ij} are scalars, and therefore the fermionic Green's function Ξ is invariant with respect to global $SU(2)$ rotations. Therefore, to get a non-zero projection wee need to form a singlet bosonic combination $\sum c_m (B_1^\dagger)^m (B_2^\dagger)^{N_h - m}$. But no such singlet exist at $N_h > 0$. This proves the non-existence of doped zero-flux $SU(2)$ wave function. An alternative diagrammatic proof is presented in the "loop-soup" section. A possible remedy for a zero-flux wave function is the non-zero "chemical potential" μ which we shall briefly discuss in section 2.2.5.

2.2.2 Variational wave function in the staggered-flux gauge.

In this section we derive an explicit form for the components of the projected wave function starting from the sF description. As a result, the wave function is expressed

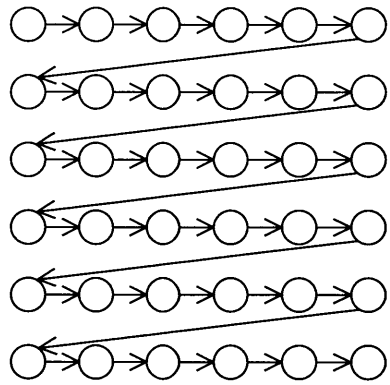

Figure 2-1: Ordering convention for the wave function.

as a sum of $C_{N_h}^{N_h/2}$ determinants of matrices of fermionic Green's functions in the sF mean-field phase. That expression will be used further for the "loop-soup" description of the wave function.

We perform our construction on a finite $N \times N$ lattice. Assume that the lattice size N is even (to avoid spin frustrations). It is convenient to choose the boundary conditions in a way to avoid the nodal points $(\pm\pi/2, \pm\pi/2)$ in the momentum lattice (e.g. periodic boundary conditions with N not divisible by four, or mixed periodic-antiperiodic boundary conditions). The number of holes N_h is also taken to be even, since in a half-filled system, the numbers of empty sites ($b_1^\dagger$-sites) and of doubly-occupied sites ($b_2^\dagger$-sites) must be equal.

Now the GP wave function may be written as

$$\Psi = \sum \Psi(j_1^\uparrow, \ldots, j^\uparrow_{\frac{N^2-N_h}{2}}; j_1^\downarrow, \ldots, j^\downarrow_{\frac{N^2-N_h}{2}}; j_1^\star, \ldots, j_{N_h}^\star) c^\dagger_{1;\sigma(1)}, \ldots, c^\dagger_{N^2;\sigma(N^2)}|0\rangle. \quad (2.15)$$

Here the sum is performed over all possible partitions of the lattice sites $1, \ldots, N^2$ into "spin-up" sites $j_1^\uparrow, \ldots, j^\uparrow_{\frac{N^2-N_h}{2}}$, "spin-down" sites $j_1^\downarrow, \ldots, j^\downarrow_{\frac{N^2-N_h}{2}}$, and holes $j_1^\star, \ldots, j_{N_h}^\star$. In the product of the electron creation operators $c^\dagger_{j,\sigma(j)}$, the operators are ordered along the contour shown in Fig. 2-1. $\sigma(j)$ denotes the spin located at the site j. For the sites with holes, the electron operators are skipped in the product. We adopt the notational convention that within each list of arguments $j^\uparrow$, $j^\downarrow$, and $j^\star$, the sites are also ordered as shown in Fig. 2-1. We introduce the special notation $[\uparrow]$,$[\downarrow]$, and $[\star]$ for these ordered sequences, respectively. Below we write the explicit formulas for the wave-function components $\Psi([\uparrow], [\downarrow], [\star])$.

We use the form of the Hamiltonian (2.1) with the sF hopping amplitudes given by (2.6). It will be convenient to get rid of the imaginary prefactor in the expression of U_{ij} by an additional gauge transformation. The resulting Hamiltonian is:

$$H = J \sum_{ij,\sigma} (f_{i\sigma}^\dagger e^{ia_{ij}} f_{j\sigma}) + \text{h.c.} + t \sum_{ij} (b_{i1}^\dagger e^{ia_{ij}} b_{j1} - b_{i2}^\dagger e^{-ia_{ij}} b_{j2}) + \text{h.c.} \quad (2.16)$$

One possible choice of gauge fields a_{ij} is shown in Fig. 2-2. The unit cell consists of

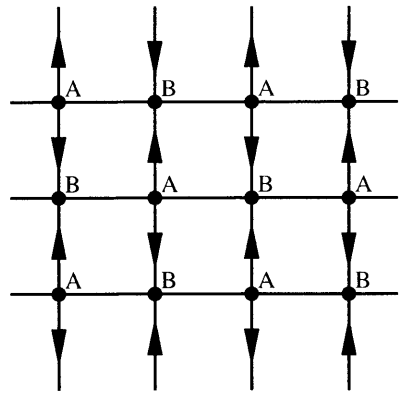

Figure 2-2: A possible realization of the staggered-flux phase in the abelian gauge. Links with arrows correspond to $a_{ij} = \varphi/2$ in the direction of the arrow. Links without arrows have $a_{ij} = 0$. The two sublattices A and B are labeled.

two sites, and there is a natural partition of the lattice into two sublattices (labeled A and B in the figure). The spectrum of the fermions in this parametrization is

$$E(k) = \pm\sqrt{(\cos k_x)^2 + (\cos k_y)^2 + 2\cos\frac{\varphi}{2}\cos k_x \cos k_y} \tag{2.17}$$

and it has four nodal points at $k = (\pm\pi/2, \pm\pi/2)$. Denote the states with positive energies Ψ_k^+, and the states with negative energies Ψ_k^-. Since the fermionic and the bosonic Hamiltonians are proportional to each other, the bosons $b_1^\dagger$ condense into the state Ψ_0^-, the bosons $b_2^\dagger$ — into the state $(\Psi_0^+)^*$.

To conveniently handle the sign of fermionic expressions, we introduce the sign function $P(j_1, \ldots, j_n)$ which is equal to the sign of the permutation of $j_1, \ldots, j_n$ required to bring them into the order of Fig. 2-1. For example, $P([\uparrow]) = P([\downarrow]) = P([\star]) = 1$, because these sets are already ordered. The explicit expression for the wave function (2.15) may be written as

$$\begin{aligned}\Psi([\uparrow],[\downarrow],[\star]) = \sum_{\times\cup\uparrow\downarrow=\star} &\mathrm{Slater}_-([\uparrow],[\uparrow\downarrow])\mathrm{Slater}_-([\downarrow],[\uparrow\downarrow]) \times \\ &\times \prod_{j\in\times}\Psi_0^-(j)\prod_{j'\in\uparrow\downarrow}(\Psi_0^+(j'))^* P([\uparrow],[\downarrow]).\end{aligned} \tag{2.18}$$

Here the sum is taken over all partitions of the set of holes $\star$ into the two sets $\times$ and $\uparrow\downarrow$ containing $N_h/2$ elements each and corresponding to $b_1^\dagger$ and $b_2^\dagger$ sites respectively. As mentioned above, $[A]$ denotes the set A ordered according to Fig. 2-1. $\mathrm{Slater}_-(A)$ (for any set A consisting of $N^2/2$ elements) is the Slater determinant

$$\mathrm{Slater}_-(A) = \det_{j\in A}^{k}(\Psi_k^-(j)). \tag{2.19}$$

The ordering of the quantum numbers k is of no importance — it can only change the overall sign of the wave function. Similarly, we define $\mathrm{Slater}_+(A)$ as the Slater

determinant of positive-energy states.

Further we derive a more symmetric expression for the wave function (2.31) using the identities similar to those used by Laughlin and Zou [11].

The first identity is

$$\text{Slater}_-([A]) = e^{i\alpha} P([A],[\bar{A}])(\text{Slater}_+([\bar{A}]))^*, \tag{2.20}$$

where α is an unimportant phase depending on gauge, but not on the choice of the set A. The above identity holds for any set A of $N^2/2$ lattice sites. $\bar{A}$ denotes the set complementary to A.

The proof is straightforward:

$$\begin{aligned} \text{Slater}_-([A]) &= \langle 0|c_{j_1}\dots c_{j_{N^2/2}}(\Psi^-_{k_1})^\dagger\dots(\Psi^-_{k_{N^2/2}})^\dagger|0\rangle, \\ (\text{Slater}_+([\bar{A}]))^* &= \langle *|c^\dagger_{j'_1}\dots c^\dagger_{j'_{N^2/2}}\Psi^+_{k_1}\dots\Psi^+_{k_{N^2/2}}|*\rangle, \end{aligned} \tag{2.21}$$

where j_k and j'_k are the elements of $[A]$ and $[\bar{A}]$ respectively, $|*\rangle$ is the fully filled state.

$$|*\rangle = (\Psi^+_{k_{N^2/2}})^\dagger\dots(\Psi^+_{k_1})^\dagger(\Psi^-_{k_1})^\dagger\dots(\Psi^-_{k_{N^2/2}})^\dagger|0\rangle = e^{i\alpha}c^\dagger_1\dots c^\dagger_{N^2}|0\rangle \tag{2.22}$$

for some phase α. Substituting these expressions into (2.21) immediately proves (2.20).

In the model (2.16) on a bipartite lattice, any negative-energy state Ψ^-_k may be converted into a positive-energy state Ψ^+_k by simply changing the sign of its wave function on one of the two sublattices. Therefore, up to an irrelevant sign,

$$\text{Slater}_+(A) = T(A)\text{Slater}_-(A) \tag{2.23}$$

where $T(A)$ denotes the function taking values ± 1 depending on the parity of the number of the elements of the set A on one (fixed) of the sublattices.

We may use the above identities to rewrite the expression (2.18) for the GP wave function as

$$\begin{aligned} \Psi([\uparrow],[\downarrow],[\star]) = \sum_{\uparrow\downarrow\cup\times=\star} &\text{Slater}_-([\uparrow],[\uparrow\downarrow])(\text{Slater}_-([\uparrow],[\times]))^* \prod_\times \Psi^-_0(\times)\prod_{\uparrow\downarrow}(\Psi^-_0(\uparrow\downarrow))^*\times \\ &\times P([\uparrow],[\downarrow])P([\downarrow],[\uparrow\downarrow])P([\uparrow],[\times])P([\downarrow\cup\uparrow\downarrow],[\uparrow\cup\times])T(\uparrow\cup\times)T(\uparrow\downarrow), \end{aligned} \tag{2.24}$$

(again, we omit an unimportant overall phase). The two extra P-functions arise from reordering the arguments inside Slater determinants, and the extra factor $T(\uparrow\downarrow)$ — from converting Ψ^+_0 into Ψ^-_0. The product of the sign factors in the above expression may be conveniently converted into

$$T(\uparrow)P([\uparrow\cup\downarrow],[\star])T(\star)P([\uparrow\downarrow],[\times]). \tag{2.25}$$

The first three factors in this product do not depend on the partition of $\star$ into $\times$

and $\uparrow\downarrow$, but only on the positions of holes. Next, if we had chosen the ordering scheme which alternates the two sublattices, the second and the third factors would have canceled each other. The ordering scheme shown in Fig. 2-1 does not obey this property: there is no change of sublattice every time we pass to the next row (for even N). In this case instead of cancellation we get the parity of the number of holes in even (or, equivalently, odd) rows:

$$R(\star) \equiv (-1)^{\#\{(x,y)\in\star | x\equiv 0 \bmod 2\}}. \tag{2.26}$$

Note that for the half-filled case all hole-dependent factors drop out, and the wave function becomes

$$\Psi([\uparrow],[\downarrow]) = |\text{Slater}_-(\uparrow)|^2 T(\uparrow). \tag{2.27}$$

In agreement with Marshall's sign rule [12], it changes sign when nearest-neighbor spins of opposite directions are transposed.

We further transform the expression for the GP wave function by replacing the product of the Slater determinants in (2.24) by the determinant of the product. Define

$$G(j_1, j_2) = \sum_k \Psi_k^-(j_1)(\Psi_k^-(j_2))^* = \langle c(j_1)c^\dagger(j_2)\rangle_0 \tag{2.28}$$

— the Green's function of the half-filled fermionic system or, equivalently, the projector onto the negative-energy states. For any ordered sets A and B of size $N^2/2$ define

$$DG(A|B) = \det_{j_1\in A}^{j_2\in B}(G(j_1, j_2)). \tag{2.29}$$

Then the expression for the wave function becomes

$$\Psi([\uparrow],[\downarrow],[\star]) = T(\uparrow)R(\star) \sum_{\uparrow\downarrow\cup\times=\star} P([\uparrow\downarrow],[\times]) DG([\uparrow],[\uparrow\downarrow]|[\uparrow],[\times]) \times$$

$$\times \prod_\times \Psi_0^-(\times) \prod_{\uparrow\downarrow} (\Psi_0^-(\uparrow\downarrow))^*, \tag{2.30}$$

or, incorporating the bosonic factors in the determinant,

$$\Psi([\uparrow],[\downarrow],[\star]) = T(\uparrow)R(\star) \sum_{\uparrow\downarrow\cup\times=\star} P([\uparrow\downarrow],[\times]) DG^\#([\uparrow],[\uparrow\downarrow]|[\uparrow],[\times]), \tag{2.31}$$

where

$$DG^\#(A|B) = \det_{j_1\in A}^{j_2\in B}(G^\#(j_1, j_2)), \tag{2.32}$$

$$G^\#(j_1, j_2) = (\Psi_0^-(j_1))^* G(j_1, j_2) \Psi_0^-(j_2). \tag{2.33}$$

($G^\#(j_1, j_2)$ is a $U(1)$ gauge invariant quantity, i.e. it does not depend on the particular choice of a_{ij}, but only on fluxes through plaquets).

2.2.3 Variational wave function in the pairing gauge.

In this section, we review the explicit expression for the wave function in the pairing gauge derived by Gros [6]:

$$\Psi([\uparrow],[\downarrow],[\star]) = \det_{i\in\uparrow}^{j\in\downarrow}(a(r_{ij}))\, P([\uparrow],[\downarrow]), \tag{2.34}$$

where $a(r_{ij})$ is the Fourier transform of v_k/u_k [13]:

$$a(r) = \sum_k a_k \cos(kr), \tag{2.35}$$

$$a_k \equiv \frac{v_k}{u_k} = \frac{\Delta(k)}{\xi_k + \sqrt{\xi_k^2 + \Delta(k)^2}}, \tag{2.36}$$

$$\xi_k = -2(\cos(k_x) + \cos(k_y)), \tag{2.37}$$

$$\Delta(k) = \tilde{\Delta}(\cos(k_x) - \cos(k_y)), \tag{2.38}$$

the rest of notation is defined in the previous section, and $\tilde{\Delta}$ is related to the flux φ by (2.8). The above expression for the components of the wave function follows directly from its BCS form (2.10) by the conventional Gutzwiller projection onto no-doubly-occupied states with a fixed number of particles which has been shown to be equivalent in this case to the $SU(2)$ projection. (We put the chemical potential of the fermions to be zero. Gros [6], as well as Yokoyama and Ogata [7], found that a negative chemical potential close to that of non-interacting fermions further improves the ground-state energy. We shall comment on this in the next section, here we simply remark that zero chemical potential is required for the equality of the sF and pairing wave functions.)

To make the Fourier transform of a_k well-defined, we need to avoid its singular points in the momentum space. It can be most conveniently achieved by imposing antiperiodic boundary conditions in one direction (x) and periodic in the other direction (y) for a square lattice $N \times N$ with arbitrary even N [7]. Most of the numerical results reported in this paper were obtained in this setup.

Remarkably, the equation (2.34) gives the same result as much more complicated expressions derived in the previous section. The pairing gauge appears much more convenient for performing numerical computations. On the other hand, in the sF gauge the wave function is expressed in terms of rapidly decaying free-fermion Green's function $G(r)$ (it decays with distance as r^{-2}), while the "singlet bonds" $a(r)$ in the pairing gauge are long ranged (due to singularities in a_k), and correlations in the projected wave function arise from a strong interference of multiple singlet configurations. Thus, the sF expressions may be more useful for qualitative understanding of the physics of the wave function; we shall use them for the "loop-soup" interpretation in section 2.3.

2.2.4 Symmetry of the wave function.

The following properties of the wave function easily follow from its definition.

1. Time-reversal invariance.

Under time-reversal symmetry, the set of "hopping amplitudes" U_{ij} in (2.1) transforms into its gauge-equivalent. Therefore, from our theorem about $SU(2)$-equivalence, it follows that the projected wave-function remains the same. It can also be seen from explicit expressions: the wave function in (2.34) is explicitly real, the wave function in (2.31) can be shown to be real for even $N_h/2$ and purely imaginary for odd $N_h/2$.

2. Translational and rotational invariance.

Similarly to time-reversal symmetry, it follows directly from the $SU(2)$ invariance. Of course, it is also obvious in the symmetric d-wave gauge.

3. Spin-rotational invariance.

The unprojected wave function is a singlet, and the projection is spin-invariant. Therefore, the projected wave function is also a spin singlet.

2.2.5 Optimizing the wave function and the "chemical potential" μ.

The $SU(2)$ wave function, as constructed in the previous section, should further be optimized by adjusting its only variational parameter φ (or, equivalently, $\tilde{\Delta} = 2\tan(\varphi/4)$). This optimization has been done in the work of Yokoyama and Ogata [7] (they used one more variational parameter μ which we shall discuss later). The optimal flux φ_{opt} is a function of the doping n_h and of the ratio t/J. At zero doping, $\varphi_{opt} \approx 0.32..0.35\pi$ [9, 7], which corresponds to $\tilde{\Delta} \approx 0.51..0.57$ (contrary to the renormalized mean-field result $\varphi_{opt} = \pi$, $\tilde{\Delta} = 2$ of [8]). In the parameter range $J/t < 1$, the optimal value of the flux φ_{opt} decreases with doping (according to Yokoyama and Ogata, φ_{opt} has a slight increase at small doping, which should probably be attributed to the antiferromagnetic instability, see below). The gap closes ($\varphi_{opt} \to 0$) at the doping of about 30..40% for $J/t \approx 0.3$ [7].

Even at the optimal value of the flux, the $SU(2)$ wave function is known to be non-optimal. It can be further improved in one of the two ways: either with a staggered magnetization (at low doping) [14, 15] or with a non-zero chemical potential [6, 7].

The instability towards antiferromagnetic order at low doping smoothly arises from the Neel phase of the spin-1/2 Heisenberg antiferromagnet. The variational energy of the antiferromagnetic wave function turns out to be better than that of the d-wave projected one, independent of the way to impose the long-range order [7, 10, 14, 15, 9]. The critical value of the doping destroying antiferromagnetism is estimated as 5..10% for $J/t = 0.2..0.4$ [14, 15]. A remarkable feature of such wave functions is that they predict the co-existence of the superconductivity and antiferromagnetism. While we cannot a priori rule out the possibility of antiferromagnetic superconductors, it is definitely a point requiring further analysis. In the present paper we restrict our discussion to the paramagnetic state, in the belief that our RVB-type wave function

is adequate outside the region of antiferromagnetic instability.

The "chemical potential" μ has been introduced by Gros and by Yokoyama Ogata [6, 7] as an additional variational parameter in the d-wave formalism, the equation (2.37) being modified as

$$\xi_k = -2(\cos(k_x) + \cos(k_y)) - \mu. \tag{2.39}$$

They found that a non-zero value of μ close to its free-fermion value μ_0 improves the variational energy with respect to $\mu = 0$ by approximately 0.2%.

The zero value of μ is the point of higher $SU(2)$ symmetry than finite μ, in the sense that it is invariant under a larger subgroup of $SU(2)$ rotations. The symmetry at $\mu = 0$ can be reduced by introducing a non-zero value of the "Lagrange multipliers" for the no-double-occupancy constraint a^0_α [1]. These Lagrange multipliers play the role of the temporal components of the gauge field and form an $SU(2)$ triplet. A non-zero value of $\mu \equiv a^0_3$ (in the pairing gauge) does not break the time-reversal or translational symmetry, while nonzero values of a^0_1 or a^0_2 do. In the staggered-flux phase, the μ-term is represented by an on-site pairing

$$\Delta(\theta_i) = \mu e^{i\theta_i} f^\dagger_{i\uparrow} f^\dagger_{i\downarrow} + \mu e^{-i\theta_i} f_{i\downarrow} f_{i\uparrow} \tag{2.40}$$

with a special choice of the phases θ_i consistent with the choice of gauge fields a_{ij}.

As a consequence of the reduction of the symmetry by a nonzero value of μ, the space Ψ_{GP} defined in (2.14) is no longer one-dimensional. In other words, condensation of different mixtures of the two species of bosons leads to different wave functions. The μ-dependence of the variational energy derived by Yokoyama and Ogata [7] allows us to suggest that $\mu < 0$ favors $B^\dagger_1$ bosons in the pairing gauge, i.e. the energy is minimized by taking $c_{N_h} \neq 0$, $c_{m<N_h} = 0$. The same structure of the condensate is derived in the $SU(2)$ mean-field theory [1], but as a consequence of satisfying the constraint.

In the mean-field theory μ plays a more important role than just a variational parameter. It represents the mean-field value of the temporal component of the gauge field a^0_3 or, equivalently, of the Lagrange multiplier enforcing the constraint [1]. In the mean-field theory, the non-zero value of μ leads to a specific mechanism of Bose condensation at finite temperature. Thus, a finite μ may be a signature of superconductivity.

The role of μ appears somewhat less significant in the variational approach. Already at $\mu = 0$ the ground-state wave function exhibits a long-range superconducting order. A non-zero value of μ somewhat suppresses antiferromagnetic spin correlations at large distances. Numerically, the effect of allowing a non-zero μ is found to be small. Therefore, in the present paper we mostly study the wave function at zero μ, and only briefly discuss the possible physical meaning of $\mu \neq 0$.

2.3 Loop-soup interpretation of the wave function.

The BCS expression (2.10) for the wave function admits an RVB-type interpretation with singlet amplitudes $a(r)$ given by (2.35) [13, 6]. In turn, RVB wave functions can be described in terms of "loop-soup" [16, 17]: correlation functions can be computed as statistical averages over all partitions of the lattice into non-intersecting loops, with statistical weights depending on the singlet amplitudes $a(r)$.

However, this description is not physically transparent, because the amplitudes $a(r)$ are long ranged. Instead, we shall build an alternative loop-soup construction starting from the sF wave function (2.31). In the sF gauge, we shall use the R^{-2}-decaying fermionic Green's functions $G^{\#}(i,j)$ instead of $a(r)$, and most of the statistical weight falls on small-size loops. We find this picture suitable for qualitative understanding of the physics behind the projected wave function and make conjectures about the behavior of correlation functions.

Our construction is based on representing the determinant of a matrix as a sum over permutations. In turn, each permutation is a product of non-intersecting cycles. Therefore, for any matrix M (of size $m \times m$), we may write

$$\det M = (-1)^m \sum_{\{C_1,\ldots,C_k\}} (-1)^{\#\{C_i\}} \prod_i (\prod_{C_i} M_{**}), \tag{2.41}$$

where the sum is taken over all partitions of indices $1,\ldots,m$ into non-intersecting cycles $C_1,\ldots,C_k$, $\#\{C_i\}$ denotes the number of cycles (including cycles of length one), and the last product is taken along each of the cycles C_i (i.e. for a cycle $(j_1,\ldots,j_n)$ the product reads $M_{j_1j_2}M_{j_2j_3}\ldots M_{j_nj_1}$). Notice that every cycle produces an additional factor of (-1) (the same as that for fermionic loops in the usual diagrammatic technique).

With the use of (2.41) we shall rewrite the GP wave function as a sum over partitions of the lattice into non-intersecting cycles. We first consider the undoped case (the Heisenberg antiferromagnet), and then expand the rules to include holes.

We start from computing the normalization of the wave function $\langle\Psi|\Psi\rangle$ as defined in the previous section. The following diagrammatic rules may be derived for computing $\langle\Psi|\Psi\rangle$:

1. Consider all partitions of the lattice into non-intersecting cycles. Every site must belong to exactly one cycle. The cycles are directed, i.e. (123) and (321) count as different cycles. An example of such a partition is shown in fig. 2-3. (Note that $G^{\#}(j_1,j_2)=0$ when connecting two different sites at the same sublattice. Therefore, all cycles of length greater than one have even number of links.)

2. Label each cycle by a spin index ($\uparrow$ or $\downarrow$).

3. Add a factor of (-1) per cycle. (This fermionic minus sign cannot be represented as a product over link amplitudes. This distinguishes loop-soup rules for Gutzwiller-projected-type wave functions from those for spin-basis RVB wave functions considered by Liang et al [16].

4. Multiply $G^{\#}(j_1,j_2)$ (defined in eq.(2.33)) along cycles and sum over all parti-

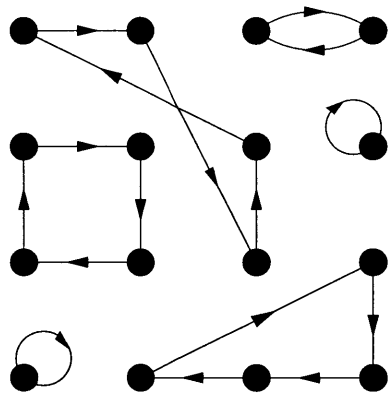

Figure 2-3: An example of partitioning the lattice into non-intersecting cycles. All cycles have either length one or even length.

tions. (For the undoped system we may multiply the bare Green's functions $G(j_1, j_2)$, with the same result. With holes, it will be more convenient to work with $G^{\#}(j_1, j_2)$ instead.)

Symbolically, the recipe may be written as

$$\langle\Psi|\Psi\rangle = \sum_{\{C_i\}} (-2)^{\#\{C_i\}} \prod_i (\prod_{C_i} G^{\#}(*,*)) \tag{2.42}$$

The derivation of the above rules proceeds in the following way: we use the expression (2.31) for the ket-vector $|\Psi\rangle$ and its spin-symmetric version for $\langle\Psi|$ (with the determinants on the spin-down sites). Then $\langle\Psi|\Psi\rangle$ is a quadratic expression in determinants whose size is half the number of lattice sites. Writing each of the determinants as a loop sum (2.41), we arrive to the loop-soup (2.42). The (-2) factor for each loop comes from (-1) fermionic sign and 2 for two possible spin orientations.

If $G^{\#}(j_1, j_2)$ were local (exponentially decaying at large distances), $\langle\Psi|\Psi\rangle$ might be considered as a partition function of a classical model (with non-positive statistical weights). In that case, $\langle\Psi|\Psi\rangle \propto e^{-FV}$ for lattices with large number of sites V, F is the "free energy" per unit cell [17].

In the staggered-flux phase, $G^{\#}(j_1, j_2)$ is not local, but decays as R^{-2} at large distances. However, we believe that our analogy with statistical mechanics is still valid. The "long-range interaction" will result in power-law correlation functions for some observables.

Consider now the spin-spin correlation function, $\langle\sigma_z(i)\sigma_z(j)\rangle$. To compute $\langle\Psi|\sigma_z(i)\sigma_z(j)|\Psi\rangle$ we simply multiply the corresponding diagrams by the product of the spin indices at the two points i and j. Obviously, only the partitions with i and j in the same cycle will contribute. This implies that the spin correlations decay as probability to find large cycles. Again, if we had a gap without nodes, i.e. if $G^{\#}(j_1, j_2)$ were local, the spin correlations would decay exponentially. In the sF phase, $G^{\#}(j_1, j_2)$ decays as power law, and we expect the spin correlations to decay as power law, although we are unable to predict the exact exponent. In the next

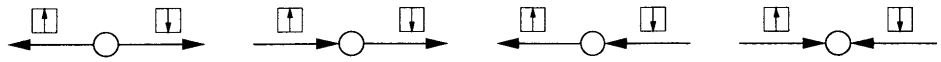

Figure 2-4: The four possible configurations of a hole in the "loop-soup".

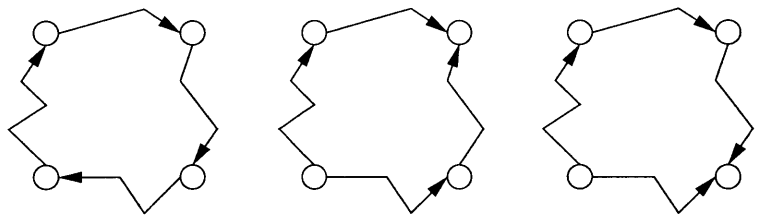

Figure 2-5: An illustration of the "alignment" sign rule. The loop (A) is aligned ("alignment" sign +1). The loop (B) requires the direction of two segments to be reversed for alignment (sign +1). The loop (C) requires the direction of one or three segments reversed (sign -1).

section we shall verify this prediction with VMC results.

Now turn to the case of a finite doping. From the expression (2.31) for the wave function, the diagrammatic rules for holes are as follows:

5. Every hole has two lines attached: one with a spin-up label, and one with a spin-down label. Each line may be either in-going or out-going, so that the total number of possible configurations is four (Fig. 2-4).

6. Any connected loop with holes counts as one cycle. The statistical weight for such a loop is calculated in the same way as for cycles without holes (product of $G^{\#}(j_1, j_2)$ times the fermionic (-1)) multiplied by an additional sign factor due to holes.

7. The sign factor due to holes is calculated as follows. First, each hole on the A-sublattice gives an additional factor of (-1). (We could take B-sublattice instead, it is of no importance as soon as the number of holes is fixed). And second, an additional factor of (-1) comes from each part of the loop between two adjacent holes whose direction need to be reversed to make all such segments aligned (the direction of the alignment is unimportant, because the total number of the segments is even) — see Fig. 2-5.

Using the "alignment" sign rule we may present a "diagrammatic" proof that a doped wave function vanishes as the flux φ goes to zero. Indeed, at $\varphi = 0$, the Green's function $G^{\#}(j_1, j_2)$ is real, and reversing any single segment of a hole-containing loop produces an exactly opposite contribution to $\langle\Psi|\Psi\rangle$, so that the total sum is zero.

Equal-time correlation functions can be represented as sums over loop configurations. Spin and hole-density correlation functions are shown pictorially in Fig. 2-6. The shaded box in the figure denotes the sum over loop coverings, lines without arrows assume summation over allowed directions.

Remarkably, the loop-soup description explains attraction between holes discovered numerically by Gros [6]. Consider two holes in a $N \times N$ lattice. Then the

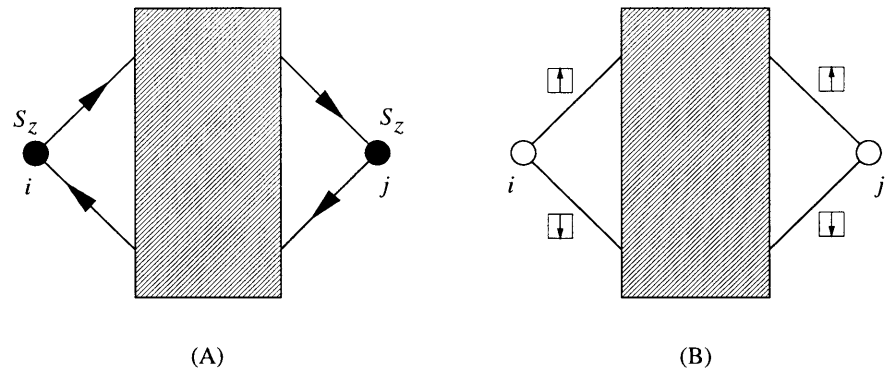

Figure 2-6: Diagrams for spin-spin (A) and hole-density (B) correlation functions. The shaded box denotes the summation over loop coverings; lines without arrows assume summation over directions.

diagram in Fig. 2-6B requires that these two holes belong to the same loop. On general grounds, we argue that the hole-density correlation must decay with distance as power law: $\langle n_h(0)n_h(R)\rangle \propto R^{-\alpha}$. If $\alpha > 2$, this correlation function is normalizable in the limit $N \to \infty$, and the holes are truly confined. If $\alpha \leq 2$, the holes become deconfined in the thermodynamic limit. The mean-field value of α is four, but it is strongly renormalized by the no-double-occupancy constraint. We expect that α is non-universal and continuously depends on the gap $\tilde{\Delta}$. The diagrammatic rules suggest that α may be equal to the spin exponent. We do not have a rigorous proof of this fact. Our numerical results appear to agree with this conjecture, except for the small gap $\tilde{\Delta} = 0.1$, where finite-size effects are strong, and our numerical data are inconclusive. For all values of the gap, in the system with two holes, our numerical simulations indicate that $\alpha < 2$, which means that two holes are always deconfined. However, as we shall see later, this does not rule out superconductivity at finite doping.

In Figs. 2-7,2-8 we present diagrams for the single-particle Green's function and for pairing correlations. [The dashed lines in the figures denote the way to visualize the loops (a line entering the site j is thought to be exiting the site i) for the purpose of counting the sign of the diagram for each loop configuration.] At large distances, the pairing correlations factorize $\langle\Delta^\dagger\Delta\rangle_{L\to\infty} = \langle\Delta^\dagger\rangle\langle\Delta\rangle$ (Fig. 2-8), which might serve as a proof of superconductivity. The long-range superconducting order in this wave function has been indeed found numerically by Gros and by other authors [6, 18]. However, our diagrammatic "proof" is deceptive: it relies only on the phase coherence of condensed bosons. In fact, it may turn out that $\langle\Delta\rangle$ would vanish as the size of the system goes to infinity, i.e. electron pairs become unbound. Numerically, we have found that this is not the case at doping as small as 5% and at intermediate values of the gap $\tilde{\Delta}$. The unbound state of two holes, however indicates that the superconductivity may disappear at very low doping or at a very small gap (which occurs at high doping).

Finally, we want to speculate on the possible effect of the "chemical potential" μ. In the sF gauge, $\mu \neq 0$ corresponds to the on-site pairing (2.40). Accordingly,

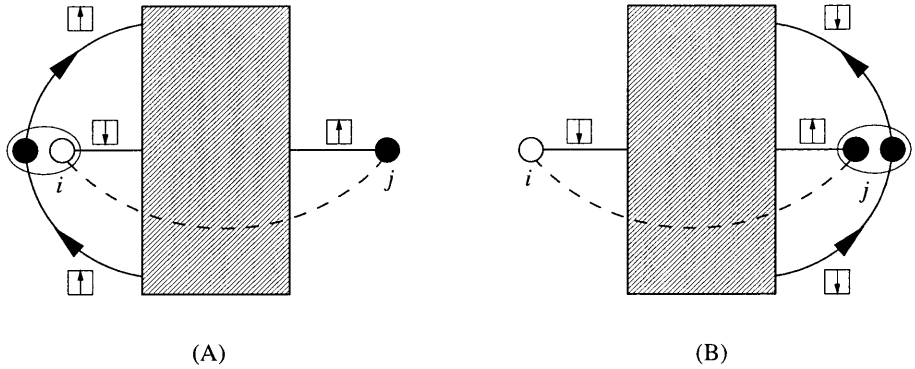

Figure 2-7: Diagrams for the Green's functions $\langle c_\uparrow(i)c_\uparrow^\dagger(j)\rangle$ (A) and $\langle c_\downarrow(i)c_\downarrow^\dagger(j)\rangle$ (B).

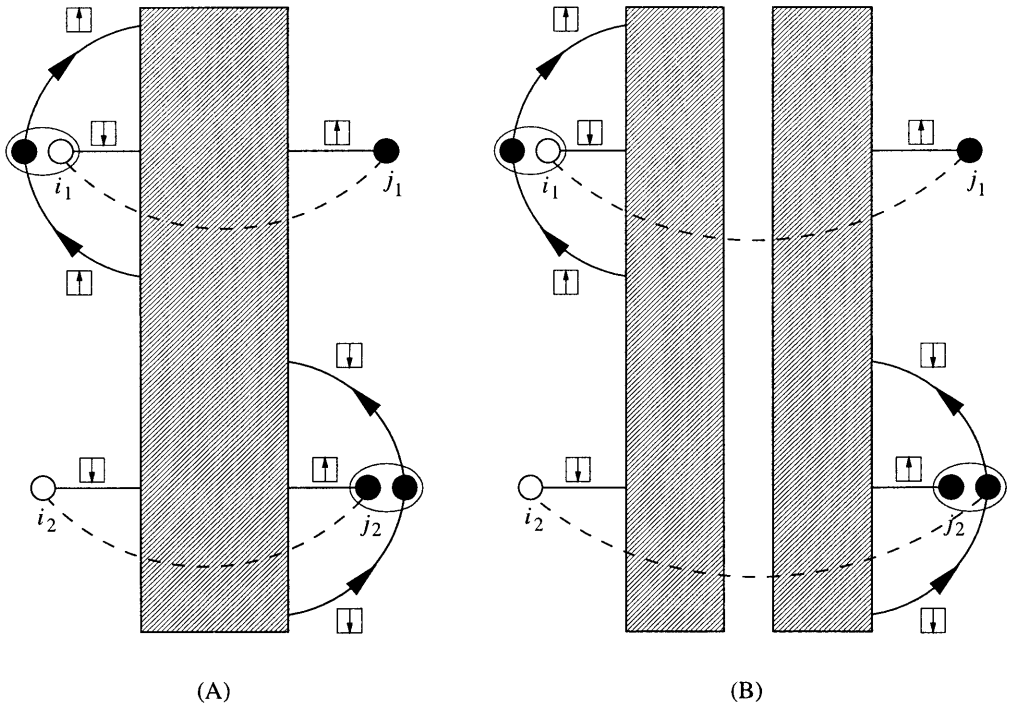

Figure 2-8: Diagram for the pairing correlation $\langle c_\uparrow(i_1)c_\downarrow(i_2)c_\downarrow^\dagger(j_1)c_\uparrow^\dagger(j_2)\rangle$ (A). As the distance between the pairs of sites (i_1, i_2) and (j_1, j_2) goes to infinity, the correlation function factorizes (B).

the Green's function $G^{\#}(i,j)$ acquires an anomalous part (which, in the diagrammatic representation, reverses the direction of the loop and flips the spin index). As a consequence, for large loops, a finite correlation length may appear, beyond which the correlations decay much faster than the short-length-scale power law (at large distances, we expect R^{-4} decay of spin and charge correlations, the same as in the mean-field theory). For doping of order 10% and for realistic values of μ, this correlation length is of the order of the size of our systems, which makes it difficult for numerical studies.

2.4 Correlation functions computed by the VMC method.

In this section we report the results of variational Monte Carlo (VMC) computations to test our conjectures and to illustrate our discussion of the properties of the projected wave function. We compute spin, density, single-particle and superconducting correlation functions some of which have previously been studied by other authors [6, 7].

The last part of the section is devoted to current-current correlations. We discover a novel type of correlations which we call "staggered vorticity". We explain these correlations from the staggered-flux picture, which suggests that pairs are formed of holes of opposite staggered vorticity.

In our VMC computations we use the scheme employed by Yokoyama and Ogata [7]. Metropolis trials [19] are performed for exchanging states at nearest-neighbor sites; the updating of determinants is optimized to $O(n^2)$ operations by method of Ceperley et al [20]. We use the square lattice $N \times N$ with maximum size 20×20 sites. The boundary conditions are mixed periodic-antiperiodic to satisfy the closed-shell condition. The sampling is performed every N^2 Monte Carlo steps. The first $20 \cdot N^2$ steps are used to thermalize the system. The error bars represent mean-square deviation and are deduced from 10 independent VMC runs. A typical number of samples in a run for 20×20 system is 10^3 (which amounts to $4 \cdot 10^6$ VMC steps in 10 runs).

2.4.1 Spin correlations.

It has been known that our variational wave function does not have a long-range spin order, even in the undoped case [9, 7]. We find, more precisely, that the spin-spin correlations decay with distance as power law, in agreement with our loop-soup picture:

$$\langle \sigma_z(0)\sigma_z(R)\rangle \propto R^{-\alpha}. \tag{2.43}$$

The exponent α non-universally depends on the gap $\tilde{\Delta}$ and on the doping $n_h = 1-n$. In Fig. 2-9 we plot the staggered spin correlations $(-1)^{R_x+R_y}\langle \sigma_z(0)\sigma_z(R)\rangle$ as a function of R^2 for the undoped system at various values of $\tilde{\Delta}$. The exponent is maximal at $\tilde{\Delta} = 2$ (π-flux phase): $\alpha \approx 1.6$. At the "optimal flux" $\tilde{\Delta} = 0.55$, $\alpha \approx 1.2$,

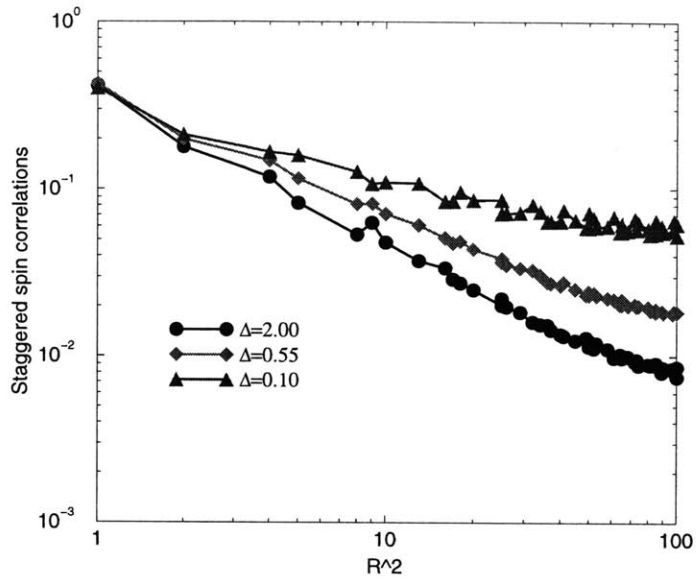

Figure 2-9: Staggered spin correlation $(-1)^{R_x+R_y}\langle\sigma_z(0)\sigma_z(R)\rangle$ as a function of R^2 for the undoped system. Lattice size 20×20, number of samples 10^4.

and at $\tilde{\Delta} = 0.1$ $\alpha \approx 0.6$. These results confirm our expectation that the correlations decay faster at larger gaps. The data at smaller gaps reveal some anisotropy of the prefactor in the power law (2.43).

Further, in Fig. 2-10 we plot the spin correlations at constant $\tilde{\Delta} = 0.55$ at various values of hole doping. Naturally, doping with holes leads to a more rapid decay of spin correlations. Still, it apparently remains power law: we find $\alpha \approx 2.4$ at $n_h = 5\%$, $\alpha \approx 3.4$ at $n_h = 10\%$.

2.4.2 Density correlations.

We start our numerical study of density correlations with the ground state of two holes. Based on the loop-soup interpretation of the wave function, we claim that within our variational ansatz, the density-density correlations of two holes exhibit a power-law behavior. The existence of a bound state then depends on whether the exponent is greater or less than two, as the correlation function must satisfy the sum rule: $\int d^2R\,\langle n_h(0)n_h(R)\rangle = n_h$. Figs. 2-11-2-13 show the correlation function for two holes in 14×14 lattice at various values of the gap $\tilde{\Delta}$. Similarly to the spin correlations, a larger gap results in faster decay. Fitting the data with the power law

$$\langle n_h(0)n_h(R)\rangle \sim CR^{-\alpha} \tag{2.44}$$

we find $\alpha \approx 1.6$ at $\tilde{\Delta} = 2$, and $\alpha \approx 1.2$ at $\tilde{\Delta} = 0.55$, which coincides with the exponents for the spin correlations in the undoped systems. At $\tilde{\Delta} = 0.1$ we observe

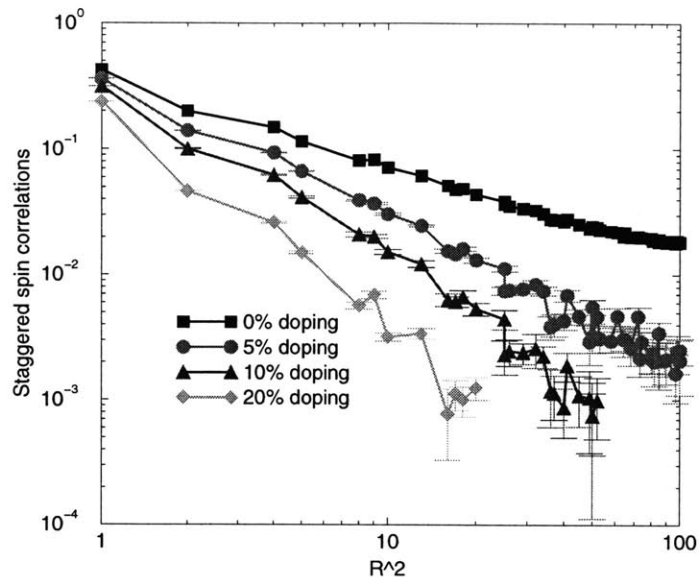

Figure 2-10: Staggered spin correlation $(-1)^{R_x+R_y}\langle\sigma_z(0)\sigma_z(R)\rangle$ as a function of R^2 at various values of doping x. The gap value is $\tilde{\Delta} = 0.55$ (optimal gap at zero doping). Lattice size 20×20, number of samples 10^4.

strong finite size effects, and our estimate $\alpha \approx 0.3$ differs from the spin exponent. Since at any gap the charge exponent is less than two, we conclude that within our variational ansatz the two holes are always unbound.

To confirm this conclusion, we compute the nearest-neighbor and $(1,1)$ next-nearest-neighbor (at the distance of $\sqrt{2}$) density correlations for two holes doped in the systems of different size, at a fixed value of the gap $\tilde{\Delta} = 0.55$. The results are plotted in Fig. 2-12. For the power law (2.44), the normalization C must scale as

$$C \propto N^{-\gamma}, \qquad \gamma = 2 - \alpha, \tag{2.45}$$

with the linear size of the lattice N. From the data in Fig. 2-14 we find $\gamma \approx 0.6$. This slightly disagrees with $\alpha \approx 1.6$ found from both the density correlations. The disagreement is probably due to the fact that the nearest-neighbor and next-nearest-neighbor correlations do not represent accurately the normalization constant C. In any case, the data clearly indicate that these correlations decay with the size of the system, contrary to the conclusion of Gros [6] about the saturation of such correlations.

An interesting feature of the density correlations is that they may additionally depend on whether the two points belong to the same or to different sublattices, and further in the case of the same sublattice, on whether the distance has odd or even R_x or R_y. As a general rule, we find that the correlations are enhanced for odd sites on the same sublattice and suppressed for even sites on the same sublattice, see

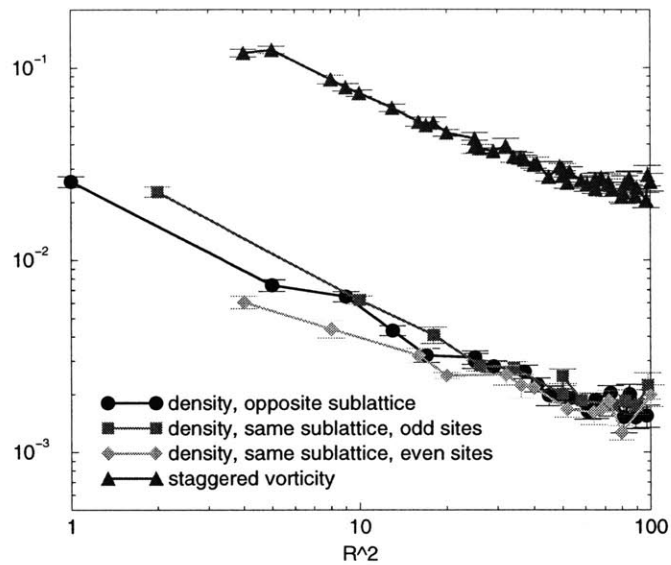

Figure 2-11: Hole density and staggered vorticity correlations for two holes in the 18×18 lattice at $\tilde{\Delta} = 0.55$ as a function of R^2. Number of samples: $2 \cdot 10^4$. Both correlation functions are normalized to the density of holes n_h.

Figs. 2-11-2-13. For the special value of $\tilde{\Delta} = 2.0$, the correlations at even sites on the same sublattice (with both R_x and R_y even) identically vanish, as a signature of an additional symmetry.

At finite doping, the density correlations exhibit only a short range attraction, screened at the average inter-hole distance. Beyond that distance, the correlation function quickly equilibrates to its value at infinity n_h^2 (Figs. 2-15,2-16).

2.4.3 Single-particle equal-time Green's function.

We performed numerical computation of the single-particle equal-time Green's function $\langle c_\alpha^\dagger(i) c_\alpha(j)\rangle$. Its Fourier transform is the electron density in the momentum space

$$n(k) = \langle c_{\uparrow k}^\dagger c_{\uparrow k}\rangle = \langle c_{\downarrow k}^\dagger c_{\downarrow k}\rangle \tag{2.46}$$

(with the normalization $(1/N^2)\sum_k n(k) = (1 - n_h)/2$). Our results confirm the characteristics of $n(k)$ known from high-temperature series [21] and from quantum Monte Carlo data [22]: a very sharp "Fermi surface" near $(\pi/2, \pi/2)$ smeared out along $(0,0) - (0,\pi) - (\pi,\pi)$. is a consequence of the $d_{x^2-y^2}$ superconducting gap vanishing on the diagonal of the Brillouin zone. We can tune the sharpness of the Fermi surface away from the zone diagonal by varying the gap parameter $\tilde{\Delta}$. The "chemical potential" μ shifts the position of the Fermi surface from $(\pi/2, \pi/2)$ along the diagonal. We also observe that the sharpness of the drop near $(\pi/2, \pi/2)$ decreases

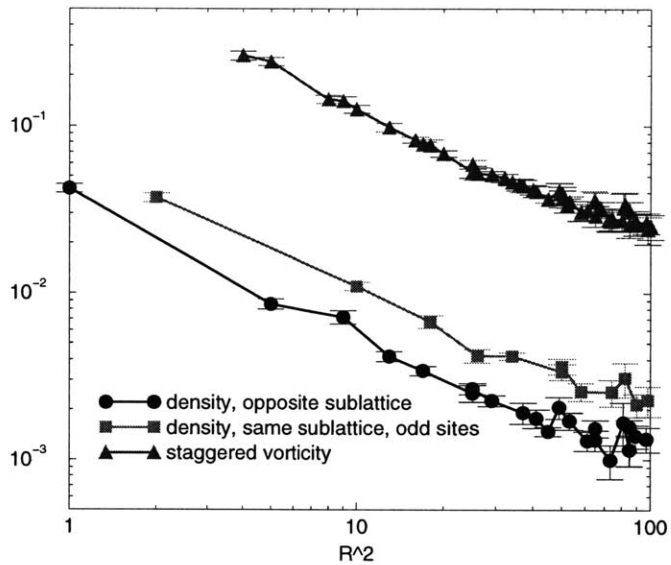

Figure 2-12: The same as previous figure, but at $\tilde{\Delta} = 2.0$. The hole correlations at the even sites of the same sublattice (with even R_x and R_y) identically vanish.

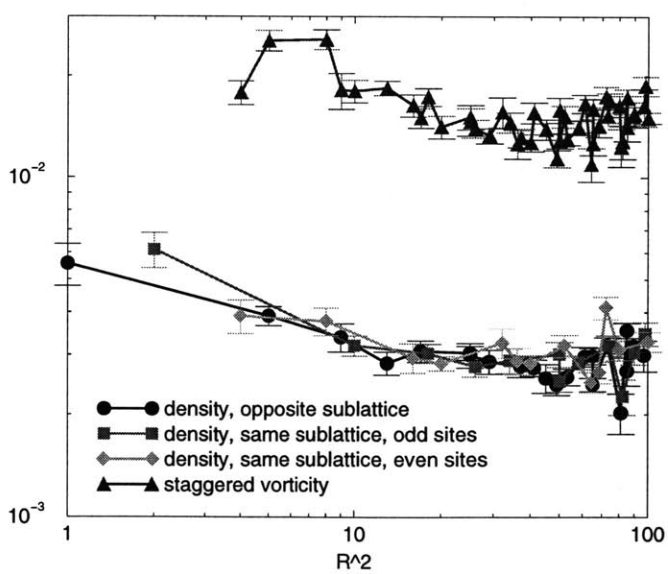

Figure 2-13: The same as previous figure, but at $\tilde{\Delta} = 0.1$.

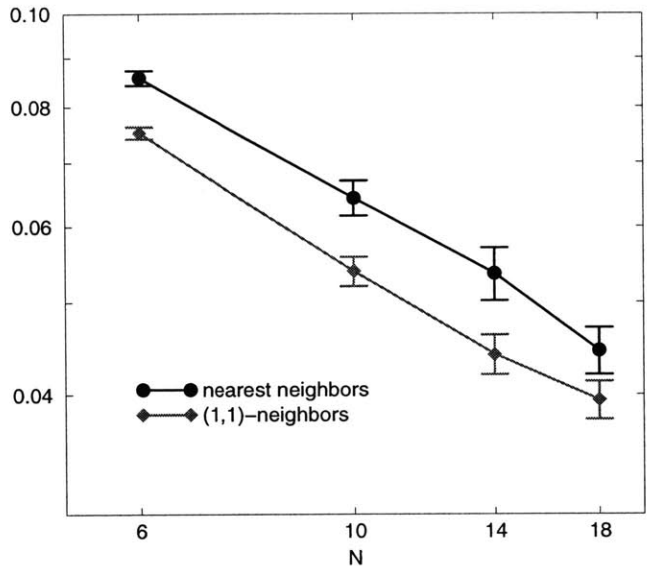

Figure 2-14: Nearest-neighbor and $(1,1)$-neighbor hole correlations for two holes in the $N \times N$ lattice as a function of N (in log-log scale). The gap value is fixed $\tilde{\Delta} = 2.0$. Each point is the result of averaging over $2 \cdot 10^4$ samples.

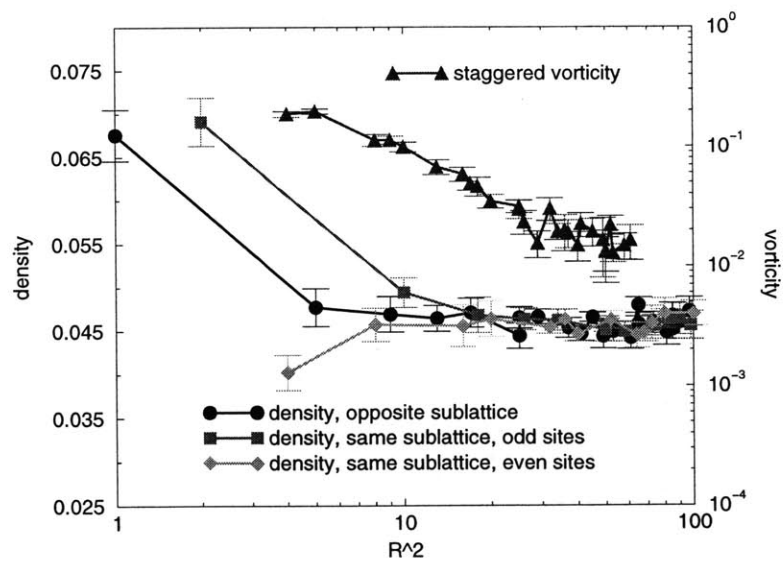

Figure 2-15: The same as fig. 2-11, but for 16 holes in the 18×18 lattice. $\tilde{\Delta} = 0.55$. Log-log scale for vorticity and log-linear scale for density. Number of samples: $2 \cdot 10^3$.

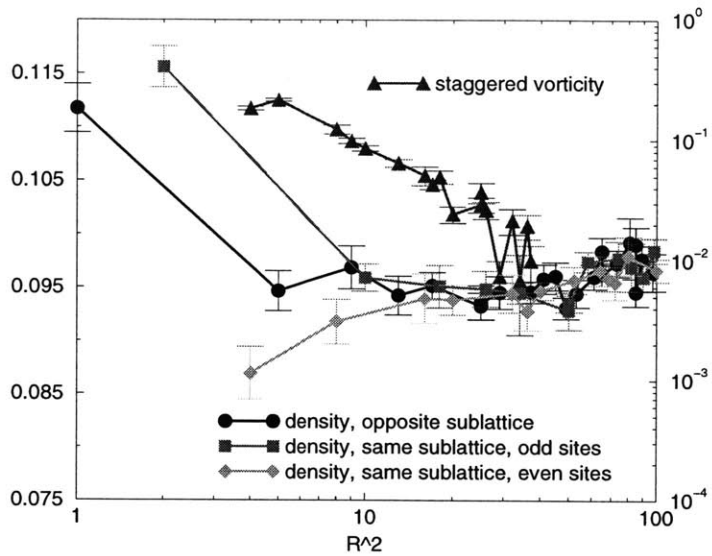

Figure 2-16: The same as the previous figure, but for 32 holes in the 18×18 lattice. $\tilde{\Delta} = 0.55$. Log-log scale for vorticity and log-linear scale for density. Number of samples: $1 \cdot 10^3$.

at large doping (as the electrons gather at the center of the zone).

In Fig. 2-17 we present a typical distribution of the *hole* momentum $n_h(k)$ (the hole momentum distribution is normalized by $(1/N^2)\sum_k n_h(k) = n_h$ and is related to the electron momentum distribution $n(k)$ by $n(k) = (1 + n_h)/2 - n_h(k)$).

2.4.4 Vorticity correlations.

Perhaps, one of the strongest arguments in favor of staggered-flux-type theories is the staggered vorticity correlations which we observe in the $SU(2)$ wave function. We define a vorticity at any plaquet as the sum of currents j_{ij} around the plaquet,

$$V = (j_{12} + j_{23} + j_{34} + j_{41})_\square, \tag{2.47}$$

with current being defined as

$$j_{ij} = i\left(c^\dagger_\sigma(i)c_\sigma(j) - c^\dagger_\sigma(j)c_\sigma(i)\right) \tag{2.48}$$

for nearest-neighbor sites i and j. In Fig. 2-18A we present data for current-current correlations for 10 holes in the 10×10 lattice at $\Delta = 0.55$ and $\mu = -0.16$ (close to the optimal values). Except for the case of two links being the opposite sides of a plaquet, the current correlations obey a staggered-vorticity pattern (we did not compute the current correlations for intersecting links, because of the ambiguity with ordering non-commuting current operators). By a double-summation over sides of plaquets,

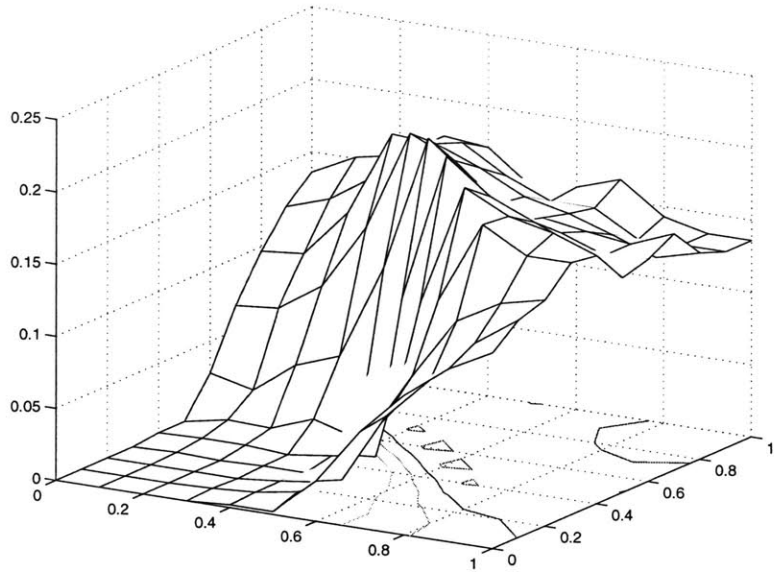

Figure 2-17: Momentum distribution of holes for 10% doping of 10×10 lattice and $\tilde{\Delta} = 0.57$.

the current current correlations may be converted into vorticity correlations (Fig. 2-18B). The correlations of vorticity have alternating sign, with the half-period shift, so that the correlation function at a vector (R_x, R_y) has the sign $(-1)^{R_x+R_y+1}$. The correlations decay with distance, and, similarly to spin and density correlations, the increase of doping or the increase of the gap leads to a faster decay.

Similarly to the case of density correlations, we find it instructive to first study the system with only two holes. Remarkably, we find that the staggered-vorticity correlations decay as power law, with (apparently) the same exponents as density (and, possibly, spin) correlations (see Figs. 2-11-2-13). This, together with the sign of the correlations, suggests that the staggered vorticity of a hole corresponds to its $SU(2)$ index in the staggered-flux description.

In the mean-field sF phase, spinons carry a non-zero staggered vorticity (let us call it type-A vorticity). Then the $B_1^\dagger$ holes represented by zero-spinon sites carry the opposite, type-B, vorticity, while the $B_2^\dagger$ holes have two spinons per site and carry type-A vorticity. Then the staggered vorticity correlations are proportional to the correlations of the $SU(2)$ index of holes. In the case of only two holes in the system, they always carry opposite $SU(2)$ labels, and the staggered-vorticity correlations are proportional to the density correlations. Also, the above picture predicts the correct sign of the correlations. It must be kept in mind though, that, after the projection, the time-reversal symmetry is restored, and the average staggered vorticity of an *individual hole* is zero, but it is the *relative* staggered vorticity of the two holes that produces the correlations.

As we dope the system further, the decay of correlations becomes faster, but still can be best fitted with power-law (Figs. 2-15,2-16), we find (with $\tilde{\Delta} = 0.55$) $\alpha \approx 2.2$ at 5% doping and $\alpha \approx 2.4$ at 10%, the latter being noticeably smaller than the spin

exponent. The staggered vorticity correlations show the increased probability to find a hole of opposite staggered vorticity around a given hole. Thinking of the pairing of holes of opposite staggered vorticity, we interpret the staggered-vorticity correlations as the hole correlations within one pair which may far exceed the average distance between holes. In this "soup" of overlapping pairs, the staggered-vorticity correlations provide a good measure of the size of the hole pair, more meaningful than the density correlations.

2.5 Discussion and conclusion.

To summarize, we present a new interpretation of the physics of the $d_{x^2-y^2}$-pairing variational wave function for the $t-J$ model. This wave function is shown to appear naturally from the $SU(2)$ slave-boson theory in the staggered-flux or d-wave-pairing phase. The staggered-flux origin of the wave function produces the staggered-vorticity pattern in the current correlations. This can be interpreted as pairing of holes of opposite staggered vorticity.

Further, we have studied the properties of the wave function at the zero value of the chemical potential (μ) for spinons. In this case, the only variational parameter of the wave function is the staggered flux which at the same time serves as the mean-field gap for spin excitations. The wave function exhibits power-law decay of spin correlations as well as of vorticity correlations and, in the two-hole system, of hole-hole correlations. Such a critical behavior can be understood from the loop-soup representation of the wave function. Those correlations require that the two points are connected by a continuous loop made out of spinon propagators.

The exponent of the power-law dependence in the correlations of staggered vorticity governs the binding-unbinding transition for the hole pairs. At zero doping, this exponent is less than two, which results in an unbound state of two holes in the thermodynamic limit. This agrees with the numerical studies by Shih et al [23]. As the doping increases, so does the exponent in the staggered-vorticity correlations, which we believe to coincide with the exponent for the hole correlations in a superconducting pair. Numerically, we find this exponent to be only slightly greater than two, which means a very large pair with a diverging average distance between the paired holes. The large size of superconducting pairs may be responsible for some numerical indications of absence of superconductivity at small J/t, when probing only nearest-neighbor pairing Δ_{ij} [23, 24]. For very large hole doping, the gap closes and the system returns back to a non-superconducting state.

In this description of superconducting transition at zero temperature, it is very important to understand the role of the additional variational parameter μ (the chemical potential in the pairing gauge). We conjecture that a finite value of μ moves the wave function away from the "critical point" with an infinite correlation length towards a truly superconducting state characterized by a finite size of superconducting pairs. (In spite of a finite size of superconducting pairs, we expect the vorticity correlations to decay only as R^{-4} at large distances, as a signature of nodes in the d-wave gap).

The $\mu = 0$ $SU(2)$ wave function is a universal starting point for variational de-

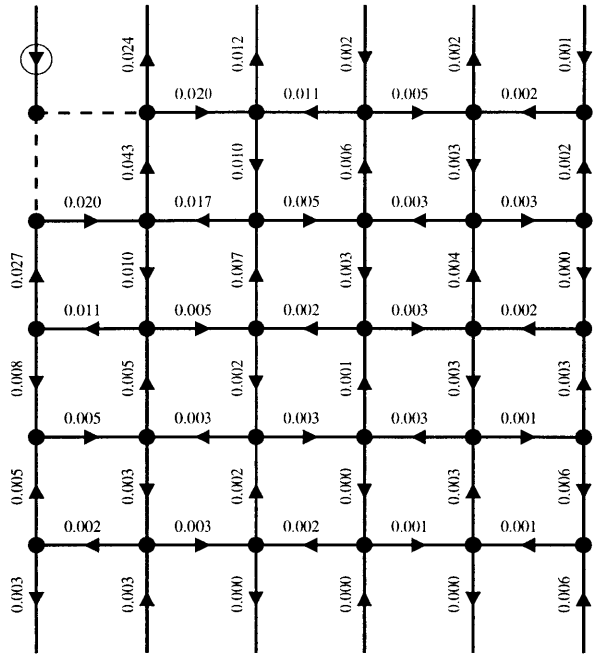

(A)

		-0.20	0.11	-0.05	0.03
		0.22	-0.09	0.05	-0.04
-0.20	0.22	-0.12	0.06	-0.04	0.04
0.11	-0.09	0.06	-0.05	0.04	-0.03
-0.05	0.05	-0.04	0.04	-0.04	0.04
0.03	-0.04	0.04	-0.03	0.04	-0.06

(B)

Figure 2-18: (A) Current-current correlations for 10 holes in the 10×10 lattice at $\tilde{\Delta} = 0.55$ and $\mu = -0.16$ (normalized to hole density). The number on a link is the correlation of the current on this link and of the current on the circled link. The arrows point in the direction of the positive correlations of the current. The error bars are one or two units in the last digit. (B) The same, but in the form of vorticity correlations. The number on a plaquet is the vorticity correlation of this plaquet and the crossed plaquet.

scription of quantum phase transitions. Besides the possibility to continuously tune it into an antiferromagnetically-ordered state, other types of phase transitions are possible via generating non-zero values of the $SU(2)$ counter-parts of μ (corresponding to on-site pairing in the d-wave gauge). Such phases have a broken translational or time-reversal symmetry and, at certain conditions, they may be favored over a superconducting state.

Bibliography

[1] X.-G. Wen and P. A. Lee, Phys. Rev. Lett. 76 (1996), 503.

[2] P. A. Lee, N. Nagaosa, T.-K. Ng, and X.-G. Wen, Phys. Rev. B 57 (1998), 6003.

[3] X.-G. Wen and P. A. Lee, Phys. Rev. Lett. 80 (1998), 2193.

[4] M. C. Gutzwiller, Phys. Rev. Lett. 10 (1963), 159; Phys. Rev. A 134 (1965), 1726.

[5] G. Kotliar and A. E. Ruckenstein, Phys. Rev. Lett. 57 (1986), 1362.

[6] C. Gros, Phys. Rev. B 38 (1988), 931; Ann. Phys. 189 (1989), 53.

[7] H. Yokoyama and M. Ogata, J. Phys. Soc. Jpn. 65 (1996), 3615.

[8] F. C. Zhang, C. Gros, T. M. Rice, and H. Shiba, Supercond. Sci. Technol. 1 (1988), 36.

[9] D. V. Dmitriev, V. Ya. Krivnov, V. N. Likhachev, and A. A. Ovchinnikov, Fiz. Tv. Tela. 38 (1996), 397. [Solid State Physics]

[10] T. C. Hsu, Phys. Rev. B 41 (1990), 11379.

[11] R. B. Laughlin and Z. Zou, Phys. Rev. B 41 (1989), 664.

[12] W. Marshall, Proc. R. Soc. London A 232 (1955), 48.

[13] P. W. Anderson, Science 235 (1987), 1196.

[14] T. Giamarchi and C. Lhuillier, Phys. Rev. B 43 (1991), 12943

[15] T. K. Lee and S. Feng, Phys. Rev. B 38 (1988), 11809

[16] S. Liang, B. Doucot, and P. W. Anderson, Phys. Rev. Lett. 61 (1988), 365.

[17] B. Sutherland, Phys. Rev. B 37 (1988), 3786.

[18] H. Yokoyama and H. Shiba, J. Phys. Soc. Jpn. 57 (1988), 2482.

[19] N. Metropolis, A. W. Rosenbluth, M. N. Rosenbluth, A. H. Teller, and E. Teller, J. Chem. Phys. 21 (1953), 1087.

[20] D. Ceperley, G. V. Chester, and M. H. Kalos, Phys. Rev. B 16 (1977), 3081.

[21] W. O. Putikka, M. U. Luchini, and R. R. P. Singh, Phys. Rev. Lett. 81 (1998), 2966.

[22] Y. Asai, "The ground state and Low Lying Excited States of the Two-Dimensional Hubbard Model", preprint cond-mat/9904310.

[23] C. T. Shih, Y. C Chen, H. Q. Lin, and T. K. Lee, Phys. Rev. Lett. 81 (1998), 1294.

[24] E. S. Heeb and T. M. Rice, Europhys. Lett. 27 (1994), 673.

Chapter 3

An SU(2) theory of t-J two-leg ladders

3.1 Introduction

Theoretical studies of t-J ladders have proven to be valuable for understanding Hi-T_c cuprate compounds. While containing certain features of the two-dimensional t-J model, the ladders are quasi-one-dimensional, which greatly simplifies the treatment of the problem. Recently, cuprate compounds with ladder structures have been produced experimentally, and data on their electronic properties have been obtained [1]. The ladder compounds may be used for verification of models and mechanisms of superconductivity proposed for layered cuprates. The experimental works are now complemented by numerical results on t-J and Hubbard models [2, 3]. Together with experimental results, they provide a good testing ground for any analytical treatment.

The challenge of theoretically solving the t-J model on ladders arises from its strongly correlated nature. In the real ladder compounds the coupling is nearly isotropic, i.e. the interchain coupling parameters (t and J) are close to the intrachain coupling. Thus, the problem does not have a small parameter and cannot be treated by a standard perturbation theory. Several works exist based on starting from uncoupled chains and then including interchain hopping and spin exchange as perturbations [4, 5]. While weak-coupling approach is the most consistent and controlled of the existing analytic methods, it is not completely reliable as the interchain coupling increases and approaches the single-chain bandwidth. We shall further comment on possible corrections to this treatment.

In the present paper we employ the $SU(2)$ slave-boson mean-field approach [6, 7]. Although not a controlled approximation, we believe that it can correctly capture the low-energy physics of the systems with a spin gap. In the paper we specialize to two-leg ladders, but our treatment may be further extended to any even-leg ladders which are known to exhibit spin gap. The spin gap ensures that most of the fluctuations around the mean-field state are massive. The only massless fluctuation is the 1+1-dimensional abelian gauge field which can be explicitly included as a pair-binding potential.

The general idea of slave-boson method is to represent the vacant sites (holes) by an auxiliary bosonic field, which allows us to rewrite the non-linear no-double-occupancy condition as a linear constraint in terms of fermions (representing spin degrees of freedom) and bosons (representing charge degrees of freedom) [6, 7, 8]. Introducing auxiliary bosons expands the Hilbert space of states, and the system acquires an additional gauge symmetry. The mean-field ansatz breaks this symmetry, which is restored for physical correlation functions after averaging over all gauge-equivalent configurations.

We use the $SU(2)$ version of the slave-boson construction developed earlier for the two-dimensional problem [6, 7]. In this method, the auxiliary boson has two components (we call the corresponding degree of freedom isospin; it is distinct from the actual spin) which describe holes in the two different ways: either as sites with no fermions or as sites doubly occupied by fermions. Thus extended, the system has a $SU(2)$ gauge symmetry (rotating isospin). We choose to use the $SU(2)$ formalism instead of $U(1)$ version of the slave-boson method developed previously for two-dimensional t-J model [8, 9]. We note that both analytic and numerical works [2, 5, 10] point to a bipolaron picture where the holes are bound in pairs. As we shall see, this picture naturally emerges out of the $SU(2)$ formulation as the confinement between two species of bosons, while the $U(1)$ formalism fails to give the correct low-energy physics. We believe that the $SU(2)$ mean-field theory has an advantage at low doping where it generalizes the $SU(2)$ symmetry of t-J model at half-filling [6]. A discussion of relation between $U(1)$ and $SU(2)$ approaches may be found in [7].

We find that the low-temperature mean-field phase is the staggered-flux phase (similar to that found for the two-dimensional problem in [6, 7]). The fluctuations about this mean-field state are described by gauge fields which have a gap, except for the in-phase fluctuations which form a 1+1-dimensional abelian gauge field. As a result, we find that the low-energy effective theory consists of two degenerate bands of holons with a short-range interaction and coupled to a $U(1)$ gauge-field. The dynamics of this gauge field arises from its interactions with spinons. Spinons have a gap and, therefore, give a nonsingular dynamics to the gauge field with the energy scale J. The two bands of holons have opposite charges with respect to this gauge field and, therefore, form confined pairs. This leads us to the conclusion that the resulting theory for the hole excitations is the Luther-Emery liquid of hole pairs. This agrees with the bipolaronic picture of charge excitations proposed earlier both analytically and numerically [2, 5, 10]. It is known that the Luther-Emery liquid has two competing orders: superconducting singlet pairing (SS) and charge density wave (CDW) [4, 5, 11]. We point out the necessity to distinguish between the hole density (two-particle operator) and the pair density (four-particle operator). While the product of the correlation exponents for the SS and CDW order parameters is equal to one when CDW is understood as hole-density correlations, this relation does not necessarily hold for four-particle pair-density correlations. The relation between the single-hole and pair CDW exponents depends on the degree of the overlap of the bipolaronic pairs. At low density of holes, when the pairs do not overlap, these two exponents coincide. On the other hand, in the limit of highly overlapping pairs we find that the effective exponents may differ by 2. This possibly explains the unexpected

numerical results for the correlation exponents obtained by Noack et al. [2].

Further, we discuss the possible implication of our model for the superconducting transition via pair condensation (of course, interladder correlations would be necessary). We describe the superconducting order by the nearest-neighbor order parameter Δ_{ij}. We extend our discussion for a more general case of a weakly doped antiferromagnet on a bi-partite lattice with a spin gap. This class of systems includes all even-leg ladders as a particular case. We assume that at low temperature such a system is in the staggered flux phase, which results in two degenerate interacting holonic bands. Under these assumptions we find that the order parameter obeys the modified d-wave relation:

$$\sum_j t_{ij}\Delta_{ij} = 0, \tag{3.1}$$

where the sum is performed over all nearest neighbors of a site i. This relation holds in the limit of zero doping, with corrections involving the hole concentration. This relation was first derived by S. C. Zhang as an exact result for the Hubbard model [12]. Our derivation should be understood as a verification that the $SU(2)$ mean-field approximation preserves this exact property. When specialized to the case of the two-leg ladder with isotropic coupling, the above equation becomes $\Delta_\perp = -2\Delta_\parallel$. This agrees very well with the earlier numerical results [2, 3].

The rest of the paper is organized in three sections. In the first section, we review the $SU(2)$ slave-boson method and present the results of the mean-field theory computations. In the second section we discuss the effective theory for the holons and the correlation exponents for SS and CDW pairing. Finally, the third part is devoted to the discussion of the modified d-wave relation for the superconducting order parameter.

3.2 $SU(2)$ mean-field theory of the ladder

In this section we present the $SU(2)$ mean-field theory for the t-J Hamiltonian

$$H = \sum_{\{ij\}} J(\vec{S}_i\vec{S}_j - \frac{1}{4}n_i n_j) - t\mathcal{P}(c^\dagger_{\alpha i}c_{\alpha j} + \text{h.c.})\mathcal{P} \tag{3.2}$$

on the ladder (Fig. 3-1).

The sum is performed over nearest-neighbor site pairs $\{i,j\}$, $c^\dagger_{\alpha i}$ and $c_{\alpha i}$ are the electron creation and annihilation operators on site i (α is the spin index), $\vec{S}_i$ is the electron spin, $\vec{S}_i = \frac{1}{2}c^\dagger_{\alpha i}\vec{\sigma}_{\alpha\beta}c_{\beta i}$, n_i is the occupation number of the site i ($n_i = c^\dagger_{\alpha i}c_{\alpha i}$), $\mathcal{P}$ is the projector onto the no-double-occupancy states (with $n_i \leq 1$ for any i). t and J are the parameters of the Hamiltonian. In the real ladder compounds t and J are estimated to be about 4000K and 1300K respectively [1]. In what follows we assume that the interchain and the intrachain couplings are equal ($t_\perp = t_\parallel = t$, $J_\perp = J_\parallel = J$) and as a realistic approximation we take $t/J = 3$.

Following the usual procedure of the $SU(2)$ slave-boson method [6, 7], we introduce

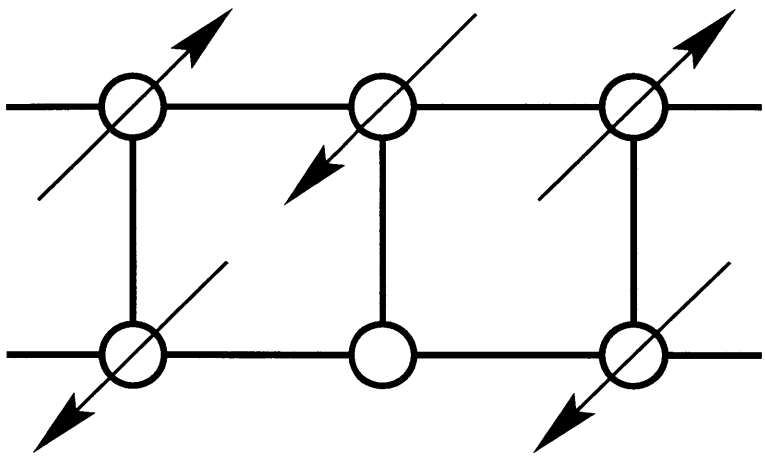

Figure 3-1: Two-leg t-J ladder.

two fermionic and one bosonic isospin doublets on each site:

$$\psi_{1i} = \begin{pmatrix} f_{1i} \\ f_{2i}^\dagger \end{pmatrix} \qquad \psi_{2i} = \begin{pmatrix} f_{2i} \\ -f_{1i}^\dagger \end{pmatrix} \qquad h_i = \begin{pmatrix} b_{1i} \\ b_{2i} \end{pmatrix} \tag{3.3}$$

with the electronic operators written in terms of bosons h_i and fermions $\psi_{\alpha i}$ as

$$c_{\alpha i} = \frac{1}{\sqrt{2}} h_i^\dagger \psi_{\alpha i} \tag{3.4}$$

The resulting Hilbert space is larger than that of the original t-J system. To select the subspace of physical states (which is invariant under the Hamiltonian of the original system) we impose a linear constraint (replacing the non-linear no-double-occupancy constraint):

$$(\frac{1}{2}\psi_{\alpha i}^\dagger \vec{\tau} \psi_{\alpha i} + h_i^\dagger \vec{\tau} h_i)|phys\rangle = 0 \tag{3.5}$$

($\vec{\tau}$ are identical to the Pauli matrices $\vec{\sigma}$, but they act in the isospin space, and we denote them by a different letter to distinguish from the Pauli matrices $\vec{\sigma}$ acting on true spin). On a given site, this constraint allows only three states: $f_1^\dagger|0\rangle$, $f_2^\dagger|0\rangle$, and $\frac{1}{\sqrt{2}}(b_1^\dagger + b_2^\dagger f_1^\dagger f_2^\dagger)|0\rangle$, which correspond to spin up, spin down electrons and a vacancy respectively. Thus in the $SU(2)$ formulation, a vacancy may be represented by both two-spinon and no-spinon states corresponding to different isospins of the holon h_i.

Thus formulated, the extended system is invariant under an $SU(2)$ gauge symmetry:

$$\psi_{\alpha i} \mapsto g_i \psi_{\alpha i}, \qquad h_i \mapsto g_i h_i. \tag{3.6}$$

This gauge symmetry acts on the isospin of fermions and bosons, and mixes creation operators $f_{\alpha i}^\dagger$ with the annihilation operators of opposite spin $f_{-\alpha i}$.

Introducing the nearest-neighbor mean-field parameters

$$U_{ij} = \langle \psi_{\alpha i} \psi_{\alpha j}^\dagger \rangle - \frac{t}{J}(\langle h_i h_j^\dagger \rangle + \mathbf{I}\langle h_j h_i^\dagger \rangle^T \mathbf{I}) \tag{3.7}$$

with

$$\mathbf{I} = \begin{pmatrix} 0 & 1 \\ -1 & 0 \end{pmatrix} \tag{3.8}$$

and the Lagrange multipliers a_i^μ ($\mu = 1, 2, 3$) for enforcing the linear constraint (3.5), the mean-field Hamiltonian becomes

$$H = \sum_{\{ij\}} \left[\frac{J}{4} \mathrm{Tr}(U_{ij} U_{ij}^\dagger) + \frac{J}{2} \psi_{\alpha i}^\dagger U_{ij} \psi_{\alpha j} + \frac{t}{2} (h_i^\dagger U_{ij} h_j + \mathrm{h.c.}) \right] +$$

$$+ \sum_i a_i^\mu (\frac{1}{2} \psi_{\alpha i}^\dagger \tau_\mu \psi_{\alpha i} + h_i^\dagger \tau_\mu h_i). \tag{3.9}$$

In the present paper we use combinatoric coefficients in (3.9) different from those used in [6, 7, 9]. Our choice of coefficients in (3.9) gives the correct combinatoric factors for tadpole diagrams, and they differ from those obtained from the Hubbard-Stratonovich transformation. This ambiguity in the numeric factors of order one is of no practical significance, since it falls within the uncertainty of the mean-field approximation.

The mean-field Hamiltonian (3.9) is accurate only up to four-boson terms which we neglect in the usual way [8]. The four-boson terms give rise to only short-range interactions between holons and can be omitted at this level of approximation.

In [6] it was argued that the non-zero values of a_i^μ correspond to Bose condensation. We do not expect Bose condensation in a quasi-one-dimensional system and set mean-field value $a_i^\mu = 0$. This implies that we in fact release the no-double-occupancy constraint (it is satisfied only on average). Afterwards, the constraint may be imposed by including the fluctuations of the field a_i^μ.

Introducing the chemical potential μ, we arrive at the mean-field Hamiltonian

$$H = \sum_{\{ij\}} \left[\frac{J}{4} \mathrm{Tr}(U_{ij} U_{ij}^\dagger) + \frac{J}{2} \psi_{\alpha i}^\dagger U_{ij} \psi_{\alpha j} + \frac{t}{2} (h_i^\dagger U_{ij} h_j + \mathrm{h.c.}) \right] - \mu \sum_i (h_i^\dagger h_i - \delta), \tag{3.10}$$

where δ is the concentration of holes (doping). The matrices U_{ij} have the form

$$U_{ij} = \begin{pmatrix} \chi_{ij} & \Delta_{ij} \\ \Delta_{ij}^* & -\chi_{ij}^* \end{pmatrix} = U_{ji}^\dagger = i a_{ij} G_{ij}, \tag{3.11}$$

where a_{ij} are positive real numbers (amplitudes), $G_{ij} \in SU(2)$ are 2×2 matrices.

The mean-field saddle point at temperature T is found as the extremum of the free energy

$$F[U_{ij}] = -T \log \mathrm{Tr}_{h,\psi} \exp(-H/T). \tag{3.12}$$

$F[U_{ij}]$ is invariant under $SU(2)$ gauge transformations

$$U_{ij} \mapsto W_i U_{ij} W_j^\dagger \tag{3.13}$$

for any set of $SU(2)$ elements W_i.

The mean-field solution breaks this gauge symmetry. Only gauge invariant quan-

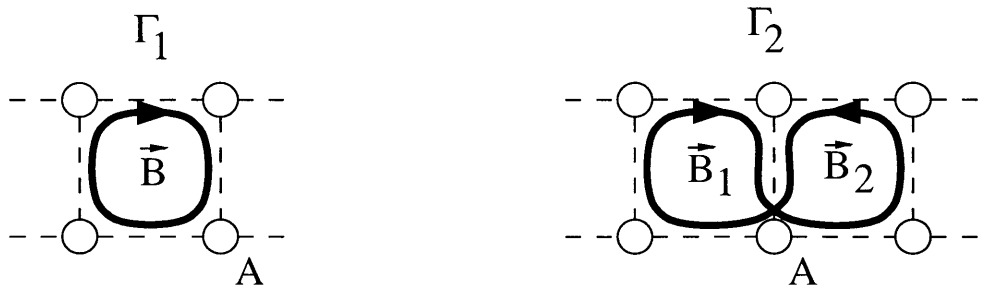

Figure 3-2: The two closed contours used in constructing mean-field order parameters.

tities correspond to physical observables. Any non-gauge-invariant expression will vanish after averaging over all gauge-equivalent configurations of U_{ij}.

Now we turn to describing possible phases. Phases should be parametrized by gauge-invariant functions of U_{ij}. We assume that the translational symmetry is unbroken, i.e. a translation of the mean-field solution $\{U_{ij}\}$ along the ladder transforms it to a gauge equivalent configuration. We also assume that the symmetry of reflection about the ladder axis (interchanging the two legs) is also preserved in the mean-field solution. Under these assumptions all possible phases may be parametrized by four real parameters: the two amplitudes $a_{\|}$ and $a_{\perp}$ (intrachain and interchain respectively), and two $SU(2)$ order parameters:

$$b = \frac{1}{2}\mathrm{Tr}\prod_{\Gamma_1} G_{ij}, \tag{3.14}$$

$$c = \frac{1}{2}\mathrm{Tr}\prod_{\Gamma_2} G_{ij} \tag{3.15}$$

with the products taken along the contours Γ_1 and Γ_2 shown in Fig. 3-2 (the first product contains four matrices, the second one — eight matrices).

The meaning of the order parameter b is analogous to the cosine of the flux through plaquet in the $U(1)$ formulation [8]. To explain this analogy we may introduce the $SU(2)$ flux $\vec{B}$ defined by

$$\exp(i\vec{B}\cdot\vec{\tau}) = \prod_{\Gamma_1} G_{ij}, \tag{3.16}$$

where the product starts and ends at a site A of the contour Γ_1 (Fig. 3-2). Then $b = \cos|\vec{B}|$ (obviously, the direction of the vector $\vec{B}$ depends on the choice of the starting point A, but its magnitude $|\vec{B}|$ does not).

The order parameter c measures the relative orientation of neighboring $SU(2)$ fluxes. Namely, define the two fluxes $\vec{B}_1$ and $\vec{B}_2$ through neighboring plaquets with a common starting point A (Fig. 3-2). Then

$$c = \frac{1}{2}\mathrm{Tr}\left(\exp(i\vec{B}_1\cdot\vec{\tau})\exp(-i\vec{B}_2\cdot\vec{\tau})\right) = \cos|\vec{B}_1|\cos|\vec{B}_2| + \frac{(\vec{B}_1\cdot\vec{B}_2)}{|\vec{B}_1||\vec{B}_2|}\sin|\vec{B}_1|\sin|\vec{B}_2|. \tag{3.17}$$

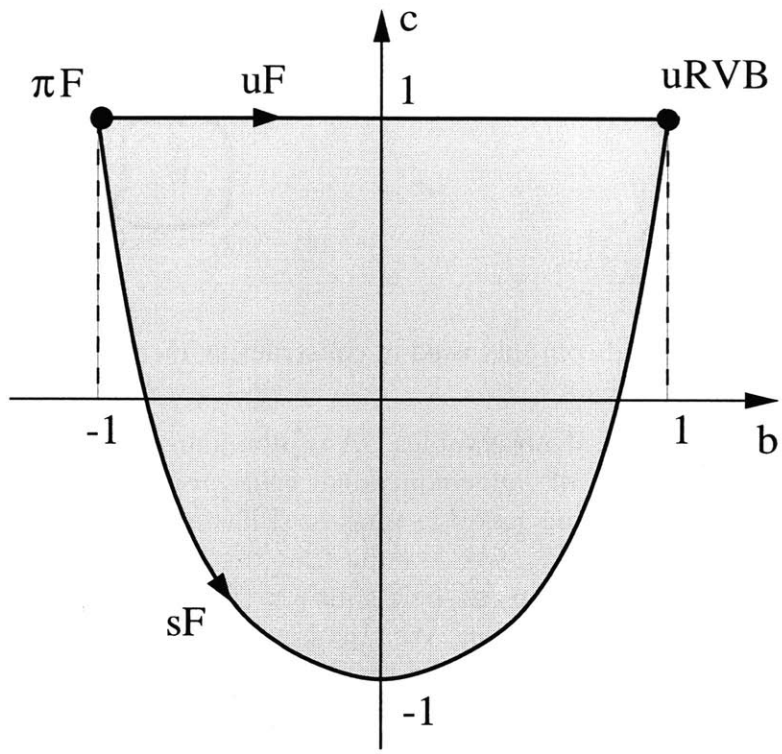

Figure 3-3: Space of mean-field phases. The two corners correspond to the π-flux and uRVB phases, boundaries — to the uniform-flux and staggered-flux phases.

Then we see that for any $G_{ij} \in SU(2)$ the order parameters b and c are restricted to

$$-1 \leq b \leq 1, \tag{3.18}$$

$$2b^2 - 1 \leq c \leq 1. \tag{3.19}$$

Thus, the $SU(2)$ order may be represented by a point in a two-dimensional domain (Fig. 3-3) with the two corners representing the π-flux and the uRVB phases, the boundaries corresponding to the uniform flux (uF) and staggered flux (sF) phases analogous to their $U(1)$ counterparts [9], but preserving translational and time-reversal symmetries. In the uF phase the neighboring $SU(2)$ fluxes are parallel, in the sF phase they are antiparallel, and inside the shaded region in Fig. 3-3 they form angles ranging between 0 and π.

By numerically minimizing the free energy (3.12) (at $t/J = 3$) we find the following mean-field phase diagram in the (δ, T) coordinates:

where

1. $\emptyset$ denotes the high-temperature free spin phase ($a_{\|} = a_{\perp} = 0$);
2. uRVB is the phase with $a_{\|} \neq 0$, $a_{\perp} \neq 0$, $G_{ij} = \mathbf{1}$ (so that $b = c = 1$);
3. D is the dimer phase: $a_{\perp} \neq 0$, $a_{\|} = 0$;
4. sF is the staggered-flux phase with $a_{\perp} \neq 0$, $a_{\|} \neq 0$, $-1 < b < 1$, $c = 2b^2 - 1$.

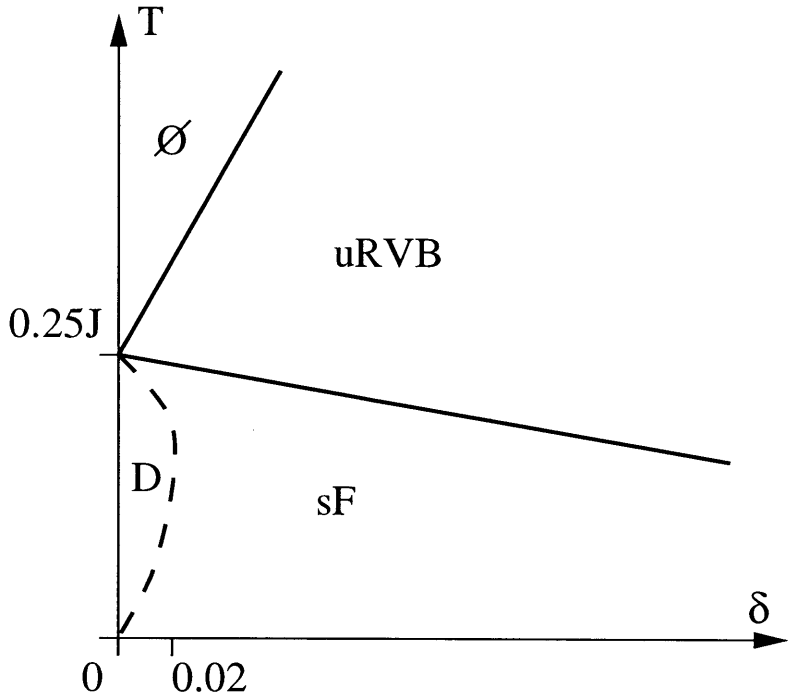

Figure 3-4: Mean-field phase diagram at isotropic coupling and $t/J = 3$.

Numerically we find that the transition between D and sF phases is a very soft first-order transition. In fact, the dimer phase D has flat spectra for bosons and fermions and will be destroyed by the fluctuations (correlations along the ladder will appear). We shall disregard the dimer phase as an artifact of the mean-field approximation and for the rest of the paper we restrict our discussion to the sF phase.

The sF phase may be described by different gauge-equivalent configurations of U_{ij}. One of the *translationally invariant* configurations (analogous to d-wave pairing phase in the $U(1)$ mean-field theory [9]) is (Fig. 3-5):

$$G_\perp = i\tau_1, \qquad G_\parallel = i(\cos\frac{\varphi}{2}\tau_1 + \sin\frac{\varphi}{2}\tau_2), \tag{3.20}$$

or, equivalently,

$$U_\perp = \begin{pmatrix} 0 & a_\perp \\ a_\perp & 0 \end{pmatrix}, \qquad U_\parallel = \begin{pmatrix} 0 & a_\parallel e^{i\frac{\varphi}{2}} \\ a_\parallel e^{-i\frac{\varphi}{2}} & 0 \end{pmatrix}. \tag{3.21}$$

Further, we shall use a different, the so called "abelian" parametrization with

$$G_\parallel = \mathbf{1}, \qquad G_\perp = \cos\frac{\varphi}{2} + (-1)^m i\tau_3 \sin\frac{\varphi}{2}, \tag{3.22}$$

(Fig. 3-6) which corresponds to

$$U_\parallel = i\begin{pmatrix} a_\parallel & 0 \\ 0 & a_\parallel \end{pmatrix}, \qquad U_\perp = i\begin{pmatrix} a_\perp e^{i(-1)^m\frac{\varphi}{2}} & 0 \\ 0 & a_\perp e^{-i(-1)^m\frac{\varphi}{2}} \end{pmatrix}, \tag{3.23}$$

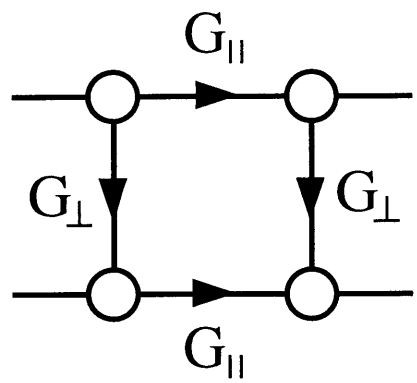

Figure 3-5: sF phase order parameters in the translationally invariant gauge.

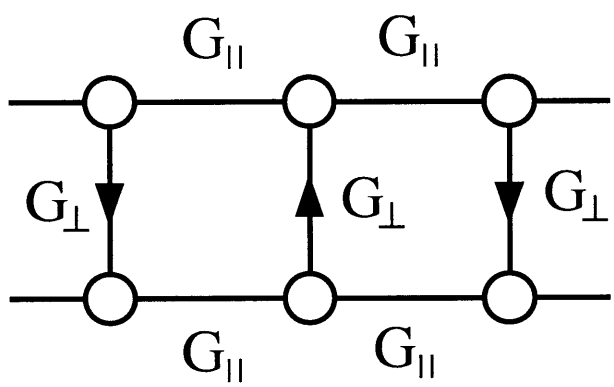

Figure 3-6: sF order parameters in the abelian gauge.

where m is the number of the rung. This gauge fixing is not translationally invariant, but instead it has the property that all U_{ij} commute. This choice of gauge resembles the staggered-flux $U(1)$ phase [9]. In the U(1) formalism, the staggered-flux and d-wave pairing phases are different, but their $SU(2)$ counterparts are gauge-equivalent [6].

In the $SU(2)$ mean-field theory bosonic and fermionic spectra are proportional to each other (with the scales t and J respectively). In the sF phase we obtain the spectrum

$$\frac{E_f}{J} = \frac{E_b}{t} = \pm\frac{1}{2}\sqrt{a_\perp^2 + (2a_\parallel)^2\cos^2 k + 2(2a_\parallel)a_\perp \cos\frac{\varphi}{2}\cos k} \tag{3.24}$$

($k \in [0; 2\pi]$ is the wave vector) and each of these two bands is doubly degenerate (four bands total). We remark that labeling the states by wave vectors k may depend on the gauge, but, because gauge-dependent shift of k involves equally bosons and fermions, the gauge-invariant quantities remain unchanged.

The double degeneracy of states is a characteristic feature of the staggered-flux phase. It is due to the fact that a certain non-abelian subgroup of the full symmetry group of the extended Hamiltonian remains unbroken by the mean-field ansatz. In the

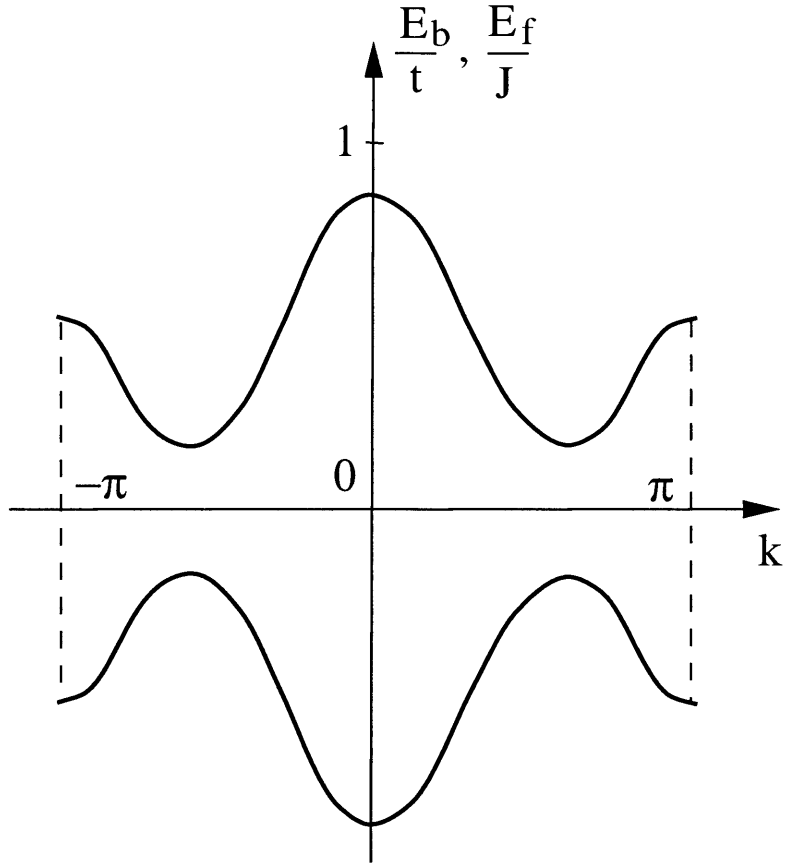

Figure 3-7: Typical fermionic-bosonic spectrum. Both bands are doubly degenerate.

staggered-flux phase the order parameters U_{ij} are invariant under a U(1) subgroup of global isospin rotations (in the abelian gauge (3.22) – (3.23) these are simply global rotations by τ_3). Besides, there remains a particular symmetry of U_{ij}, which is the combination of time reversal (transforming $U_{ij} \mapsto U_{ij}^*$) and global isospin rotation (exchanging isospins up and down in the abelian gauge). This symmetry operation does not commute with the $U(1)$ rotation, but extends them to a non-abelian group. The two degenerate bands form a two-dimensional representation of this group, with time reversal mapping one band onto the other.

The typical numerical values for $a_{||}$, $a_\perp$ and $\cos\frac{\varphi}{2}$ are $a_{||} = 0.5$, $a_\perp = 0.9$, $\cos\frac{\varphi}{2} = 0.4$ (found by minimizing free energy at $\delta = 0.05$, $T = 0.1J$, $t/J = 3$). This means that the upper bands of the spectrum are separated from the lower bands by a gap of order J for fermions and of order t for bosons (Fig. 3-7). The fermionic spectrum is half-filled, i.e. the lower bands are completely filled whereas the upper bands are empty. The fermionic excitations have a gap of order of J. This agrees with the prediction of spin gap in two-leg ladders and is crucial for the stability of the phase.

Finally, we need to include the fluctuations about the mean-field phase. These fluctuations are described by the spatial $SU(2)$ gauge fields $A_{ij} = U_{ij}^{-1}\delta U_{ij}$ defined on the links and their temporal counterparts $a_i = a_i^\mu \tau_\mu$ defined on the sites [6, 7, 8]. The temporal components of the gauge field a_i coincide with the constraint-fixing

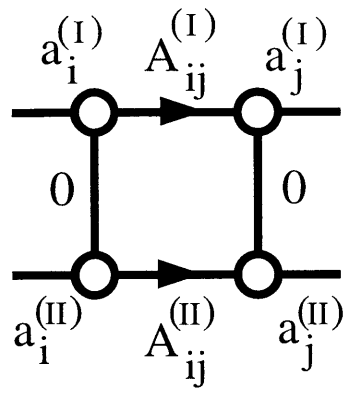

Figure 3-8: Gauge fields describing the fluctuations of the order parameter. We choose the gauge with $A_\perp = 0$.

Lagrange multipliers in (3.9) when expressed in units of J. The effective action for the fields A_{ij} and a_i is invariant under the (time-dependent) gauge transformations

$$A_{ij} \mapsto W_i(t) A_{ij} W_j^\dagger(t), \qquad a_i \mapsto a_i + i\partial_t W_i(t) \tag{3.25}$$

for arbitrary $SU(2)$ matrices $W_i(t)$ defined on sites.

In the sF phase the $SU(2)$ gauge symmetry is broken down to U(1) global symmetry. In the abelian gauge, this residual symmetry is realized by rotations by τ_3. As shown in the Appendix B of [7], the free energy will contain terms proportional to $\mathrm{Tr}\prod U_{ij}$, where the products are taken along closed loops on the lattice. When expanded in gauge-field fluctuations, these terms give rise to mass for the gauge modes proportional to τ_1 and τ_2. Thus, massless modes of the gauge field must be proportional to τ_3 [7], and we may treat A_{ij} and a_i as $U(1)$ gauge fields.

To proceed further, we may make use of the symmetry (3.25) (now an $U(1)$ gauge symmetry with all $W_i(t)$ being rotations by τ_3). The analysis appears to be particularly simple in the gauge where $A_{ij} = 0$ across the rungs (Fig. 3-8).

Then the remaining gauge fields split into the in-phase and out-of-phase modes

$$A_\pm = A_{ij}^{(I)} \pm A_{ij}^{(II)}, \qquad a_\pm = a_i^{(I)} \pm a_i^{(II)} \tag{3.26}$$

(where the superscripts (I) and (II) label the two legs of the ladder). The dynamics of the gauge fields arises from their coupling to the spinons and can be found by computing the polarization diagram (Fig. 3-9), solid lines denote spinons):

In contrast to the two-dimensional model, where there exist massless transverse fluctuations of the gauge field, it is not the case in the ladder. The ladder geometry restricts the transverse wave vector to two values $k_\perp = 0$ and $k_\perp = \pi$ which correspond to the modes (A_+, a_+) and (A_-, a_-) respectively. The out-of-phase modes A_- and a_- (describing the fluctuations of the flux φ through the plaquet) acquire a finite mass of order J and, therefore, can be neglected, giving only a short-range interactions between holons.

On the other hand, the modes A_+ and a_+ become 1+1 QED gauge fields with the

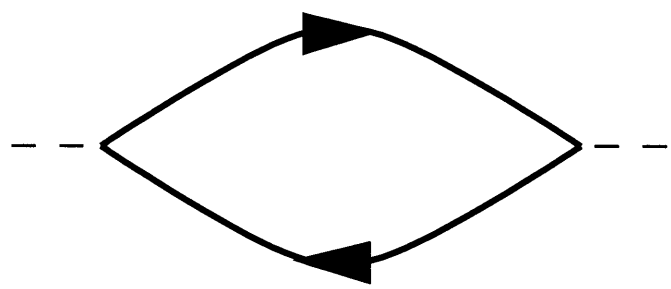

Figure 3-9: Lowest-order diagram responsible for the dynamics of the gauge field. Solid lines denote spinon propagators. This diagram gives mass to the out-of phase mode and 1+1-dimensional QED dynamics for the in-phase mode.

long-wavelength action

$$S = \frac{1}{J^*} \int (\partial_t A_+ + \partial_x a_+)^2 \, dx \, dt \tag{3.27}$$

with J^* of order J. This action arises from expanding the polarization diagram in Fig. 3-9. The particular value of J^* depends on the values of mean-field parameters, and for the typical values cited above differs from J only by a factor of order unity.

Since the two lower bosonic bands have different isospin, they have opposite charges with respect to the gauge field (A_+, a_+). In 1+1 dimension, electromagnetic field leads to a confining (linearly growing with the distance) potential between charges:

$$U(r) = \pm J^* |r|. \tag{3.28}$$

In the limit of low hole density, the bosons will form isospin-neutral dipole pairs (bipolarons) which produce no field outside each pair. Therefore, bipolarons will interact only by short-range forces.

We may estimate the size of bipolaron by solving a simple quantum-mechanical problem of two particles interacting via the potential (3.28). The holon hopping amplitude is of order t, therefore the kinetic energy of bipolaron is of order $t\xi_{pair}^{-2}$. The potential energy, on the other hand, is of order $J\xi_{pair}$. Thus from variational principle we find that the size of bipolaron is $\xi_{pair} \sim (t/J)^{1/3}$ up to a factor of order one. For our assumption $t/J = 3$, this gives $\xi_{pair} \sim 1$, which means that now the other short-range (repulsive) terms, which we omitted before, give a comparable contribution. Due to the no-double-occupancy constraint, the two species of bosons must be subject to a substantial on-site repulsion. It increases the estimated size of the pair by several lattice spacings, but does not change the long-range attractive force. Since we omitted the short-range part of the interaction from the very beginning, we cannot compute the size of the pair more precisely. From the numerics [2] we know that the characteristic decay length for the pairing correlation function is about four lattice spacings, in agreement with our discussion.

A simple classical explanation of the confinement may be obtained from the picture of fluctuating singlet bonds (somewhat in the spirit of [10]). We may think of the

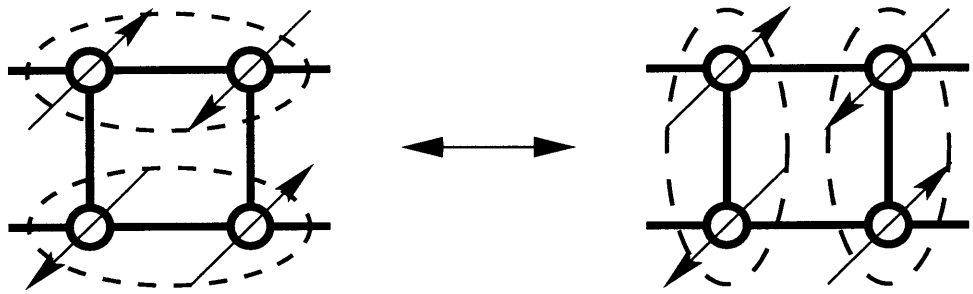

Figure 3-10: Fluctuating singlets in the spin ladder.

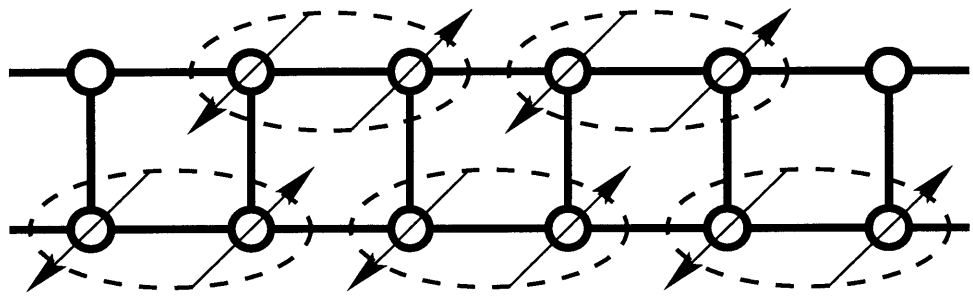

Figure 3-11: Misplaced singlet bonds between two holes in the t-J ladder. The energy cost is proportional to the distance between the holes.

spin structure of the Heisenberg antiferromagnet on the ladder as of spins forming fluctuating singlet bonds with nearest neighbors (Fig. 3-10).

Once we have a single hole, it leads to the appearance of a localized spin, which costs a finite energy of order J. When putting two holes, the spins between the holes must form singlet bonds in a non-favorable way without a freedom to fluctuate (Fig. 3-11).

Naturally, this string of singlets costs certain energy J^*r, where r is the distance between the holes and J^* is of order J. We believe that this naive picture gives a correct understanding of the holon confinement which we derived starting from the mean-field sF phase.

3.3 Luther-Emery liquid and correlation exponents

In the previous section we have shown that the low-energy excitations in our model are pairs of holons — bipolarons — which are bound by long-range confining interaction. Due to complete screening of the confining interaction by a single particle in one dimension, bipolarons interact only via short-range forces, and this recovers the picture of Luther-Emery liquid of hole pairs proposed earlier in [10].

In fact, this simple picture is valid at low hole concentration $\delta \ll \xi_{pair}^{-1}$, when bipolarons do not overlap. The purpose of this section is to show that as overlap increases, the charge-density-wave exponents for single-particle and for pair densities

may differ.

For quantitative description of bipolarons we introduce the three different correlation exponents as follows. Let $n(x) = n^{(I)} + n^{(II)} - 2\delta$ be the fluctuation of the number of holes on the rung (x is the coordinate along the ladder, superscripts refer to the two chains). Let further $n_{pair} = (n^{(I)} - \delta)(n^{(II)} - \delta)$ be the fluctuation of the probability that both sites of the same rung contain holes. Finally, let $\Delta(x) = c_{\downarrow}^{(I)} c_{\uparrow}^{(II)} - c_{\uparrow}^{(I)} c_{\downarrow}^{(II)}$ be the singlet superconducting order parameter on the rung at the position x. Then define the correlation exponents α_1, α_2 and γ by

$$\langle n(x) n(y) \rangle_{2k_F} \propto |x - y|^{-\alpha_1}, \tag{3.29}$$

$$\langle n_{pair}(x) n_{pair}(y) \rangle_{2k_F} \propto |x - y|^{-\alpha_2}, \tag{3.30}$$

$$\langle \Delta^{\dagger}(x) \Delta(y) \rangle \propto |x - y|^{-\gamma}, \tag{3.31}$$

where $\langle \ldots \rangle_{2k_F}$ is the coefficient at $\cos[2k_F(x - y)]$ in the expansion of the correlation function [14]:

$$\begin{aligned} \langle n(x) n(y) \rangle = A_0 |x - y|^{-\theta_0} + A_1 |x - y|^{-\theta_1} \cos[2k_F(x - y)] + \\ + A_2 |x - y|^{-\theta_2} \cos[4k_F(x - y)] + \ldots \end{aligned} \tag{3.32}$$

The correlation function (3.29) describes charge-density-wave (CDW) ordering, and the correlation function (3.31) — singlet superconductivity (SS) ordering.

By k_F we denote the "Fermi wavevector" for the holons in the lower bands, so that $2k_F = 2\pi\delta$. For comparison with other works, we must remark that $2k_F$ in our notation corresponds to $4k_F$ in the notation of [2] and [5].

In the limit of dilute gas of bipolarons (the doping is much less than the inverse size of a bipolaron: $\delta \ll \xi_{pair}^{-1}$) we may describe the low-energy states of the system in terms of bipolaron creation and annihilation operators (similarly to the large $|U|$ limit in the attractive Hubbard model [11, 13]). Bipolarons interact repulsively and, from a naive classical picture, it is likely that the repulsion is nearly hard-core. In this limit $\alpha_1 = \alpha_2$, because on the bipolaronic subspace of the total Hilbert space the matrix elements of the operators $n(x)$ and $n_{pair}(x)$ differ only by a numerical factor (the probability of the two holons in the pair to occupy the same rung). For hard-core repulsion $\alpha_{1,2} = 2$, since hard-core bosons can be mapped to free fermions by a Jordan-Wigner-type transformation, so that density-density correlations coincide with those of free fermions. From the theory of Luther-Emery liquid it is known that CDW and SS correlations are described by dual phases, and the corresponding exponents are therefore reciprocal: $\gamma = 1/\alpha$ [11, 13]. A more detailed discussion of the Luther-Emery theory of bipolaronic excitations may be found in [10].

The opposite limit of highly overlapping bipolarons is more subtle. In this limit ($\delta \ll (t/J)^{1/3}$) bipolarons can exchange particles. Exchanging a particle would cost interaction energy of order $J\delta^{-1}$, while the gain of kinetic energy would be of order $t\delta^2$. Thus, in this limit we cannot speak of isolated bipolarons, but rather of two species of bosons with attraction much smaller than the bandwidth. We suggest that in this case we may replace the screened long-range interaction by a short-range

one. In the long-wavelength limit the system may be described as two Luther-Emery liquids with a weak attraction:

$$H = H_1 + H_2 + H_{int}, \tag{3.33}$$

$$H_i = \frac{1}{2\pi}\int dx[v_J(\nabla\varphi_i)^2 + v_N(\nabla\theta_i)^2], \qquad i = 1, 2, \tag{3.34}$$

$$H_{int} = -V\int dx\rho_1(x)\rho_2(x), \tag{3.35}$$

where φ_i and θ_i are dual phases,

$$[\varphi_i(x), \theta_j(y)] = \delta_{ij} i\frac{\pi}{2}\mathrm{sign}(x-y), \tag{3.36}$$

v_J and v_N are the parameters depending on the short-range properties of the interaction, and $\rho_i(x)$ are the density fluctuations expressed by [14]

$$\rho_i(x) = \frac{1}{\pi}\nabla\theta_i(x) + 2\rho_0\cos(2k_F x + 2\theta_i(x)) + \text{higher order terms.} \tag{3.37}$$

The interaction (3.35) contains a term proportional to

$\cos 2(\theta_1(x) - \theta_2(x))$ and locks the relative phase $\theta_- = \theta_1 - \theta_2$. The only remaining gapless mode is the in-phase fluctuations ($\theta_+ = \theta_1 + \theta_2$ and $\varphi_+ = \varphi_1 + \varphi_2$) corresponding to propagation of bipolarons.

If we at first approximation neglect higher-order terms in the density expansion (3.37), we find

$$\langle\Delta^\dagger(x)\Delta(y)\rangle \sim \langle e^{i[\varphi_+(x)-\varphi_+(y)]}\rangle, \tag{3.38}$$

$$\langle n(x)n(y)\rangle_{2k_F} \sim \langle e^{i[\theta_+(x)-\theta_+(y)]}\rangle, \tag{3.39}$$

$$\langle n_{pair}(x)n_{pair}(y)\rangle_{2k_F} \sim \langle\nabla\theta_+(x)\nabla\theta_+(y)e^{i[\theta_+(x)-\theta_+(y)]}\rangle, \tag{3.40}$$

which yields $\alpha_2 = \alpha_1 + 2$, $\gamma = 1/\alpha_1$. This would explain the numerical results of [2] who found $\alpha_2 \approx \gamma \approx 2$ (at $\delta = 1/8$, $\xi_{pair} \sim 4$). Our prediction of power-law correlations (3.29) also explains the small, but relatively narrow peak at $2k_F$ in the Fourier transform of $\langle n(x)n(y)\rangle$ in [2].

As it was pointed out by Haldane [14], in general one must also include higher-order terms in the density expansion (3.37). These terms proportional to $\cos[m(2k_F x + 2\theta_i(x))]$ with $m > 1$ are absent in the free fermion theory (and, consequently, in hard-core boson theory), but arise as we include interactions mixing left- and right-moving excitations. They produce terms proportional to $\exp i[m\theta_1(x) - (m \pm 1)\theta_2(x)]$ in the $n_{pair}(x)_{2k_F}$ expansion, and give a contribution to $\langle n_{pair}(x)n_{pair}(y)\rangle_{2k_F}$ decaying with the exponent α_1 instead of $\alpha_1 + 2$. This effect that originally higher-order terms result in leading correlation exponents is not paradoxical in view of the crossover to the dilute limit where the binding interaction is strong and the higher-order corrections to (3.37) play a dominating role. we suggest that the crossover from $\alpha_2 = \alpha_1$ in the dilute limit to $\alpha_2 = \alpha_1 + 2$ in the weak-coupling limit is governed by the overlap of

bipolarons. Namely,

$$\langle n_{pair}(x) n_{pair}(y)\rangle_{2k_F} = \frac{A}{(x-y)^{\alpha_1}} + \frac{B}{(x-y)^{\alpha_1+2}} \tag{3.41}$$

with relative weights of A and B depending on the average pair overlap ($A \gg B$ at $\xi_{pair}\delta \ll 1$ and $A \ll B$ at $\xi_{pair}\delta \gg 1$). The actual behavior of the coefficients A and B strongly depends on the short-scale features of the interaction, and cannot be found in our rude treatment.

The whole discussion of this section is equally applicable to the negative-U (attractive) Hubbard model. In the low-density (or large $|U|$) limit the exponents α_1 and α_2 coincide, while in the small U limit we expect a crossover (3.41) to $\alpha_2 = \alpha_1 + 2$. In other words, because of screening, the long-range gauge interaction between holons in one dimension leads to the same behavior at large distances as a short-range attraction.

Finally, we comment on our disagreement with the prediction of Nagaosa [5] that the correlations $\langle n_{pair}(x) n_{pair}(y)\rangle_{2k_F}$ decay exponentially (note again that $2k_F$ in our notation corresponds to $4k_F$ in the notation of [5]). The disagreement my be explained from the fact that Nagaosa starts from two uncoupled chains and treats the interchain couplings ($t_\perp$ and $J_\perp$) as perturbations. In that picture, power-law correlations $\langle n_{pair}(x) n_{pair}(y)\rangle_{2k_F}$ will appear as a correction for the nonlinearity of the spectrum as the coupling increases and approaches the bandwidth. In contrast to the weak-coupling approach, our model starts directly from diagonalizing a strong-coupling Hamiltonian (3.10), and the correlations (3.29) are present from the very beginning.

3.4 Modified d-wave relation on superconducting order parameter

In this section we verify that our approximation scheme is consistent with the exact relation for the superconducting order parameter derived by S. C. Zhang for the Hubbard model [12] (and later translated to t-J model in [15]).

Let us define the pairing operator

$$\Delta_{ij} = c_{i\downarrow} c_{j\uparrow} - c_{i\uparrow} c_{j\downarrow} \tag{3.42}$$

and consider the quantity

$$\Delta_{ij}^{(0)} = \langle 2|\Delta_{ij}|0\rangle, \tag{3.43}$$

where $|0\rangle$ and $|2\rangle$ are the ground states with zero and two holes respectively. Should a superconducting transition happen, $\Delta_{ij}^{(0)}$ will become the superconducting order parameter.

From now on, we restrict i and j to be nearest-neighbor sites. Zhang's results

states that on a bipartite lattice in the limit of zero doping $\Delta_{ij}^{(0)}$ obey the relation

$$\sum_j \Delta_{ij}^{(0)} = 0, \tag{3.44}$$

where the sum is over the nearest neighbors of the site i. On the two-dimensional square lattice this implies the d-wave symmetry of pairing; thus we may call Eq.(3.44) the modified d-wave relation.

Below we re-derive this result within the $SU(2)$ slave-boson mean-field approximation. For the sake of generality, we extend our further discussion to the t-J model on an arbitrary quasi-one-dimensional bi-partite lattice, provided it exhibits a spin gap (the most popular examples of this type are even-leg ladders). Further, assume that the low-temperature mean-field phase is analogous to the sF phase of the two-leg ladder. Namely, we require that the $SU(2)$ order parameter may be brought to the diagonal form (by a suitable choice of gauge):

$$U_{ij} = \begin{pmatrix} \chi_{ij} & 0 \\ 0 & -\chi_{ij}^* \end{pmatrix}. \tag{3.45}$$

This requirement means that spinons and holons form doubly degenerate bands related by the symmetry of simultaneous time-reversal and isospin flip. In such a phase a superconductivity may evolve by pair formation between the holons at the bottom of the two lowest bands (of course, superconductivity is possible only when stabilized by inter-ladder interactions, see e.g. [11]).

For simplicity, let the coupling be isotropic (t and J are the same on all links), as it was assumed in the previous sections. At the end of this section we shall extend the result to non-isotropic coupling.

Using our slave-boson representation, we express Δ_{ij} (for nearest-neighbor i and j) in terms of spinons and holons as

$$\Delta_{ij} = \frac{1}{2}\left[(h_i^\dagger \psi_{2i})(h_j^\dagger \psi_{1j}) - (h_i^\dagger \psi_{1i})(h_j^\dagger \psi_{2j})\right]. \tag{3.46}$$

At low doping, the fermionic part of the correlation function (4.2) may be replaced by the mean-field order parameters

$$\chi_{ij} = \langle f_{1i} f_{1j}^\dagger + f_{2i} f_{2j}^\dagger \rangle, \tag{3.47}$$

and we find

$$\Delta_{ij}^{(0)} = \frac{1}{2}\left(\chi_{ij}\langle 2|b_{1i}^\dagger b_{2j}^\dagger|0\rangle + \chi_{ij}^*\langle 2|b_{2i}^\dagger b_{1j}^\dagger|0\rangle\right), \tag{3.48}$$

where $|0\rangle$ and $|2\rangle$ now denote the states in the holonic sector. Let $b_1(k)$ and $b_2(k)$ be the operators destroying holons at a wave vector k in the two lowest bands (subscripts denote the isospin). Then the single-pair wave-function $|2\rangle$ has the form

$$|2\rangle = \int \frac{dk}{2\pi} \Psi_0(k) b_1^\dagger(k) b_2^\dagger(-k)|0\rangle, \tag{3.49}$$

where $\Psi_0(k)$ is the relative wave function of the two holons in a pair. Eq.(3.48) becomes

$$\Delta_{ij}^{(0)} = \int \frac{dk}{2\pi} \Psi_0(k) \Delta_{ij}(k), \tag{3.50}$$

where

$$\Delta_{ij}(k) = \frac{1}{2}\left(\chi_{ij}\langle 0|b_2(-k)b_1(k)b_{1i}^\dagger b_{2j}^\dagger|0\rangle + \chi_{ij}^*\langle 0|b_2(-k)b_1(k)b_{2i}^\dagger b_{1j}^\dagger|0\rangle\right) =$$
$$= \frac{1}{2}\left(\chi_{ij}\langle 0|b_2(-k)b_{2j}^\dagger|0\rangle\langle 0|b_1(k)b_{1i}^\dagger|0\rangle + \chi_{ij}^*\langle 0|b_2(-k)b_{2i}^\dagger|0\rangle\langle 0|b_1(k)b_{1j}^\dagger|0\rangle\right). \tag{3.51}$$

Since $b_1(k)$ and $b_2(k)$ are related by the time-reversal symmetry (accompanied by a gauge transformation), $\langle 0|b_2(-k)b_{2i}^\dagger|0\rangle = (-1)^i\langle 0|b_{1i}b_1^\dagger(k)|0\rangle$, and for nearest-neighbor sites i and j

$$\begin{aligned}\Delta_{ij}(k) &= \frac{1}{2}((-1)^j\chi_{ij}\langle 0|b_{1j}b_1^\dagger(k)|0\rangle\langle 0|b_1(k)b_{1i}^\dagger|0\rangle + \\ &+(-1)^i\chi_{ij}^*\langle 0|b_{1i}b_1^\dagger(k)|0\rangle\langle 0|b_1(k)b_{1j}^\dagger|0\rangle) = \\ &= (-1)^i\langle k|\frac{1}{2}(-\chi_{ij}b_{1i}^\dagger b_{1j} + \chi_{ij}^* b_{1j}^\dagger b_{1i})|k\rangle,\end{aligned} \tag{3.52}$$

where $|k\rangle$ is a single-holon plane wave created by $b_1^\dagger(k)$. The state $|k\rangle$ is an eigenvector of the free Hamiltonian proportional to the bosonic part of Eq.(3.10)

$$H_0 = \frac{1}{2}\sum_{\{ij\}}(b_{1i}^\dagger\chi_{ij}b_{1j} + b_{1j}^\dagger\chi_{ij}^* b_{1i}) \tag{3.53}$$

(with the sum performed over nearest-neighbor pairs of sites). Therefore

$$\sum_j \Delta_{ij}(k) = (-1)^i\langle k|[b_{1i}^\dagger b_{1i}, H_0]|k\rangle = 0, \tag{3.54}$$

where the sum is over the nearest neighbors of the site i. This immediately implies the result (3.44).

The above derivation holds also at a non-zero temperature (with ground-state expectation values replaced by thermal averages). However, it is strictly limited to zero doping: at finite doping Eq.(3.47) is no longer valid. A remarkable feature of the relation (3.44) is its independence of the coupling parameters t and J.

For the two-leg ladder the modified d-wave relation (3.44) turns into

$$\Delta_\perp = -2\Delta_{||}. \tag{3.55}$$

This result agrees with the available numerical results [2, 3]. It would provide a good test for possible numerical models on ladders with a higher number of legs.

The d-wave relation (3.44) may be easily extended to a non-isotropic coupling. In fact, the whole slave boson mean-field theory may be re-derived for arbitrary coupling constants t_{ij} and J_{ij}, differing at different links. One just needs to replace t and J in

Eqs. (3.7) – (3.10) by t_{ij} and J_{ij}. The whole argument of this section may be repeated down to Eq.(3.53) which we must now replace by the Hamiltonian

$$H_0 = \frac{1}{2} \sum_{\{ij\}} t_{ij} (b_{1i}^\dagger \chi_{ij} b_{1j} + b_{1j}^\dagger \chi_{ij}^* b_{1i}). \tag{3.56}$$

Finally, this leads to the following generalization of the d-wave relation (3.44):

$$\sum_j t_{ij} \Delta_{ij}^{(0)} = 0. \tag{3.57}$$

This equation implies that as the hopping on a link increases, the weight of the superconducting order parameter on this link decreases. Of course, Eq.(3.57) may also be derived exactly for the Hubbard model (with the site- and link-dependent U and t) by the method of [12].

3.5 Conclusion

We presented the low-energy effective theory for charge excitations in two-leg t-J ladder, based on the mean-field treatment of spin degrees of freedom. We found that the $SU(2)$ slave-boson formalism predicts bipolaronic picture of charge excitations, as expected from earlier analytic and numerical works. While capturing well the low-energy physics, our approximation is not reliable for spin and single-electron excitations which have a gap of order J. In the framework of the model developed in the paper, single-hole excitations may be constructed as holon-spinon pairs bound by confining gauge-field interaction. The similarity of the boson-fermion spectrum in Fig. 3-7 to the single-hole spectrum found numerically in [10] makes this possibility very appealing. However, spin structure of the ladder was included in the lowest mean-field order, and to restore correctly spin excitations requires a more elaborate treatment.

We wish to thank Christopher Mudry for illuminating discussions of one-dimensional systems and for many helpful remarks. We are grateful to N. Nagaosa, X.-G. Wen, and D. H. Kim for useful discussions. This work is supported by NSF under the MRSEC program, DMR 94-0034.

Bibliography

[1] T. Osafune, N. Motoyama, H.Eisaki, and S. Uchida, Phys. Rev. Lett. 78 (1997), 1980;
M. Uehara, T. Nagata, J. Akimitsu, H. Takahashi, N. Môri, and K. Kinoshita, J. Phys. Soc. Jpn. 65 (1996), 2764;
N. Motoyama, T. Osafune, T. Kakashita, H. Eisaki, and S. Uchida, Phys. Rev. B 55 (1997), R3386;
Z. Hiroi, M. Takano, Nature 377 (1995), 41;
K. Ishida, Y. Kitaoka, K. Asayama, M. Azuma, Z. Hiroi, and M. Takano, J. Phys. Soc. Jpn. 63 (1994), 3222;
M. Azuma, Z. Hiroi, M. Takano, K. Ishida, and Y. Kitaoka, Phys. Rev. Lett. 73 (1994), 3463.

[2] R. M. Noack, S. R. White, and D. J. Scalapino, Physica C 270 (1996), 281.

[3] M. Sigrist, T. M. Rice, F. C. Zhang, Phys Rev. B 49 (1994), 12058.

[4] D. V. Khveshchenko, Phys. Rev. B 50 (1994), 380;
D. V. Khveshchenko and T. M. Rice, Phys. Rev. B 50 (1994), 252.

[5] N. Nagaosa, Solid State Commun. 94 (1995), 495.

[6] X.-G. Wen and P. A. Lee, Phys. Rev. Lett. 76 (1996), 503.

[7] P. A. Lee, N. Nagaosa, T.-K. Ng, and X.-G. Wen, Phys. Rev. B 57 (1998), 6003.

[8] P. A. Lee and N. Nagaosa, Phys. Rev. B 46 (1992), 5621.

[9] M. U. Ubbens and P. A. Lee, Phys. Rev. B 46 (1992), 8434.

[10] M. Troyer, H. Tsunetsugu, and T. M. Rice, Phys. Rev. B 53 (1996), 251.

[11] K. B. Efetov and A. I. Larkin, Sov. Phys. JETP 42 (1976), 390.

[12] S. C. Zhang, Phys. Rev. B 42 (1990), 1012.

[13] V. J. Emery, in "Highly Conducting One-Dimensional Solids", ed. J. T. Devreese et al. (Plenum, New York, 1979).

[14] F. D. M. Haldane, Phys. Rev. Lett. 47 (1981), 1840;
F. D. M. Haldane, J. Phys. C 14 (1981), 2585.

[15] Y. Yu and Z. Zhu, Phys. Rev. B 45 (1992), 12502.

Chapter 4

Staggered-spin contribution to nuclear spin-lattice relaxation in two-leg antiferromagnetic spin-1/2 ladders.

Recent NMR experiments on Cu_2O_3 ladders in $A_{14}Cu_{24}O_{41}$ compounds (A_{14}=La_6Ca_8, Sr_{14}, $Sr_{11}Ca_3$) reveal unexpected behavior of the nuclear spin-lattice relaxation rate $1/T_1$ at temperatures of order of the spin gap [1]. While both $^{63}(1/T_1)$ and $^{17}(1/T_1)$ exhibit activation-type behavior at low temperature, a well-pronounced crossover is observed in ^{63}Cu nuclear spin relaxation rate. There exist numerous theoretical studies of $1/T_1$ in antiferromagnetic two-leg ladders [2, 3, 4, 5], but none of them predicts a similar crossover. In this paper we argue that the observed crossover is due to the processes with the momentum transfer $q = (\pi, \pi)$.

We describe the spin ladder by the Heisenberg Hamiltonian

$$H = \sum_n \left[J(\vec{S}_n^{(I)} \vec{S}_{n+1}^{(I)} + \vec{S}_n^{(II)} \vec{S}_{n+1}^{(II)}) + J_\perp \vec{S}_n^{(I)} \vec{S}_n^{(II)} \right]. \tag{4.1}$$

Here n is an integer labeling the rungs of the ladder, the superscripts refer to the two chains. J and $J_\perp$ are the coupling constants. From analyzing experimental data on magnetic susceptibility [6] and on ^{17}O NMR Knight shift [1], it has been suggested that in Cu_2O_3 ladders $J_\perp/J \approx 0.5$.

Both the strong-coupling ($J_\perp/J \gg 1$) and the weak-coupling ($J_\perp/J \ll 1$) approaches confirm that the low-lying magnetic excitations in the ladder are spin-1 magnons with the minimal gap at $k = (\pi, \pi)$; in the physically relevant range $J_\perp/J \approx 0.5$, the value of the gap is known to be $\Delta \approx 0.5 J_\perp$ [7, 5, 8]. We believe that the weak-coupling limit captures the characteristic features of the nuclear spin relaxation. For the sake of simplicity we assume that $T, J_\perp \ll J$ (with no assumptions on the relative magnitudes of $J_\perp$ and the temperature T). Then all excited magnons have momenta close to the wave vector $k = (\pi, \pi)$. The relaxation rate $1/T_1$ is given

by

$$\frac{1}{T_1} = 2\sum_q F(q)S(q,\omega_0) = \sum_q F(q)\frac{2T}{\omega_0}\mathrm{Im}\chi(q,\omega_0), \tag{4.2}$$

where $F(q)$ are the appropriate coupling constants, ω_0 is the nuclear resonance frequency ($\omega_0 \ll \Delta, T$), $S(q,\omega)$ is the dynamical structure factor, and $\chi(q,\omega)$ is the dynamical magnetic susceptibility. We employ the system of units with $\hbar = k_B = \mu_B = 1$. Since the excited magnons have momenta close to (π,π), there are two major contributions to $1/T_1$: that with $q \approx (0,0)$ (via even-magnon-number processes) and that with $q \approx (\pi,\pi)$ (via odd-magnon-number processes). Accordingly, define

$$\left(\frac{1}{T_1}\right)_{q=0} = 2\int_{q\approx 0}\frac{dq}{2\pi}S((q,0),\omega_0), \qquad \left(\frac{1}{T_1}\right)_{q=\pi} = 2\int_{q\approx\pi}\frac{dq}{2\pi}S((q,\pi),\omega_0) \tag{4.3}$$

(defined this way, the quantities $(1/T_1)_{q=0}$ and $(1/T_1)_{q=\pi}$ do not have the dimension of inverse time). Then the total relaxation rate $1/T_1$ is a linear combination of $(1/T_1)_{q=0}$ and $(1/T_1)_{q=\pi}$.

The coupling constants $F(q)$ for the oxygen sites vanish at $q = (\pi,\pi)$ [1], so

$$^{17}\left(\frac{1}{T_1}\right) \propto \left(\frac{1}{T_1}\right)_{q=0}. \tag{4.4}$$

The experiments on $SrCu_2O_3$ suggest that in Cu_2O_3 ladders the coupling constant $F(q)$ for the copper site is dominated by the on-site hyperfine interaction and therefore only weakly depends on q [9]. Thus we expect that $^{63}(1/T_1)$ is a linear combination of $(1/T_1)_{q=0}$ and $(1/T_1)_{q=\pi}$ with the coefficients of the same order of magnitude. Next, the available numerical studies[4] indicate that at temperatures of order of the spin gap the contributions $(1/T_1)_{q=0}$ and $(1/T_1)_{q=\pi}$ have comparable magnitudes. Therefore, we suggest that $^{63}(1/T_1)$ in the experimentally relevant temperature range is not dominated by the $q = 0$ contribution, in contrast with other studies [2, 3].

A simple argument shows that the contribution $(1/T_1)_{q=\pi}$ has gap 2Δ as opposed to gap Δ for $(1/T_1)_{q=0}$ (this argument was originally proposed for spin-1 chains [10], but it also remains valid for spin-1/2 ladders). In $(1/T_1)_{q=0}$, the nuclear spin is relaxed by the quasi-elastic scattering of a thermally excited magnon, which requires a gap of Δ. On the other hand, $(1/T_1)_{q=\pi}$ assumes an elastic scattering with momentum transfer near (π,π), which means that the total number of incoming and outcoming magnons must be odd (each magnon carries momentum close to (π,π)). Processes of creating and annihilating a single magnon cannot occur at zero energy because of the gap. Therefore, the leading contribution comes from three-magnon processes: two thermally excited magnons are converted into a single magnon carrying the total energy of the incoming magnons (up to the NMR frequency ω_0), or vice versa (see Fig. 1 below). Such processes require energy at least 2Δ.

On the basis of the above argument, the contribution $(1/T_1)_{q=\pi}$ was usually neglected. However, several recent works conclude that the effective gap in $(1/T_1)_{q=0}$ is somewhat larger than Δ (determined from susceptibility), either because of magnon interaction [3] or due to the singlet excitation mode [2]. A larger gap in $1/T_1$ than in

the susceptibility is indeed reported in Cu_2O_3 ladders [11, 9]. In view of these results, our suggestion of importance of $q = \pi$ contribution to ^{63}Cu nuclear spin relaxation rate appears more plausible.

For the rest of the paper we focus on computing $(1/T_1)_{q=\pi}$ in the weak-coupling limit $J_\perp \ll J$. Although we are unable to find a closed analytic form for $(1/T_1)_{q=\pi}$ in the whole range of temperatures, we find the high- and low-temperature asymptotics and estimate the crossover temperature.

According to the results of [8], in the weak-coupling limit, the spin-1/2 two-leg ladder is equivalent to four massive Majorana fermions, combined into a triplet of mass Δ and a singlet of mass 3Δ:

$$H_f = H_\Delta[\xi_1] + H_\Delta[\xi_2] + H_\Delta[\xi_3] + H_{3\Delta}[\rho] + H_{int}, \tag{4.5}$$

where each $H_m[\xi]$ is a free massive Hamiltonian of a Majorana fermion ξ; H_{int} is the four-fermion interaction arising from the marginal term in the interchain coupling [8]. It has been argued in [3] that the interaction would lead to nonperturbative effects in $(1/T_1)_{q=0}$. However, the staggered magnetization is nonlocal in terms of fermions, and we expect that the interaction will play a smaller role in $(1/T_1)_{q=\pi}$. Following [8], we neglect H_{int}. (See also Appendix B on neglecting the interaction.)

In the continuum limit, the local magnetization $\vec{S}^{(\alpha)}$ may be split into the uniform and staggered components:

$$\vec{S}_n^{(\alpha)} = \vec{J}^{(\alpha)} + (-1)^n \vec{n}^{(\alpha)}. \tag{4.6}$$

While $\vec{J}$ has a quadratic expression in terms of the Majorana fermions, $\vec{n}$ is non-local in the fermion operators. If the Majorana fermions are mapped onto non-critical 1+1-dimensional Ising models (we need four Ising models — one for each Majorana fermion), the operator $\vec{n}$ may be expressed in terms of order (σ) and disorder (μ) parameters of the Ising models [8]. In particular,

$$n_z^- = n_z^{(I)} - n_z^{(II)} \propto \sigma_1\sigma_2\mu_3\sigma^*, \tag{4.7}$$

where σ^* is the order parameter for the Ising model with gap $\Delta^* = 3\Delta$; σ_1, σ_2, and μ_3 — order and disorder parameters of the three identical Ising models with gap Δ [8]. Conventionally, we have chosen the Ising models to be in ordered state, so that $\langle\sigma\rangle \neq 0$ at zero temperature.

The expression (4.7) would enable us to compute $(1/T_1)_{q=\pi}$ using (4.3), should we know the non-critical Ising correlation functions at finite temperature. In a recent work [12], the latter has been expressed as a series in number of fermionic excitations, and we shall use their result to match the high- and low-temperature asymptotics of the Ising correlation functions.

The proportionality coefficient in (4.7) is non-universal. To fix the relative normalization of the high- and low-temperature asymptotics, define

$$\tilde{n}_z^- = \sigma_1\sigma_2\mu_3\sigma^* \tag{4.8}$$

with the order and disorder operators normalized by their short-distance asymptotics:

$$\langle\sigma(x)\sigma(0)\rangle \sim \langle\mu(x)\mu(0)\rangle \sim \frac{1}{|x|^{1/4}}, \qquad x \to 0. \tag{4.9}$$

In what follows we normalize $(1/T_1)_{q=\pi}$ accordingly, in other words, in (4.3) we set $S(x,t) = \langle\tilde{n}_z^-(x,t)\tilde{n}_z^-(0,0)\rangle$.

In a natural way, the following three limits may be distinguished:

(i) $T \ll \Delta$. In this low-temperature limit, $(1/T_1)_{q=\pi}$ has activation-type behavior with gap 2Δ. The prefactor may be computed using the results of [12].

(ii) $T \gg \Delta^*$. In this limit the gaps presumably play no role, and the system is equivalent to two uncoupled chains ("quantum critical" phase). The result for $(1/T_1)_{q=\pi}$ in this limit may be borrowed from [13]. Although this high temperatures are beyond the experimental range, considering this limit is useful for determining the degree of applicability of the approximations being made.

(iii) $\Delta \ll T \ll \Delta^*$. In the ladder system this intermediate limit is never attained, since $\Delta^* = 3\Delta$. However we may formally take this limit assuming $\Delta^* \gg \Delta$. The validity of this approximation will be discussed further.

Below we describe in more detail the computations and the results in these three limits.

(i) $T \ll \Delta$. According to [12], the (non-ordered) Ising correlation functions may be expressed as the series in the number of fermionic excitations:

$$\langle\sigma(t,0)\sigma(0,0)\rangle = \sigma_0^2 \sum_{n \text{ even}} \frac{1}{n!} \sum_{\varepsilon_i} \int_{-\infty}^{+\infty} \prod_{i=1}^{n} \frac{d\beta_i}{2\pi} f_{\varepsilon_i}(\beta_i) e^{-i\varepsilon_i E(\beta_i)t} |F(\beta_1,\ldots,\beta_n)_{\varepsilon_1,\ldots,\varepsilon_n}|^2, \tag{4.10}$$

where $\varepsilon_i = \pm 1$ $(i = 1,\ldots,n)$ are the particle-hole indices,

$$f_\varepsilon(\beta) = [1 + \exp(-\varepsilon E(\beta)/T)]^{-1} \tag{4.11}$$

is the Fermi distribution function, β_i are the rapidities of the excitations with energies $E(\beta) = \Delta\cosh\beta$.

$$F(\beta_1,\ldots,\beta_n)_{\varepsilon_1,\ldots,\varepsilon_n} = i^{n/2} \prod_{i<j} \left(\tanh\frac{\beta_i - \beta_j}{2}\right)^{\varepsilon_i\varepsilon_j} \tag{4.12}$$

are the corresponding formfactors [12, 14].

The same expression gives $\langle\mu(t,0)\mu(0,0)\rangle$, with the only difference that the sum is taken over odd numbers of excitations n.

The zero-temperature magnetization σ_0 may be taken from the exact result on the Ising model [15, 16]:

$$\sigma_0^2 = \Delta^{1/4} 2^{1/6} e^{-1/4} A^3 \approx 1.8437\Delta^{1/4}, \tag{4.13}$$

where $A = \exp[1/12 - \zeta'(-1)] = 1.282427\ldots$ is the Glaisher constant. In the Ising model with gap 3Δ, $\sigma_0^{*2} = 3^{1/4}\sigma_0^2$.

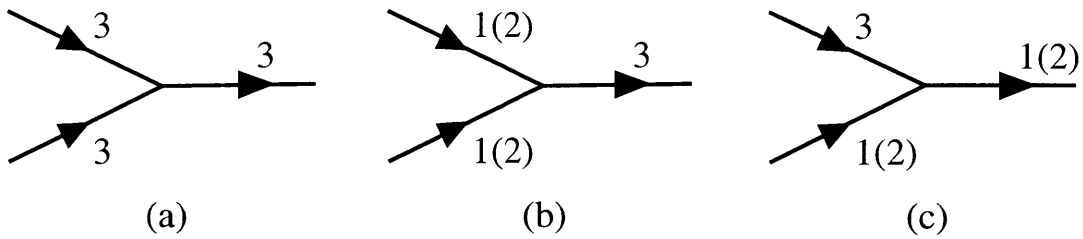

Figure 4-1: Three-magnon processes contributing to $(1/T_1)_{q=\pi}$.

Using (4.10), we express

$$\left(\frac{1}{T_1}\right)_{q=\pi} = 2\int_{-\infty}^{+\infty} dt \langle \tilde{n}_z^-(x,t)\tilde{n}_z^-(0,0)\rangle \tag{4.14}$$

as a sum of the odd-magnon-number processes with zero energy transfer. The one-magnon process has a gap and does not contribute to (4.14). In Fig. 4-1 we show the three types of three-magnon processes contributing to $(1/T_1)_{q=\pi}$.

In the diagrams, the arrows correspond to the particle-hole index ε_i in (4.10), the labels 1,2,3 — to the three different Majorana fermions (equivalently, to the spin of magnons). The contribution from the diagrams shown in Fig. 4-1 must be multiplied by two to account for the diagrams with arrows reversed. We neglect processes including the singlet channel (with gap 3Δ), since they have a larger gap 4Δ. The processes (a) and (b) in Fig. 4-1 can be shown to have temperature dependence $T^2\exp(-2\Delta/T)$, while the process (c) dominates at low temperatures with the temperature dependence $T\exp(-2\Delta/T)$. Including only the latter contribution, we find:

$$\left(\frac{1}{T_1}\right)_{q=\pi} = 4\sigma_0^6\sigma_0^{*2}\iiint_{-\infty}^{+\infty}\frac{d\beta_1}{2\pi}\frac{d\beta_2}{2\pi}\frac{d\beta_3}{2\pi}\frac{2\pi\delta\left(E(\beta_1)+E(\beta_2)-E(\beta_3)\right)}{8\cosh\frac{E(\beta_1)}{2T}\cosh\frac{E(\beta_2)}{2T}\cosh\frac{E(\beta_3)}{2T}}\coth^2\left(\frac{\beta_1-\beta_3}{2}\right). \tag{4.15}$$

The low-T asymptotics of this expression is

$$\left(\frac{1}{T_1}\right)_{q=\pi} \sim \frac{4\sqrt{3}}{\pi}\left(\frac{\sigma_0^6\sigma_0^{*2}}{\Delta}\right)\left(\frac{T}{\Delta}\right)e^{-\frac{2\Delta}{T}}. \tag{4.16}$$

Putting in the numbers,

$$\left(\frac{1}{T_1}\right)_{q=\pi} \sim 33.54\left(\frac{T}{\Delta}\right)e^{-\frac{2\Delta}{T}} \tag{4.17}$$

(with the normalization (4.9), $(1/T_1)_{q=\pi}$ is dimensionless).

(ii) In the high-temperature limit $T \gg \Delta^*$, the quantity $(1/T_1)_{q=\pi}$ is determined by the short-distance asymptotics of the correlation function

$$\langle \tilde{n}_z^-(x)\tilde{n}_z^-(0)\rangle \sim \frac{1}{x}. \tag{4.18}$$

In this case Sachdev's result [13] gives

$$(1/T_1)_{q=\pi} = \pi \approx 3.1416. \tag{4.19}$$

(iii) In this limit, we replace the operator σ^* by its zero-temperature expectation value, while pretending that the three remaining operators in (4.8) are massless. Then

$$\langle \tilde{n}_z^-(x)\tilde{n}_z^-(0)\rangle \sim \frac{\sigma_0^{*2}}{x^{3/4}}. \tag{4.20}$$

To handle this case, we redo the calculation of [13] for arbitrary exponent η in

$$\langle \tilde{n}_z^-(x)\tilde{n}_z^-(0)\rangle \sim \frac{D}{x^\eta}. \tag{4.21}$$

The magnetic susceptibility is then given by [17]

$$\chi(\omega,k) = \frac{\pi D}{(2\pi T)^{2-\eta}} \frac{\Gamma\left(1-\frac{\eta}{2}\right)}{\Gamma\left(\frac{\eta}{2}\right)} \frac{\Gamma\left(\frac{\eta}{4} - i\frac{\omega+k}{4\pi T}\right)\Gamma\left(\frac{\eta}{4} - i\frac{\omega-k}{4\pi T}\right)}{\Gamma\left(1-\frac{\eta}{4} - i\frac{\omega+k}{4\pi T}\right)\Gamma\left(1-\frac{\eta}{4} - i\frac{\omega-k}{4\pi T}\right)}, \tag{4.22}$$

which leads to

$$\left(\frac{1}{T_1}\right)_{q=\pi} = \lim_{\omega\to 0}\int_{-\infty}^{+\infty} \frac{dk}{2\pi}\frac{2T}{\omega}\mathrm{Im}\chi(\omega,k) = D\frac{\Gamma^2\left(\frac{\eta}{2}\right)}{\Gamma(\eta)}(2\pi T)^{\eta-1}. \tag{4.23}$$

In our case ($\eta = 3/4$, $D = \sigma_0^{*2}$),

$$\left(\frac{1}{T_1}\right)_{q=\pi} = \sigma_0^{*2}\frac{\Gamma^2\left(\frac{3}{8}\right)}{\Gamma\left(\frac{3}{4}\right)}(2\pi T)^{-1/4}. \tag{4.24}$$

Numerically,

$$\left(\frac{1}{T_1}\right)_{q=\pi} = 7.028\left(\frac{T}{\Delta}\right)^{-1/4}. \tag{4.25}$$

The three temperature dependences (4.17), (4.19), and (4.25) are plotted in Fig. 4-2.

The mismatch of the asymptotics (ii) and (iii) at $T \approx 3\Delta$ is due to the roughness of the approximation $\langle\sigma^*(t)\sigma^*(0)\rangle = \sigma_0^{*2}$ made in (4.20). At $T \approx \Delta^*$, this correlation function decays at time scale of order T^{-1} (the same as the triplet-channel correlation functions), which substantially decreases $(1/T_1)_{q=\pi}$. Although for $\Delta^* = 3\Delta$ the limit (iii) is never realized, it clearly indicates that at high temperature $(1/T_1)_{q=\pi}$ slowly decreases with temperature, approaching the constant value of the asymptotics (ii).

Another qualitative consequence of our discussion is the crossover from increasing activation behavior of asymptotics (i) to slowly decreasing high-temperature asymptotics (iii)–(ii). The crossover occurs at $T \approx \Delta$, in spite of the gap 2Δ of the low-temperature asymptotics. This agrees with the experimental results of T. Imai et al.,

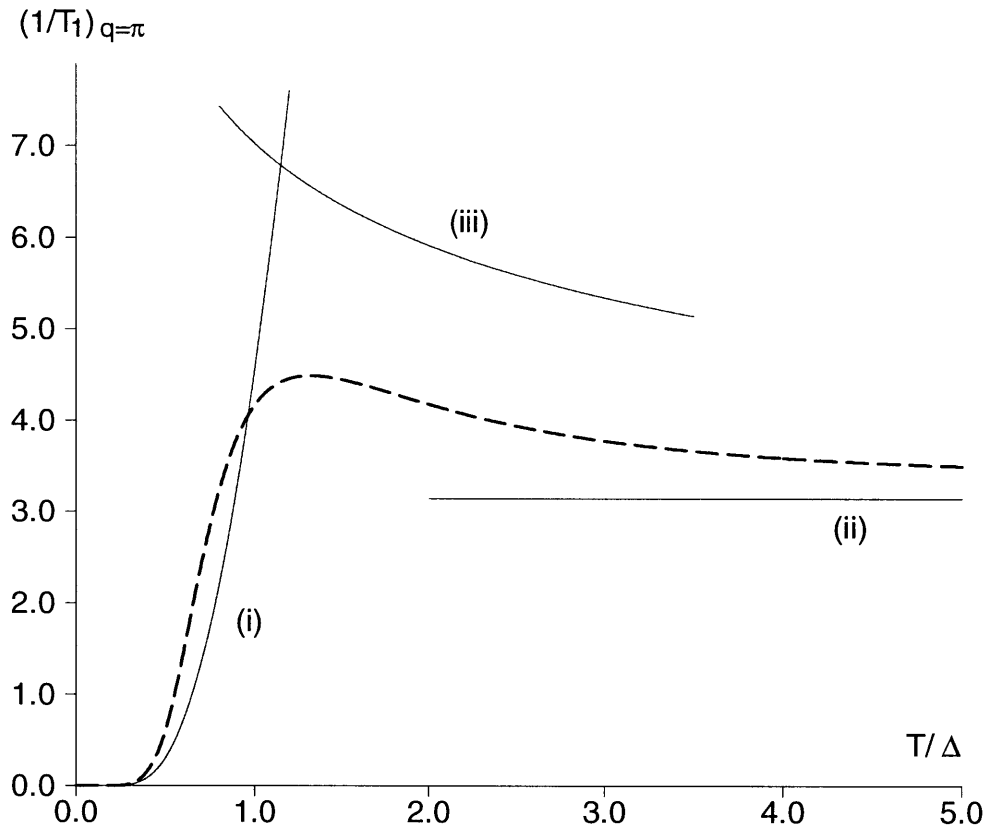

Figure 4-2: The three limiting asymptotics of the temperature dependence of $(1/T_1)_{q=\pi}$. Dashed line is the qualitative interpolation of the actual temperature dependence.

who observed a sharp crossover in $^{63}(1/T_1)$ at $T \approx 425$K in the undoped compound $La_6Ca_8Cu_{24}O_{41}$ [1]. Moreover, the form of the temperature dependence of $^{63}(1/T_1)$ in the hole-doped compounds $Sr_{14}Cu_{24}O_{41}$ and $Sr_{11}Ca_3Cu_{24}O_{41}$ appear qualitatively very close to the proposed form of $(1/T_1)_{q=\pi}$ (including a slowly-decreasing high-T behavior). We may speculate that this can possibly be explained by a different hyperfine coupling of the ^{63}Cu spin in these compounds making $(1/T_1)_{q=\pi}$ contribution dominate in $^{63}(1/T_1)$. On the other hand, hole doping may modify the temperature dependence of $(1/T_1)_{q=\pi}$, which deserves further theoretical study. (See also the discussion of the weakly doped case in Appendix A.)

It is worth mentioning that our interpolation of $(1/T_1)_{q=\pi}$ (dashed line in Fig. 4-2) is higher than the asymptotics (i) at low temperature. This comes from the fact that all terms in the low-temperature expansion (4.10) are positive, and including only the leading term underestimates $(1/T_1)_{q=\pi}$ at low temperatures. This observation ensures that the crossover from (i) to (iii)-(ii) is sufficiently sharp.

To experimentally separate $(1/T_1)_{q=\pi}$ and $(1/T_1)_{q=0}$ contributions in the total spin-lattice relaxation rate $^{63}(1/T_1)$, one can use the fact that $q = \pi$ contribution does not have a singular dependence on the external field. While $(1/T_1)_{q=0}$ singularly diverges at low magnetic fields (as $\log H$ in the free-magnon model [5] or as $H^{-1/2}$ in the spin-diffusion model [3, 18]), $(1/T_1)_{q=\pi}$ only weakly depends on the magnitude of the magnetic field.

We hope that further experimental and numerical works will provide a better understanding of the crossover in $(1/T_1)_{q=\pi}$ discussed in this paper.

We would like to thank T. Imai for sharing the experimental data prior to publication, A. M. Tsvelik for drawing our attention to ref. [12], and D. H. Kim for many helpful discussions.

This research was supported by the MRSEC program of NSF under award number DMR 94-00334.

P.S. After the publication of this work, we have learned about the preprint of Naef and Wang, whose numerical computations by DMRG method agree with our analytic weak-coupling predictions [19].

4.1 Appendix A. Case of weakly doped ladders

In this appendix we argue that, at small doping, the temperature dependence of $1/T_1$ is qualitatively similar to that in the undoped ladder (except for the renormalization of the spin gap Δ).

The spin gap persists at low doping, and the spin-gap behavior of $(1/T_1)_\pi$ will remain similar to the undoped case, with a smaller gap. The pre-exponential factor in eq. 4.17 may also change.

In the scaling regimes $T > \Delta$ one may expect the change of the conformal dimension of the staggered-spin operator n_z^- due to charge degrees of freedom. However, at low doping, the "holons" reside near the bottom of their band, and linearizing the dispersion of charge degrees of freedom near the "Fermi points" would be a bad

approximation. The finite doping will affect only the long-range part of the correlation function $\langle n_z^- n_z^- \rangle$, at distances exceeding the average inter-hole distance $1/x$ (x is the hole concentration) [20]. In the temporal correlation function, the holes affect time scales larger than $(1/x)v_c^{-1}$, where v_c is the velocity of charge excitations. It may be estimated as $v_c = Cxt$, where C is a numerical coefficient (in one-dimensional Hubbard model at $U \to \infty$, $C = 2\pi$ [20], but in the ladder it may be different), t is the hopping parameter of the $t-J$ model. At a finite temperature T, holes affect the scaling behavior if $(1/x)v_c^{-1} < T^{-1}$ or, equivalently,

$$T < Cx^2 t. \tag{4.26}$$

Therefore, for small doping, if the inequality

$$x < \sqrt{\frac{\Delta}{Ct}} \tag{4.27}$$

is satisfied, the high-temperature behavior of $1/T_1$ is not affected. In application to the experiments of Imai et al. [1], this inequality is definitely satisfied for $Sr_{14}Cu_{24}O_{41}$ with $x \sim 0.06$ and possibly for $Sr_{11}Ca_3Cu_{24}O_{41}$ with $x \sim 0.12$.

4.2 Appendix B. On the validity of neglecting magnon interaction in computing $1/T_1$

As found by Damle and Sachdev [3], the four-magnon interaction arising from the marginal interchain term in the Hamiltonian (4.1) leads to a non-perturbative renormalization of the scattering matrix at low momenta (and further to the diffusive spin dynamics). In view of this result, our neglecting interaction of magnons may appear questionable. However, a simple argument will show that the staggered component of the spin is not subject to these non-perturbative effects.

The outline of this appendix is as follows. We use the mapping of the Hamiltonian onto the sine-Gordon model with the cosine dimension slightly shifted (by interaction) from the free-fermion point. The magnons are represented by solitons and antisolitons. We observe that the exact scattering matrix for the sine-Gordon model reproduces Damle and Sachdev's result. Finally, we notice that the staggered-spin field has identical commutation relations with a soliton and with an antisoliton and, therefore, "hard-core" scattering of solitons at low momenta has no effect on the correlations of staggered spin.

Consider the "x-y part" of the ladder Hamiltonian (containing only the magnons ξ_1 and ξ_2). It is convenient to combine the two Majorana fermions into one complex fermionic field Ψ, then the Hamiltonian reads as [8]:

$$H = H_0 + H_{int}, \tag{4.28}$$

where

$$H_0 = -iv_s(\Psi_R^\dagger \partial_x \Psi_R - \Psi_L^\dagger \partial_x \Psi_L) - i\Delta(\Psi_R^\dagger \Psi_L - \Psi_L^\dagger \Psi_R) \tag{4.29}$$

is the free massive Hamiltonian,

$$H_{int} = \frac{g}{2}(\Psi_R^\dagger \Psi_R + \Psi_L^\dagger \Psi_L)^2 \tag{4.30}$$

is the interaction term with $g = J_\perp a_0$ (a_0 is the lattice constant). Now we bosonize the Hamiltonian, and the density-density term H_{int} becomes quadratic in the bosonic field φ:

$$H_{int} = \frac{g}{4\pi}(\nabla\varphi)^2. \tag{4.31}$$

By appropriate rescaling the field φ, this term may be incorporated in the kinetic energy, and we arrive to the sine-Gordon Hamiltonian

$$H = \frac{v_s}{2}\left(\Pi^2 + (\nabla\tilde{\varphi})^2\right) - \frac{\Delta}{\pi a_0}\cos(\beta\tilde{\varphi}), \tag{4.32}$$

where the dimension of the cosine term is (to lowest order in g) [8]

$$D = \frac{\beta^2}{4\pi} = 1 - \frac{g}{2\pi v_s}. \tag{4.33}$$

It is shifted from the free-fermion point $D = 1$ by interaction. Denote

$$\varepsilon = 2\pi(1 - D) \sim \frac{g}{v_s} \propto \frac{J_\perp}{J}. \tag{4.34}$$

Although, by assumption, this parameter is small, it nonperturbatively modifies the scattering matrix at very low momenta [3].

The magnons ξ_1 and ξ_2 (or rather $\Psi^\dagger$ and Ψ) correspond to solitons and antisolitons in the sine-Gordon model. The soliton-antisoliton S-matrix is known exactly [21, 22]. The scattering results in either transmission (with a possible phase shift) or in the hard-core reflection (the soliton and the antisoliton exchange their momenta). Respectively, the scattering matrix consists of the two components, t and r. In the low-momentum limit, they are given by

$$t = \frac{i\theta}{\varepsilon + i\theta}, \tag{4.35}$$

$$r = \frac{\varepsilon}{\varepsilon + i\theta}, \tag{4.36}$$

where θ is the difference of the rapidities of the soliton and the antisoliton, $\theta = \theta_1 - \theta_2$. When the momenta k_i are small, $\theta_i \approx v_s k_i/\Delta$. We see that the exact sine-Gordon result reproduces the scattering matrix obtained by Damle and Sachdev, including the numerical prefactor in the small parameter ϵ.

Here we want to make two brief remarks about the result (4.35), (4.36). First, in the sigma-model approach discussed in Damle and Sachdev's work [3] the scattering matrix is given by (4.35), (4.36) with $\varepsilon = 2\pi$. This has a natural explanation as a classical limit of the sine-Gordon model ($\varepsilon = 2\pi$ corresponds to $D = 0$). Second, the

pole in the S-matrix at $\theta = i\varepsilon$ gives the soliton-antisoliton bound state (breather). In the original ladder problem, such breathers correspond to the lowest triplet magnetic excitations at momenta near (0,0).

Let us now consider the staggered-spin operators projected onto the ξ_1-ξ_2 subsystem. In the bosonized form, they are given by [8]

$$n_z \propto \cos(\sqrt{\pi}\varphi), \tag{4.37}$$

$$n_\pm \propto e^{\pm i\sqrt{\pi}\theta}. \tag{4.38}$$

In turn, the soliton and the antisoliton are constructed from the fermionic operators

$$\Psi_{R,L} \propto e^{\pm i\sqrt{\pi}\varphi + i\sqrt{\pi}\theta}, \tag{4.39}$$

$$\Psi^\dagger_{R,L} \propto e^{\mp i\sqrt{\pi}\varphi - i\sqrt{\pi}\theta}. \tag{4.40}$$

The actual soliton (antisoliton) operator is a linear combination of Ψ_R and Ψ_L ($\Psi^\dagger_R$ and $\Psi^\dagger_L$) mixed by the mass term (up to perturbative in g corrections). The dual angles φ and θ obey the commutation relation

$$[\phi(x), \theta(y)] = i\Theta(x-y), \tag{4.41}$$

where Θ is the step function: $\Theta(x>0) = 1$, $\Theta(x<0) = 0$ (with this definition, the right- and left-movers (4.39), (4.40) correctly anticommute).

Then it is straightforward to show that

$$n_z(x)\Psi^{(\dagger)}(y) = (-1)^{\Theta(x-y)}\Psi^{(\dagger)}(y)n_z(x), \tag{4.42}$$

$$n_\pm(x)\Psi^{(\dagger)}(y) = (-1)^{\Theta(y-x)}\Psi^{(\dagger)}(y)n_\pm(x). \tag{4.43}$$

in other words, the operator product of the staggered spin and a magnon has a branch cut in either positive or negative direction. The key feature of the commutation relations (4.42), (4.43) is that they are identical for the solitons (Ψ) and for the antisolitons ($\Psi^\dagger$) [23].

This formal derivation has a simple quasiclassical interpretation. n_z reaches a nonzero value at the minima of the sine-Gordon potential. Each soliton or antisoliton shifts $\sqrt{\pi}\varphi$ by π, and n_z changes sign regardless of whether $\sqrt{\pi}\varphi$ is shifted in positive or negative direction. This argument is identical to that of Sachdev and Young for the Ising chain in a transverse magnetic field [24]. The quasiclassical treatment of that work may be used to compute the correlation functions of n_z at low temperature (in a dilute gas of solitons).

The insensitivity of the staggered spin to the sign of the soliton contrasts the situation with the uniform component of the spin. The uniform z-component of the spin is in the bosonic language $J_z = \nabla\varphi/\sqrt{\pi}$ which is obviously sensitive to the sign of the soliton. One can verify from commuting $\Psi^{(\dagger)}$ with J_z that the soliton (antisoliton) carries spin 1 (-1 respectively).

At low temperature, the gas of solitons is dilute, and in a semiclassical computa-

tion of the correlations of the staggered spin, both solitons and antisolitons may be replaced by a single species of particles (again, up to perturbative in g corrections) obeying the commutation relations (4.42), (4.43). This is possible, because in any event of the soliton-antisoliton scattering, the resulting particles have again the same momenta as the original ones; in other words, if we do not distinguish the sign of solitons, we may treat them as free particles. This is equivalent to neglecting the magnon interactions. We conclude, therefore, that our neglecting interactions leads only to perturbative in g corrections. In particular, the spin gap observed in $(1/T_1)_{q=\pi}$ equals 2Δ (plus perturbative in g corrections) as in the noninteracting model.

Bibliography

[1] T. Imai, K. R. Thurber, K. M. Shen, A. W. Hunt, and F. C. Chou, Phys. Rev. Lett. 81 (1998), 220.

[2] J. Kishine and H. Fukuyama, J. Phys. Soc. Jpn. 66 (1997), 26.

[3] K. Damle and S. Sachdev, Phys. Rev. B 57 (1998) 8307.

[4] A. W. Sandvik, E. Dagotto, and D. J. Scalapino, Phys. Rev. B 53 (1996), R2934.

[5] M. Troyer, H. Tsunetsugu, and D. Würtz, Phys. Rev. B 50 (1994), 13515.

[6] D. C. Johnston, Phys. Rev. B 54 (1996), 13009.

[7] T. Barnes, E. Dagotto, J. Riera, and E. S. Swanson, Phys. Rev. B 47 (1993), 3196.

[8] D. G. Shelton, A. A. Nersesyan, and A. M. Tsvelik, Phys. Rev. B 53 (1996), 8521.

[9] K. Ishida, Y. Kitaoka, K. Asayama, M. Azuma, Z. Hiroi, and M. Takano, J. Phys. Soc. Jpn. 63 (1994), 3222.

[10] J. Sagi and I. Affleck, Phys. Rev. B 53 (1996), 9188.

[11] M. Azuma, Z. Hiroi, M. Takano, K. Ishida, and Y. Kitaoka, Phys. Rev. Lett. 73 (1994), 3463.

[12] A. Leclair, F. Lesage, S. Sachdev, and H. Saleur, Nucl. Phys B 482 (1996), 579.

[13] S. Sachdev, Phys. Rev. B 50 (1994), 13006.

[14] V. P. Yurov and Al. B. Zamolodchikov, Int. J. Mod. Phys. A 6 (1991), 3419.

[15] T. T. Wu, B. M. McCoy, C. A. Tracy, and E. Barouch, Phys. Rev. B 13 (1976), 316.

[16] In Ref. [14] the citation of the result (4.13) has a typo.

[17] S. Sachdev, T. Senthil, and R. Shankar, Phys. Rev. B 50 (1994), 258.

[18] M. Takigawa, T. Asano, Y. Ajiro, M. Mekata, and Y. J. Uemura, Phys. Rev. Lett. 76 (1996), 2173.

[19] F. Naef and X. Wang, "Nuclear spin relaxation in two-leg ladders", preprint.

[20] H. J. Schultz, "Fermi liquids and non-Fermi liquids", in "Les Houches. Session LXI. Mesoscopic Quantum Physics." Elsevier, 1995. Amsterdam, Netherlands.

[21] V. E. Korepin, Teor. Mat. Fiz. 41 (1979), 169.

[22] A. B. Zamolodchikov, Pis'ma v Zh.E.T.F. 25 (1977), 499 [JETP Lett.].

[23] In our argument we assume that there are no non-perturbative corrections to the commutation relations (4.42), (4.43).

[24] S. Sachdev and A. P. Young, Phys. Rev. Lett. 78 (1997), 2220.

2727-5a